Quantum Dot Platform for Single-Cell Molecular Profiling

Pavel S Zrazhevskiy

A dissertation

submitted in partial fulfillment of the

requirements for the degree of

Doctor of Philosophy

University of Washington

2013

Reading Committee:

Xiaohu Gao, Chair

Patrick S Stayton

Lawrence D True

Program Authorized to Offer Degree:

Bioengineering

University of Washington

Abstract

Quantum Dot Platform for Single-Cell Molecular Profiling

Pavel S Zrazhevskiy

Chair of the Supervisory Committee:

Associate Professor Xiaohu Gao

Department of Bioengineering

In-depth understanding of the nature of cell physiology and ability to diagnose and control the progression of pathological processes heavily rely on untangling the complexity of intracellular molecular mechanisms and pathways. Therefore, comprehensive molecular profiling of individual cells within the context of their natural tissue or cell culture microenvironment is essential. In principle, this goal can be achieved by tagging each molecular target with a unique reporter probe and detecting its localization with high sensitivity at sub-cellular resolution, primarily via microscopy-based imaging. Yet, neither widely used conventional methods nor more advanced nanoparticle-based techniques have been able to address this task up to date. High multiplexing potential of fluorescent probes is heavily restrained by the inability to uniquely match probes with corresponding molecular targets. This issue is especially relevant for quantum dot probes – while simultaneous spectral imaging of up to 10 different probes is possible, only few can be used concurrently for

staining with existing methods. To fully utilize multiplexing potential of quantum dots, it is necessary to design a new staining platform featuring unique assignment of each target to a corresponding quantum dot probe. This dissertation presents two complementary versatile approaches towards achieving comprehensive single-cell molecular profiling and describes engineering of quantum dot probes specifically tailored for each staining method. Analysis of expanded molecular profiles is achieved through augmenting parallel multiplexing capacity with performing several staining cycles on the same specimen in sequential manner. In contrast to other methods utilizing quantum dots or other nanoparticles, which often involve sophisticated probe synthesis, the platform technology presented here takes advantage of simple covalent bioconjugation and non-covalent self-assembly mechanisms for straightforward probe preparation and specimen labeling, requiring no advanced technical skills and being directly applicable for a wide range of molecular profiling studies. Utilization of quantum dot platform for single-cell molecular profiling promises to greatly benefit both biomedical research and clinical diagnostics by providing a tool for addressing phenotypic heterogeneity within large cell populations, opening access to studying low-abundance events often masked or completely erased by batch processing, and elucidating biomarker signatures of diseases critical for accurate diagnostics and targeted therapy.

Table of Contents

List of Figures

List of Tables

Acknowledgements

Inception, design, and implementation of research projects comprising this dissertation could only become possible due to an outstanding education, dedicated mentorship, and unconditional support that I have enjoyed through my academic career in Russia and the United States. I would like to extend my sincerest appreciation to my teachers, mentors, colleagues, friends, and family, who have made unique and indispensable contributions to my development as a scientist and as a person. For this I am forever indebted to you.

A special word of appreciation goes to the Gao Lab. Guidance and support provided by my longtime research advisor and mentor Dr. Xiaohu Gao helped me not only to acquire expertise in the exciting field of bionanotechnology, but also to build a solid professional foundation for a future Academic career. Numerous members of the Gao Lab, in turn, brought together diverse cultural and research backgrounds to create a friendly collaborative atmosphere that nurtured creativity, collegiality, and perseverance. I would like to express particular gratitude to my lab-mates Shivang, Christine, and Emily, who relentlessly questioned my views, engaged in critical discussions, and offered insightful ideas.

Cross-disciplinary work described in this dissertation would not be possible without prominent dedication on the part of the UW College of Engineering and School of Medicine to fostering translational research and collaboration. It is our clinical collaborators, in particular Prof. Larry True, who aided in finding unique clinical applications for quantum dot technology and helped maintain clinical utility as a top priority of our technology development efforts. Open exchange of ideas between scientists from diverse research backgrounds provided a bottomless source of innovative ideas. I praise the University of Washington and affiliated institutions for creating such a unique environment for cross-disciplinary research.

My training as a scientist would be incomplete without engaging in professional development and social service activities. I thank my home Department of Bioengineering, UW Molecular Engineering & Sciences Institute, and the Center for Nanotechnology for providing numerous outreach and networking opportunities, facilitating active interaction with the general public, and supporting student organizations. Also, I would like to note the outstanding job done by the UW Career Center at promoting professional development of graduate students.

Finally, I would like to acknowledge the sources of funding that supported my training and research. I am grateful to the UW Center for Nanotechnology for a University Initiative Fund (UIF) Fellowship and to the National Science Foundation for Graduate Research Fellowship (DGE-0718124). This work was also supported in part by NIH (R01CA131797), NSF (0645080), DoD-CDMRP (W81XWH0710117), the Coulter foundation, and the UW Department of Bioengineering.

CHAPTER 1: INTRODUCTION

The development of materials, structures and systems with physical dimensions of 1 to 100 nanometers (nm) has a tremendous impact on the advancement of a wide range of fields including catalysis, computing, photonics, energy, and medicine. In contrast to widely used bulk counterparts, nanomaterials possess novel unusual and useful physicochemical properties that emerge at minute length scales. Metallic nanostructures in the presence of an electromagnetic field, for example, exhibit electron density oscillations which are highly sensitive to environmental perturbations. Iron oxide nanoparticles become superparamagnetic, exhibiting field-inducible magnetic dipoles. Carbon nanotubes possess remarkable tensile strength and controllable electrical conductivity. Semiconductor nanoparticles emit tunable and spectrally narrow fluorescence light upon excitation. These structures have been synthesized in a variety of shapes, sizes and configurations, and the theoretical framework explaining the unique optical, chemical and electronic properties of nanomaterials has been built. Meanwhile, nanomaterials have been incorporated in a variety of useful products ranging from stain-repellent fabrics and nanoparticle-containing sunscreens to lipid-encapsulated anti-cancer drugs and sensitive bioanalytical tools. With the number of nanotechnology-based patents growing exponentially [1], such items are rapidly appearing on the market. As new applications are developed, especially in such critical fields as energy generation and medicine, the impact of nanotechnology on the economy and on society will become increasingly more profound.

One of the most promising applications of nanotechnology has been in the area of biomedical research. Nanoscale sensors find their use in sensitive molecular diagnostics and high throughput bioanalytics, while nanoparticle-based drug carriers enable spatial and temporal control of drug delivery and release. Of great interest are organic and inorganic nanostructures that incorporate radiolabels and contrast agents for *in vivo* imaging techniques, such as Positron Emission Tomography (PET), Computed Tomography (CT), Single Photon Emission Computed Tomography (SPECT), Magnetic Resonance Imaging (MRI), sonography, and optical imaging. In combination with these macroscale modalities, nanoscale probes are important tools for molecular imaging – visualization, characterization, and quantification of biological processes at the molecular level within living systems [2, 3]. Further development of novel nanoparticle-based technologies should prove essential for overcoming limitations of conventional methods and advancement of biomedical research and clinical practice, especially in providing a technological foundation for implementation of the advanced personalized diagnostic and therapeutic approaches.

State-of-the-art medicine is an indispensable part of the human society. Wealth of medical knowledge accumulated over centuries of observation and experimentation, advanced diagnostic techniques made possible by the technological revolution, and innovative biomedical research done on the cellular and molecular levels provide formidable weapons against nearly any threat to human health. However, the most devastating diseases, such as cancer, immunodeficiencies, and neurological disorders to name a few, are notorious for their ability to evade current diagnostic methods and resist therapy. Significant heterogeneity on molecular level, complex interlinking of subcellular mechanisms, and integrated effects on organs and systems of the human body render generalized diagnostic and treatment methods ineffective. Instead, each individual case should be dealt with in a personalized manner,

utilizing disease-specific molecular signatures for assessing disease stage and progression, making accurate prognosis, and developing targeted therapy [4-8].

Successful implementation of personalized approach in medicine requires (i) advances in fundamental biomedical research to uncover molecular mechanisms of disease pathogenesis and elucidate relevant molecular signatures and (ii) advances in clinical diagnostics to utilize expanded set of biomarkers in making treatment decisions. Both critically depend on development of novel molecular characterization technologies capable of producing comprehensive molecular portraits of individual diseases. Current attempts of gaining access to such information rely on batch screening for genetic alterations (e.g. RT-PCR, gene chips) or differences in protein expression (e.g. protein chip, 2D gel electrophoresis, mass spectrometry) in diseased cells; yet diagnostic and predictive power of genetic screening alone is questionable [9, 10], while batch analysis of a homogenized mixture of different cell types, including healthy ones, might significantly hamper discovery of disease-specific molecular signatures. Furthermore, destructive nature of these techniques leads to a loss of valuable 3D cellular and tissue morphological information. Therefore, complementary analysis of single-cell phenotypic changes within the context of local tissue microenvironment and preserved morphology is necessary for comprehensive analysis of a pathological process, enabling accurate diagnosis and targeted therapy. Critical importance of single-cell analysis for modern medicine fuels continuous exploration of new elaborate ways for obtaining molecular and morphologic information from intact clinical specimens [11]. In particular, microscopy imaging based on specific labeling of biomarkers of interest with reporter probes followed by high-resolution 2-D or 3-D signal readout represents the most appropriate technology for this task. However, fundamental limitations faced by conventional imaging techniques, such as poor capacity for quantitative analysis and inability to analyze multiple

biomarkers on the same specimen, currently preclude comprehensive evaluation of individual cells, significantly hampering evolution of personalized medicine.

Innovations in bio-nanotechnology are introducing variety of nanoparticle-based tools promising to dramatically expand capabilities of molecular imaging. Specifically, fluorescent nanoparticles – quantum dots (QDots) – will undoubtedly play a major role in advancing the field of molecular analysis and personalized medicine, in part through enabling engineering of powerful imaging technologies taking advantage of unique photo-physical properties and versatile bio-functionalization capabilities of QDot probes [4, 5, 12-14]. Intrinsic capacity of QDots for highly multiplexed biomarker imaging and quantitative analysis of expression levels overcomes the fundamental limitations of conventional reporters (such as colorimetric stains and organic fluorophores) and provides a foundation for assessing single-cell molecular signatures in a comprehensive manner. Yet, despite substantial efforts focused on exploiting QDots for addressing most demanding biomedical applications, QDot-based tools have neither contributed to major biomedical discoveries nor found wide adoption within clinical diagnostics, suffering from unreliable staining methodologies and sophisticated probe preparation protocols.

Quantum dot platform technology described in this thesis features a fine balance of technical simplicity and analytical power necessary for straightforward single-cell molecular characterization within the context of preserved specimen morphology. Specifically, our technology enables simultaneous imaging of 5-10 biomolecular targets at sub-cellular resolution, while evaluating expression levels of each target in a quantitative manner, through multicolor fluorescence microscopy and hyperspectral imaging. Furthermore, limitations of parallel multicolor staining imposed by spectral features of QDot probes are overcome by employing sequential staining and imaging methodology, thus substantially

expanding the multiplexing capability for analysis of molecular profiles consisting of over 100 targets and enabling generation of truly comprehensive molecular and morphological phenotypes for individual cells.

1.1 Molecular profiling as a key driver for biomedical advances

Molecular profiling is a powerful technique for study of complex molecular networks underlying physiological and pathological processes through comprehensive interrogation of individual molecular components comprising such networks. It promises to become a key tool for advancing biomedical research, clinical diagnostics, and targeted therapy. Most importantly, molecular profiling, especially a more informative and powerful implementation of single-cell molecular profiling, might become an indispensable driving force for implementation of personalized medicine.

The need in personalized diagnostics and therapy is becoming apparent in all areas of medicine, especially considering steady movement to better quality of living and higher healthcare standards worldwide. In this regard, widespread transition towards personalized medicine, a practice of addressing individual diseases in a pathology-specific and patient-specific manner spanning all levels from whole-body symptoms down to molecular signatures of the disease, seems most appropriate. In particular, a personalized approach might prove essential for accurate diagnosis (i.e. pinpoint exact changes that occurred within healthy cells and tissues), prognosis (i.e. predict progression of a disease based on these changes), and treatment (i.e. specifically reverse the changes or, if not possible, target and eliminate the diseased cells without affecting healthy ones) of a variety of diseases as well as development of effective prophylaxis.

Great challenges faced by the field of oncology present one strong case in favor of extensive use of single-cell molecular profiling technologies to drive transition towards personalized medicine. Despite considerable efforts in the scientific and medical community to combat this disease, cancer still accounts for 25% of all deaths in the United States and remains one of the leading causes of death in the 21st century [15]. Mechanisms of oncogenesis and cancer response to therapy remain poorly understood, thus precluding from accurate cancer diagnosis, prognosis, and effective treatment. Elucidation of such mechanisms will undoubtedly provide insights not only for novel approaches to detection and treatment of cancers in early stages, but also for development of effective preventative measures. Yet, implementation of this task is quite challenging, as each cancer appears to be as unique as a fingerprint [5]. It is evident that different types of cancers have different biomarker expression schemes. However, even when tumors appear histologically identical between patients of the same ethnic and demographic group, cancer cells still sometimes exhibit drastically different genotypes and phenotypes [16], resulting in different (and, quite often, unpredictable) prognoses and responses to therapy. For example, Paik and colleagues have identified 21 genes that predict 10 year metastasis-free survival in patients with estrogen receptor-positive node-negative tumor, and have demonstrated that two-thirds of such patients get no benefit from chemotherapy [6]. Therefore, accurate molecular profiling of individual tumors is one key to effective treatment. Tumor-specific molecular information might identify cellular markers for targeted and effective anti-cancer therapy with minimal adverse side-effects. As such, expression levels of hormone receptors have been directly correlated with the benefit of endocrine treatment, while overexpression of Her2 protein or amplification of its gene has been identified as a requirement for effective treatment with monoclonal antibodies (such as trastuzumab) [17-19]. Successful targeted therapy has been implemented for the treatment of breast cancer [6], lung carcinoma, chronic myelogenous

leukemia, and gastrointestinal stromal tumor [20]. Therefore, the ability to thoroughly and quantitatively analyze complex panels of cancer biomarkers of individual tumors is strongly needed for comprehensive understanding of cancer pathophysiology – a prerequisite for accurate diagnostics and effective therapy.

Decreasing efficiency of the drug discovery process along with increasing demand for "smarter" targeted therapeutics presents further support for expedited development and widespread adoption of single-cell molecular profiling technologies. In recent years, remarkable technological breakthroughs in genome sequencing and combinatorial chemical synthesis have created the perfect storm for drug discovery within the pharmaceutical industry [21]. Pinpointing genetic differences between normal and diseased states enables identification of thousands of potential therapeutic targets, while generation and screening of enormous libraries of chemical compounds facilitates finding of a matching small-molecule drug to virtually any target of interest. As a result, high-throughput screening (HTS) approach has been successfully used for development of a number of small-molecule drugs [22, 23]. However, HTS is proving to be inefficient for finding treatments against the most complex and challenging diseases, as little to nothing is known about the role of targeted biomolecules in disease pathogenesis on par with lack of insight on the mechanism of action of selected drug candidates. Consequently, most drugs identified by HTS fail during downstream validation studies or clinical trials, yielding only 2-4 drugs with HTS origins reaching the market every year and, thus, demonstrating no real gains in the economics of drug development and an overall lackluster impact on improving patient outcomes [24, 25]. A fundamental gap between the "black box" drug discovery approach prevalent in pharmaceutical industry and the need for rational drug design based on an in-depth understanding of molecular mechanisms underlying pathogenesis and cellular responses to therapy has become boldly apparent. A conceptually different strategy of high-content screening (HCS) utilizing single-cell

proteomics for comprehensive molecular characterization is necessary for bridging this gap. Currently, HCS can be applied downstream of HTS hit identification to dramatically reduce the guesswork in selecting lead drug candidates by using live cell assays and an automated single-cell image processing. As a result, HCS has been successfully exploited within drug discovery for lead optimization, drug toxicity, mechanism of action, and target selectivity studies [26, 27]. However, further advances in rational drug design require substantial expansion of the HCS platform through incorporation of comprehensive single-cell molecular profiling technologies.

Successful implementation of the "personalized medicine" concept, therefore, relies on development and widespread adoption of molecular profiling technologies capable of driving fundamental advances in basic biomedical research as well as integration of novel diagnostic and therapeutic techniques into clinical practice. In fact, compilation of a database of genetic and phenotypic signatures of individual diseases appears to be critical for accurate diagnosis and prognosis, whereas untangling the complexity of intracellular molecular mechanisms and signaling pathways underlying pathogenesis and mapping their response to therapeutic intervention is indispensable for the development of next-generation therapeutics. Achieving this objective, however, is highly challenging, as it requires comprehensive interrogation of molecular and morphological detail at single-cell resolution, currently unattainable with even the most advanced state-of-the-art techniques.

1.2 Molecular profiling using conventional technologies

A variety of analytical approaches, such as two-dimensional gel electrophoresis, reverse transcription polymerase chain reaction, gene chips, protein chips, and biomolecular mass spectrometry, have been developed and routinely used for highly multiplexed genomics and

proteomics studies indispensable for describing the state of the cell population and its overall response to signaling, damage, or therapeutic intervention [28-31]. However, not only analysis of homogenized samples obscures unique states and responses of individual cells, but it also results in a loss of morphological information critical for evaluation of cell microenvironment [32, 33]. To address these issues, a number of single-cell proteomic technologies have been developed in recent years. In general, single-cell approaches generate complex data sets where each individual cell serves as an independent sample, enabling assessment of cell heterogeneity and study of intracellular processes at a mechanistic level. For example, microfluidic-based proteomic assays utilize sequestration of individual cells within separate microchambers for subsequent analysis of secreted or intracellular proteins, addressing variability of cell-to-cell behavior [34, 35]. However, such methods provide only moderate capacity for multiplexed quantitative analysis due to limitations imposed by spatial patterning of capture antibodies (**Table 1.1A**).

Flow-cytometry techniques, in turn, have been actively evolving towards expanding multiplexing capacity for comprehensive molecular profiling of suspended cells. Being a high-content technique that provides single-cell read-outs, fluorescence-based flow-cytometry can simultaneously analyze up to 17 biomarkers (using a combination of organic dyes and QDots for biomarker labeling, **Table 1.1B**), whereas recently developed mass-cytometry (which uses mass-spectrometry rather than fluorimetry for signal read-out) has enabled a remarkable 33-plexed analysis of the immune system hierarchy and provided an insight into cell signaling in response to drug intervention (**Table 1.1C**) [36, 37]. Featuring capability for multiparametric and quantitative single-cell analysis, flow cytometry has proven an extremely powerful tool for reconstructing cellular pathways, uncovering pathway crosstalk, and understanding response to therapeutic intervention. For example, use of antibodies specific for phosphorylated proteins has enabled the development of phoshoflow, a fluorescence flow

cytometry technique that has been applied to profile disease and normal signaling cascades, understand the role of aberrant signaling in cancer, and study the signaling biology of immune cell subsets. Still, without imaging capacity this technology faces significant limitations, most important of which are the inability to access morphological information (such as biomarker co-localization or translocation between intracellular compartments) and compatibility with only suspended cells (which necessarily destroys supra-cellular specimen morphology and prohibits analysis of solid tissue specimens or adherent cells), thus providing an incomplete portrayal of intracellular processes.

In contrast, conventional staining methods, such as immunohistochemistry (IHC) and immunofluorescence (IF), are well-suited for examination of specimen morphology and assessing specimen heterogeneity through single-cell analysis, but often incapable to provide sufficient analytical and multiplexing capacity necessary for meaningful molecular profiling (**Table 1.1D**). In clinics, for example, abnormal expression of cellular markers is commonly evaluated using standard pseudo-quantitative IHC methods [38], such as immunoperoxidase, which reveals biomarker location via deposition of colored product resulting from enzymatic conversion of diaminobenzidine by horseradish peroxidase. Since the density of staining is proportional to the number and distribution of biomarkers in the specimen, visual analysis of the colorimetric stains is routinely used to "quantify" biomarker expression levels. IF procedure, in turn, utilizes antibodies linked to fluorescent proteins or organic dyes for labeling of biomarkers, often providing higher contrast and sensitivity of staining and facilitating some degree of signal quantification through measurement of fluorescence intensity. However, both techniques are most well suited for single-color imaging and have limited use in single-cell molecular profiling [39]. Besides being single-color in nature, IHC analysis is prone to inconsistent staining results, as slight deviations in staining protocol (*e.g.* activity of enzyme, duration of reaction, and amount of substrate added) lead to significant

differences in staining density. Additionally, visual evaluation of stains is subjected to inter- and intra-observer variability, further limiting accurate quantification [40, 41]. Immunofluorescence method provides more room for detection of multiple markers with careful choice of fluorescent probes (2-3 colors in most cases due to the unfavorable optical properties of organic dyes), but quantitative analysis is heavily compromised by relatively quick photobleaching of organic fluorophores and significant signal interference due to tissue autofluorescence [42].

A number of procedures have been developed to overcome limitations of traditional IHC and IF, providing some degree of multiplexing for molecular profiling of cells and tissue specimens with preserved morphology. For example, Furuya et al have developed a 50-well chip for IHC staining of tissue sections, thus enabling isolated staining of 50 spots on the same section with 50 different antibodies, but not allowing molecular profiling of individual cells [43]. Englert and coworkers, on the other hand, proposed to transfer specimen proteins through a series of capture membranes that were then stained, thus maintaining 2D relationship between biomarkers for co-localization studies (**Figure 1.1A**); however, spatial resolution and multiplexing capability of this method are quite low [44]. A number of cyclic staining approaches utilizing 3-step staining procedure with tyramide signal amplification have been applied for "building-up" multicolor signal with successive cycles of staining (**Figure 1.1B**). Yet, these techniques require complete elution of antibodies after each cycle to eliminate cross-talk and still cannot offer high degree of multiplexing due to spectral overlap between different organic dyes. As such, 3-color staining using elution with microwave treatment [45] and 4-color staining using elution with pH2 Glycine-SDS [46] have been demonstrated. Sequential IHC [47] and IF [48] with image registration and de-staining on each cycle aim to overcome spectral overlap limitation (**Figure 1.1C**). For example, implementation of an automated cyclic IF has recently enabled interrogation of substantially

larger sets of antigens using organic fluorophores [49, 50]. However, numerous rounds of physical or chemical de-staining often lead to specimen degradation and loss of antigenicity, whereas alternative approach of organic dye quenching through photo-bleaching hinders consistent quantitative signal analysis. Overall, further progress of this field appears to be reaching a plateau, as conventional IF technology stumbles against fundamental limitations imposed by both organic dye-based probes and imaging instrumentation. In particular, inability to improve sensitivity, increase multiplexing capacity, and offer access to reliable quantitative analysis taken together with high instrumentation complexity and cost preclude from wide-spread use of conventional technologies for single-cell molecular profiling.

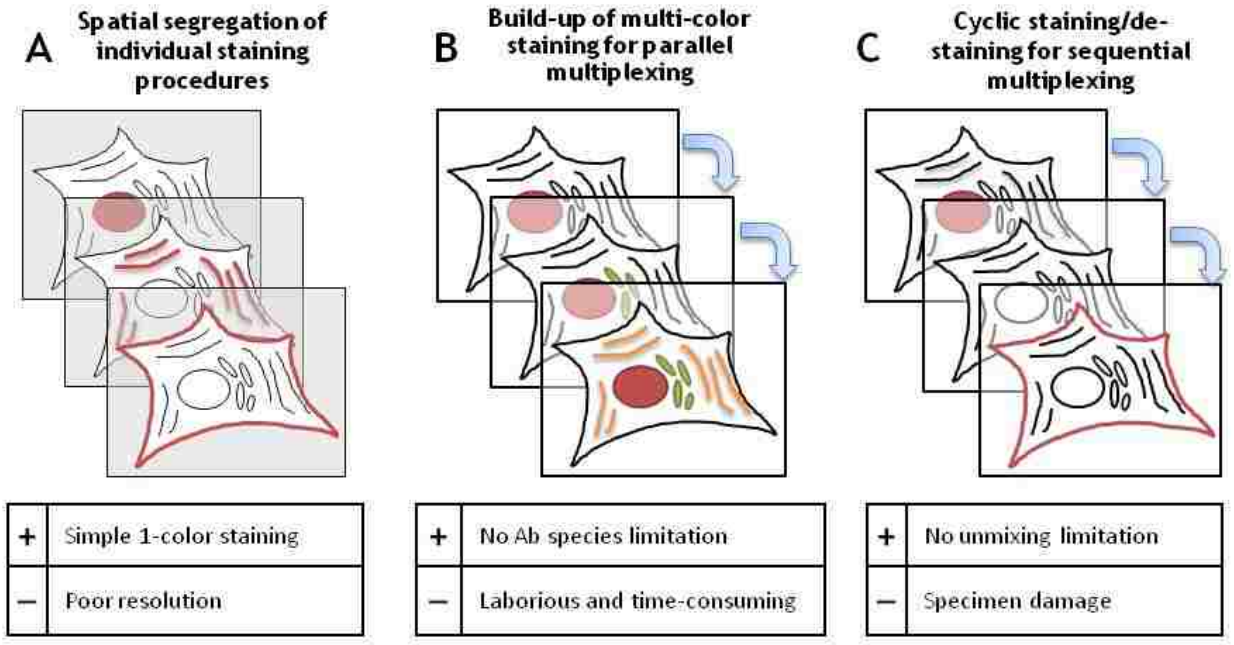

Figure 1.1 Multiplexed staining with conventional IF and IHC methods. (A) Evaluation of multiple targets on the same specimen can be achieved by spatial segregation of individual 1-color staining procedures, for example via transfer of specimen proteins through a series of capture membranes and staining of each membrane for a different target. (B) Multicolor staining can be achieved with fluorescent reporters by performing 1-color staining procedures in sequence on the same specimen, labeling each target with a different reporter. (C) Cyclic staining with signal registration followed by de-staining can be employed for interrogation of multiple targets using single-color reporter.

Realizing that demands of single-cell molecular profiling cannot be efficiently addressed through further advancements in IHC and IF techniques, conceptually different routes to engineering of molecular imaging systems are being actively explored. One successful example of stepping away from the mainstream research and approaching this problem from an alternative perspective is development of mass-spectrometry imaging, a massively multiplexed and quantitative label-free method capable of providing extensive molecular information for a small area of the specimen through parallel analysis of biomolecule-specific fragment signatures (**Table 1.1E**) [51-53]. As a result, MS imaging represents a powerful tool for elucidation of disease-related molecular changes and biomarker discovery, but it lacks single-cell resolution (having lateral resolution of 10-20 μm) and requires *a priori* identification of areas for analysis through correlation with optical imaging (still based on IHC or IF and requiring subjective evaluation by pathologist).

Despite many challenges encountered on the way towards molecular profiling, this approach is becoming more feasible due to development of highly specific and sensitive tools for uncovering physiologically and pathologically relevant molecular information. Scientists working in the field of biomedical research are constantly exploring new elaborate ways for obtaining comprehensive molecular information in order to better understand and, eventually, control normal and pathologic processes underlying complex physiological phenomena. Development of automated microscopy and image processing promise to provide this powerful functionality through high-resolution interrogation of individual cells within specimens with preserved morphology. At the same time, the bottleneck limitation of conventional microscopy tools, namely the inability to assess large libraries of biomolecules of interest due to poor multiplexing capacity, must be overcome to fulfill this promise. Since no existing method can simultaneously address the need for highly multiplexed molecular and morphological detail, many fascinating opportunities for single-cell proteomics research await

the development of new technologies. In this regard, novel nanoparticle-based tools for molecular imaging, in particular QDot technology (**Table 1.1F**), promise to finally enable exploration of single-cell molecular profiling applications [4, 54].

Table 1.1 Analytical capabilities of single-cell molecular profiling technologies

	Method	Parallel multiplexing	Quantitative analysis	Sub-cellular resolution	Specimen morphology
A	Microfluidic assay	up to 12	Moderate	No	No
B	FL Flow-cytometry	up to 17	High	No	No
C	Mass-cytometry	up to 34	High	No	No
D	IF / IHC microscopy	1-4	Low	Yes	Yes
E	MS imaging	>100	Moderate	No	Yes
F	QDot technology	up to 10	High	Yes	Yes

1.3 Quantum dots as a platform for engineering of imaging probes

Fluorescent semiconductor nanoparticles, commonly referred to as quantum dots (QDots), represent a particularly interesting class of nanoscale probes well-suited for advanced fluorescence imaging applications, such as comprehensive molecular profiling, real-time monitoring of intracellular processes, and *in vivo* molecular imaging [4, 55-62]. Such a rich functionality stems from a number of unique photo-physical and chemical properties possessed by QDots. Most notably, charge carriers in QDots undergo electronic transitions similar to those of bulk semiconductors, while also exhibiting quantum confinement effects imposed by the nanoscale dimensions (**Figure 1.2**). Bulk semiconductors are materials with a relatively small band gap (less than 4 eV) between the valence and conduction bands, thus behaving like insulators at ambient conditions and exhibiting electrical conductivity only

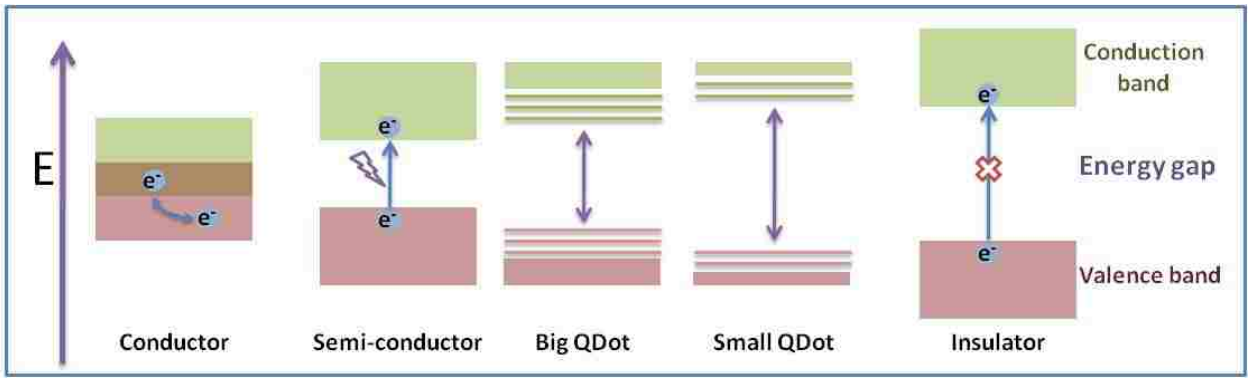

Figure 1.2 Electronic structure of bulk conductor, semiconductor, and insulator materials and semiconductor nanoparticles (QDots). Bulk semiconductor materials have fully populated valence band and empty conduction band separated by a relatively small band gap. When an energy exciding the band gap is supplied, valence-band electrons acquire sufficient energy to populate conduction band and enable electric current flow. In nanoparticles, valence and conduction bands split into discrete energy levels, with the energy gap between closest possible valence and conduction levels increasing with decreasing particle size (and increasing degree of confinement of charge carriers).

under external stimulation. Electrons in the ground state, typically localized to individual atoms (*i.e.* comprising valence band), can be promoted to higher energy levels where electrons are free to move throughout the material (*i.e.* populate the conduction band) by supplying an amount of energy that exceeds the band gap. In certain cases, relaxation of an electron results in the release of bandgap energy in the form of light (fluorescence). QDots, having physical size smaller that the exciton Bohr radius, impose a 3-dimensional quantum confinement on charge carriers and limit the number of possible energy states that an electron can occupy. Confinement results in a concentration of oscillator strength into a few discreet transitions and shifts electronic excitation to higher energy (which is inversely proportional to the square of a radius). As the particle size decreases, density of states becomes discrete on the edges of conduction and valence bands, and the spacing between allowed states increases [63].

This phenomenon results in smaller QDots requiring higher energy photons for electron excitations, while larger QDots (with smaller bandgaps) being excited with photons of lower energy. Relaxation of the newly created exciton to its ground state through electron-hole recombination is usually accompanied by release of bandgap energy in the form of a photon, thus yielding direct correlation between the particle size and the wavelength of emitted photon (**Figure 1.3**) [64-66]. Notably, photons with any energy exceeding the bandgap size can be absorbed by QDots without damaging the nanoparticle core. In fact, molar extinction

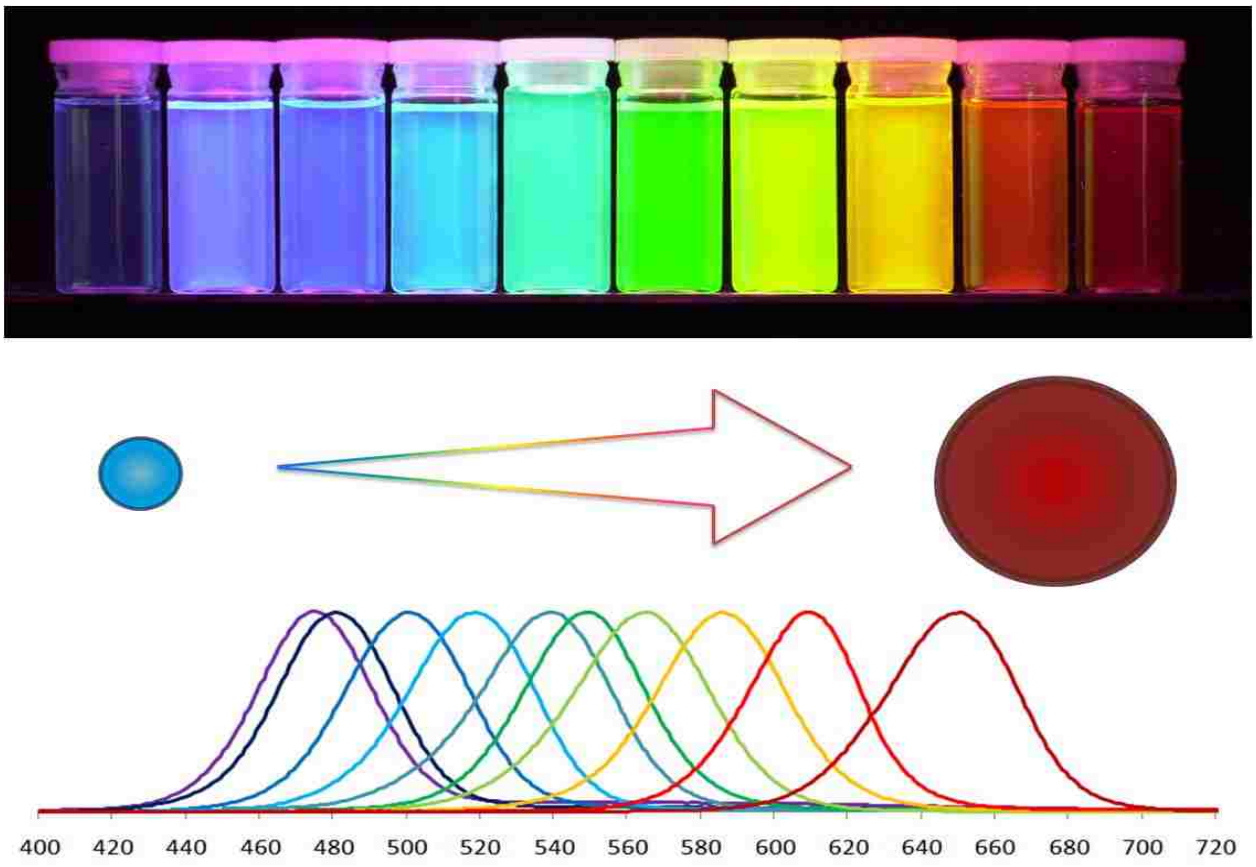

Figure 1.3 **Unique photo-physical properties of QDot probes.** Direct correlation between the nanoparticle size and the wavelength of emitted photon, originating from the quantum confinement of charge carriers, offers precise control over QDot color and yields narrow symmetrical light emission profiles (bottom). Wide absorption profile, in turn, allows simultaneous excitation of multicolor QDots with a single high-energy light source (top).

coefficient of QDots gradually increases toward shorter wavelength, producing wide absorption profile (hundreds of nanometers) and allowing simultaneous excitation of multicolor QDots by a single high-energy light source (*e.g.* UV lamp) [67]. Taken together, narrow size-tunable light emission and efficient light absorption throughout a wide spectrum provide a foundation for highly multiplexed fluorescence imaging (*e.g.* for phenotyping cell populations [68] or detection of molecular signatures of cancer [69]), as little or no cross-talk between adjacent colors enables simultaneous detection of multiple fluorescence signals within a narrow spectral range.

Unprecedented resistance to photobleaching along with well-defined symmetrical emission spectrum renders QDots the only probes capable of reliable quantitative analysis via fluorescence microscopy, especially when used together with advanced imaging instruments

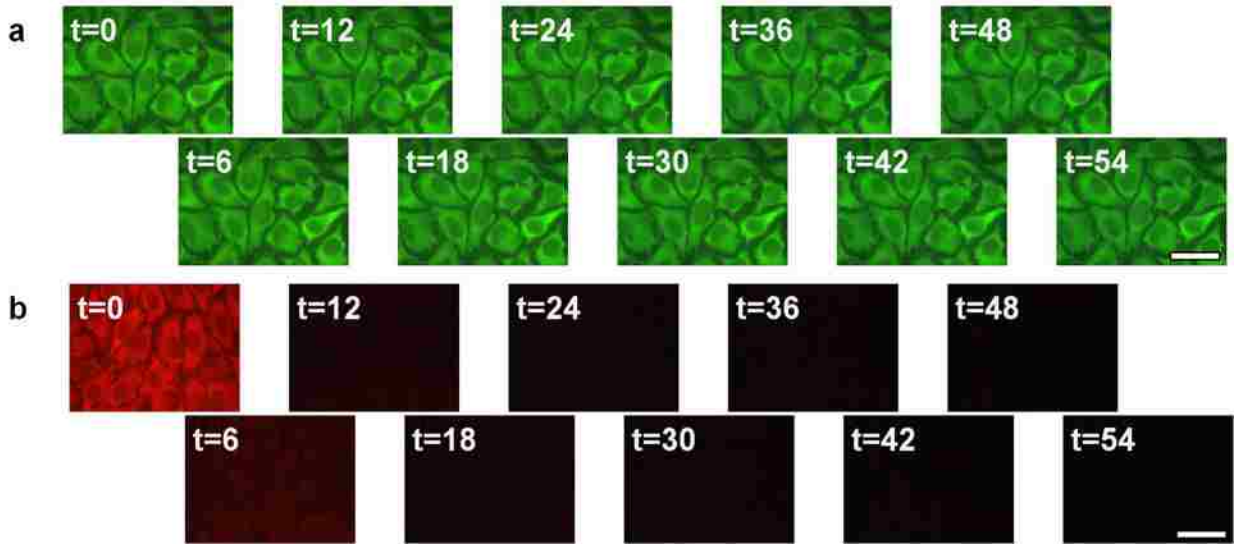

Figure 1.4 Superior photostability of QDot probes in comparison to organic fluorophores. HSP90 is stained in fixed HeLa cells with either QDot565 (a) or Alexa Fluor 568 (b). Continuous imaging of QDot-labeled specimen for 1 minute reveals lack of staining intensity fluctuation, enabling robust image acquisition and consistent quantitative analysis of staining intensity. In contrast, continuous imaging of Alexa Fluor 568-labeled cells shows quick photo-bleaching of the dye, which reduces useful time-frame for image acquisition and severely hampers quantitative signal analysis. Scale bar, 50μm.

such as hyperspectral imaging (HSI) [70]. In contrast to organic fluorophores, QDots are composed of hundreds to thousands of atoms and possess large capacity for absorption and dissipation of excess photon energy, exhibiting much greater stability of an inorganic core. It has been shown, for example, that QDots resist photobleaching for more than 30 minutes, while organic dyes fade by more than 90% in less than one minute under identical experimental conditions [71, 72]. Our own assessment of QDot photostability corroborates such observations (**Figure 1.4**).

Ghazani and coworkers have successfully employed this feature for quantitative analysis of tumor biopsies in tissue microarrays with optical spectroscopy [42]. Three-color QDot staining of lung carcinoma xenografts for epidermal growth factor receptor (EGFR), E-cadherin, and cytokeratin has been achieved and confirmed by conventional IF, while demonstrating superior QDot signal intensity and photostability essential for reliable quantitative analysis with de-noising and normalizing algorithms. Yezhelyev *et al* have demonstrated the use of QDot bioconjugates for quantitative evaluation of the three representative breast cancer markers (ER, PR, and HER2) in FFPE breast cancer cell lines, obtaining characteristic molecular profiles (**Figure 1.5**) [73].

Additionally, QDots are well suited for imaging applications when long exposure to excitation source is required while keeping signal intensity constant and allowing for consistent analysis of samples. For example, Tokumasu and Dvorak have reported the use of this property in immunocytochemical studies of human erythrocytes with high-magnification, three-dimensional reconstruction technique, where utilization of QDot probes allowed reliable collection of z-stack image data for 3D reconstruction without loss of image intensity [74]. Cui *et al* have employed high brightness and photostability for real-time tracking of intracellular transport of QDot-labeled nerve growth factor along axons of rat dorsal root

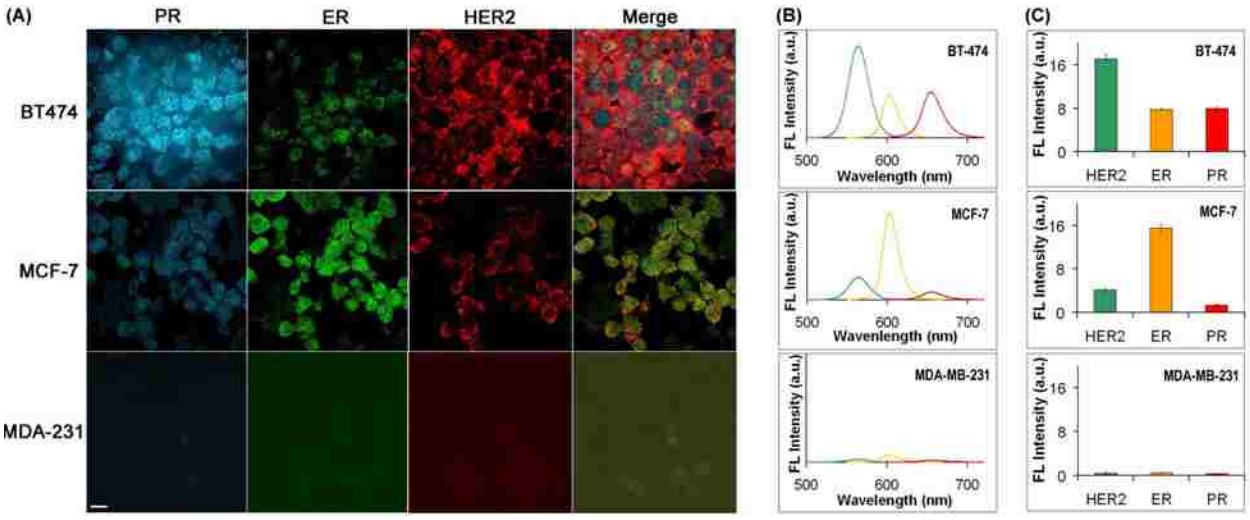

Figure 1.5 Multiplexed labeling of breast cancer cells with QDot probes. Unique optical properties of QDots enable accurate characterization of molecular profiles in FFPE breast cancer cell lines via multiplexed 3-color labeling and quantitative analysis of staining intensity. (A) Fluorescence images are deconvoluted into three individual components. (B) Representative spectra obtained with single-cell spectroscopy are used in quantitative analysis of biomarker expression levels. (C) Statistical analysis of biomarker expression obtained by averaging spectra of 100 single cells shows characteristic molecular profiles of different cell lines. Adapted from: Yezhelyev, M.V., et al. Adv. Mater., 2007. **19**(20): p. 3146.

ganglion neurons with pseudo-TIRF (total internal reflection fluorescence) microscopy [75]. It should be noted that stable surface coating, such as polymer encapsulation, is critical for QDot stability, as bare nanocrystals are quite susceptible to photolysis under extended UV illumination (since the energy of UV irradiation is close to that of covalent bonds in nanoparticles) [76-78].

Large red shift of fluorescence emission peak relative to excitation wavelength, also known as the Stokes shift, further contributes to QDot utility in molecular profiling applications. As the process of electron relaxation to its ground state following excitation to conduction band is usually accompanied by some energy loss, the emitted photon has longer wavelength (*i.e.* less energy) than the absorbed photon. While this phenomenon is common to

many fluorophores, red shift produced by QDots is much larger than that of organic fluorophores and can be as large as 300-400 nm, depending on the wavelength of the excitation light [79, 80]. This feature is particularly helpful when imaging specimens with high levels of autofluorescence, which often buries fluorescent signal of organic dyes due to close proximity of their excitation and emission profiles. QDot emission peak, on the other hand, can be red-shifted to a region of low autofluorescence, thus rendering staining clearly recognizable above the background [78, 81].

Further improvement in image contrast (measured by signal-to-noise or signal-to-background ratio) can be achieved by employing the relatively long excited state lifetime of QDots (20-50 ns, as compared to 2 ns for autofluorescence and 1-4 ns for organic fluorophores) via time-delayed data acquisition technique [81, 82]. Since QDot fluorescence intensity drops substantially slower, QDot-to-dye intensity ratio increases to ~100 in only 10 ns (assuming exponential model of fluorescence decay after a pulse excitation). For example, Dahan *et al* have demonstrated that time-gated imaging significantly and selectively reduces the autofluorescence contribution, achieving enhancement of the signal-to-background ratio by more than an order of magnitude [83]. Time-gated imaging can also be utilized in multiplexed biomarker imaging when both QDots and conventional organic fluorophores are used. In this case, the short-lived fluorophore signal is detected first, and then the QDot signal is measured [84].

In addition to a number of favorable photo-physical properties, QDots uniquely combine small protein-scale size (typically 2-10 nm in diameter) and large surface area, representing versatile nanoscaffolds for attachment of multiple proteins, peptides, and nucleic acids, thus enabling design of multifunctional nanoparticle-biological hybrids. Variety of bioconjugation approaches have been developed and utilized for QDot-based imaging applications. Covalent

bond formation between reactive functional groups (*e.g.* primary amines, carboxylic acids, alcohols, and thiols) is one of the most popular bioconjugation methods. Many proteins contain primary amine groups that can be linked to carboxyl-coated QDots via carbodiimide-mediated amide formation, genetically engineered or endogenously present sulfhydryl groups can be conjugated using active ester maleimide-mediated amine and sulfhydryl coupling, whereas a wide selection of cross-linking reagents enables conjugation of biomolecules to amine-modified QDots. Besides covalent bonding to organic QDot shell, thiolated or polyhistidine (HIS)-tagged biomolecules can be linked directly to the nanocrystal surface via coordination with metal atoms of the QDot core [85, 86]. Electrostatic interactions between nanocrystals and biomolecules have also been utilized for non-covalent self-assembly of engineered proteins on the surface of QDots. For example, avidin, a highly positively charged glycoprotein, was deposited on the surface of negatively charged QDots for further conjugation to biotinylated antibodies [87], while chimeric fusion protein was used for indirect coupling of native unmodified immunoglobulin G antibodies [88].

Rich set of unique photo-physical and chemical properties renders QDots an ideal platform for design and engineering of novel imaging probes capable of overcoming bottleneck limitations of existing methods and enabling practical implementation of single-cell molecular profiling concept [62]. Most importantly, QDots have the fundamental capacity for (i) simultaneous encoding of multiple individual targets via distinct emission spectral signatures, essential for multiplexed profiling on the same specimen, and (ii) production of bright and photo-stable fluorescence signal, critical for reliable assessment of target expression levels in a quantitative manner, while also featuring small size and versatile surface chemistry for synthesis of compact biofunctional probes.

1.4 Molecular profiling with QDot probes and its limitations

Despite the relatively recent introduction into biomedical research, QDots have already shown potential to become a powerful tool for sensitive quantitative molecular characterization of cells and tissues [5]. Possessing advantageous photo-physical properties and being compatible with conventional biomedical assays, QDots have found use in most techniques where fluorescence or colorimetric imaging of target biomolecules is utilized (*e.g.* cell and tissue staining, Western blot, ELISA, etc.) and have launched many novel applications (*e.g.* targeted *in vivo* imaging, single-molecule tracking, traceable drug delivery, etc.). Yet, arguably the major impact of wide adoption of QDot technologies will come from implementation of single-cell molecular profiling concept capable of providing unique identification of individual cell lineages, uncovering molecular signatures of pathological processes, tracing intricate networks of intracellular pathways, and guiding personalized diagnostics and rational drug design.

Initial proof-of-concept studies have already demonstrated feasibility of the single-cell molecular profiling concept and utility of QDot probes as a platform for its practical implementation. For example, QDots have been successfully employed for multi-parameter flow-cytometry analysis of cell populations and quantitative multiplexed analysis of biomarker expression in intact tissue specimens. As such, Chattopadhyay *et al* have achieved accurate immunophenotyping of antigen-specific T-cells using a 17-parameter flow-cytometry based on 8 QDot probes and 9 organic fluorophores, revealing significant phenotypic differences between T-cells specific to distinct epitopes of the same pathogen [36]. Access to molecular profiles of individual cell populations not only improves our understanding of immune response, but also might enable analysis of changes occurring during immune system

disorders, sensitive detection of metastasizing cancer cells in a bloodstream, and accurate phenotyping of heterogeneous cell populations.

Moving towards introducing QDot technology into clinical diagnostics, five-parameter characterization of breast cancer tissue specimens obtained from biopsies has been demonstrated with covalent QDot-Antibody bioconjugates (**Figure 1.6**) [73]. Comparison of the three specimens revealed distinct molecular profiles, where one tumor over-expressed such biomarkers as ER and PR, another tumor primarily expressed EGFR, and third tumor showed abundance of ER and HER2. Besides diagnostic and prognostic value of such analysis, potential targets for anti-cancer treatment can also be identified, thus enabling a "personalized" approach in therapy.

Information content of molecular profiling based on protein expression can be further enriched by analysis of gene expression via quantification of mRNA using fluorescent *in situ* hybridization (FISH). Relying on binding of oligonucleotide probes to complimentary mRNA molecules in 1:1 probe-to-target ratio, this technique offers high level of specificity, yields direct quantitative correlation between gene amplification (*i.e.* number of mRNA molecules present) and signal intensity, and provides accurate information about mRNA localization within the cell. Similar to protein-based staining, quantitative potential and sensitivity of FISH might be significantly improved by utilization of QDot probes [89]. In early proof-of-concept studies Xiao and Barker have used highly stable QDot-Streptavidin bioconjugates for monochromatic visualization of biotinylated oligonucleotide probes in FISH analysis of amplification of clinically important erbB2 gene [90]. Notably, QDot probes yielded substantially higher signal-to-noise ratio compared to organic fluorophores. Yet, utilization of the biotin-streptavidin linkage limited this 2-step procedure to detection of only one target per sample, rendering multiplexed FISH impossible.

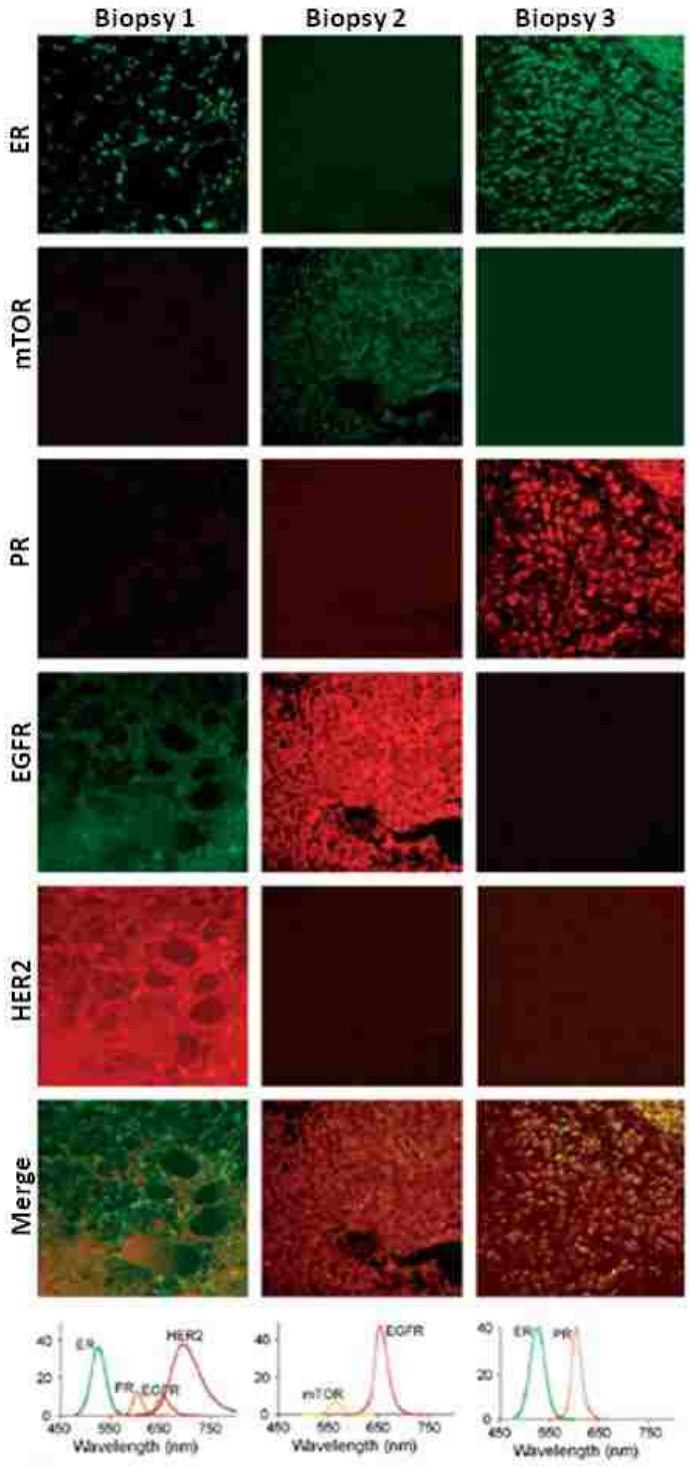

Figure 1.6 Molecular profiling of breast cancer biopsies with covalent QDot-Antibody bioconjugates. Direct labeling of targets with unique QDot probes enables simultaneous 5-color staining and quantitative evaluation of biomarker expression profiles. Adapted from: Yezhelyev, M.V., et al. Adv. Mater., 2007. **19**(20): p. 3146.

Using a modified procedure, Tholouli *et al* have achieved multiplexed staining of 3 mRNA targets within one specimen by pre-assembling QDot-Streptavidin bioconjugates with biotinylated DNA probes and directly labeling target mRNA in a 1-step FISH procedure [91]. Naturally, pre-conjugation of multiple oligonucleotides to QDots significantly increases the overall probe size, thus requiring stronger specimen permeabilization with enzymes (*e.g.* proteinase K), which necessarily degrades cell and tissue architecture and destroys most of the protein-based targets useful for IHC and IF studies. In order to reduce the size of imaging probe and improve binding stoichiometry, Chan *et al* have developed a monovalent FISH probe by blocking extra streptavidin sites with biocytin (water-soluble biotin derivative) [92]. High-resolution multiplexed FISH has been demonstrated in simultaneous detection of four mRNA targets using two different QDot probes and two different organic fluorophore probes within a single mouse midbrain neuron. Notably, reduced size of FISH probes enables staining in milder, protein-compatible specimen permeabilization conditions, which is essential for combined QDot-based FISH and QDot-based IF studies, thus offering the possibility of correlating gene expression at the mRNA level with the number of corresponding protein copies [89].

Simultaneous interrogation of multiple different types of targets (such as proteins and mRNA) and 3-dimentional mapping of their relative intracellular distribution represents an interesting and potentially highly informative avenue for future molecular profiling studies with QDot probes. In one interesting study of intracellular morphology, Matsuno *et al* have combined QDot-based FISH and IF along with confocal laser scanning microscopy for three-dimensional imaging of the intracellular localization of growth hormone (GH), prolactin (PRL), and of their mRNAs within tissue specimens [93]. With further improvements in design of QDot probes suitable for multiplexed FISH and IF, it is plausible to expect this technology provide

access to studies of intricate signaling pathways, mechanisms of pathogenesis, intracellular trafficking, and routes for drug delivery and resistance.

Despite the encouraging results obtained through initial proof-of-concept studies, current QDot-based technologies stumble at many of the same fundamental limitations faced by conventional IF methods. Specifically, use of poorly selective intermediate linkers with 2-step and 3-step procedures (such as primary/secondary antibody or biotin/streptavidin) leads to a loss of biomolecule-specific information, rendering multiplexed staining even with QDot probes highly challenging. Direct target labeling with QDot-Antibody bioconjugates, in turn, suffers from the requirement for tedious and time-consuming synthesis of custom designed probes [73, 94], finding little adoption among biomedical researchers.

In an attempt to expand multiplexing capacity of 2-step and 3-step procedures, several sequential staining approaches have been implemented. By using same links (*e.g.* primary/secondary antibody or streptavidin/biotin) on different staining cycles, detection of multiple biomarkers becomes possible. For example, 3-color staining (in 3 cycles) with 1' antibodies from the same species [95] and 4-color staining (in 2 cycles) with 1' antibodies from two different species [96, 97] have been demonstrated in 2-step format, while 2-color [98], 3-color [99], and 5-color [70] staining (in 2, 3, and 5 cycles respectively) has been achieved with 3-step format. Yet, all those methods suffer from inherent potential for cross-talk between different staining cycles and offer less consistent staining compared to parallel cocktail method [100]. As a result, QDot-based fluorescence imaging has yet to show major improvements over organic dyes, as current multiplexing capability is far below the expectation of creating a truly comprehensive molecular portrait for individual cells.

1.5 Overview of the quantum dot molecular profiling platform

Unlike variety of reporter probes utilized for detection of molecular targets, quantum dots possess intrinsic capacity for high-resolution multiplexed imaging and robust quantitative analysis of targets within specimens with preserved morphology, uniquely suited for implementation of single-cell molecular profiling applications. However, widespread realization of this potential in biomedical research is currently hampered by the complexity of probe preparation, lack of staining methodology for multiplexed target labeling, and scarcity of application-specific validation studies. In this context, novel molecular profiling platform described in this dissertation stands alone in full integration of all beneficial features of QDot probes within robust 1-step and 2-step staining methodology, while featuring technical simplicity and high analytical power. Such capability is achieved by simultaneous labeling of up to 5-10 molecular targets with unique QDot probes, either directly or via highly selective intermediate links, and quantitative evaluation of single-cell molecular profiles within preserved specimen morphology with hyper-spectral imaging. Incorporation of cyclic staining strategy, where several staining/imaging/de-staining cycles are performed on the same specimen in sequential manner, enables further dramatic expansion of the multiplexing capability of QDot imaging technology, capable of producing molecular profiles consisting of over 100 targets in just few cycles (**Figure 1.7**).

Direct labeling of molecular targets with QDot-Antibody probes in a 1-step procedure represents the most straightforward approach to implementation of multiplexed molecular imaging, as each target is unambiguously encoded by a corresponding QDot color. However, this approach has not found wide adoption due to requirement for complex synthesis of custom-designed probes, which is time-consuming (taking over 5 hours) and highly expensive (*e.g.* 1 conjugation reaction consumes ~$500 for QDot antibody conjugation kit + over $300

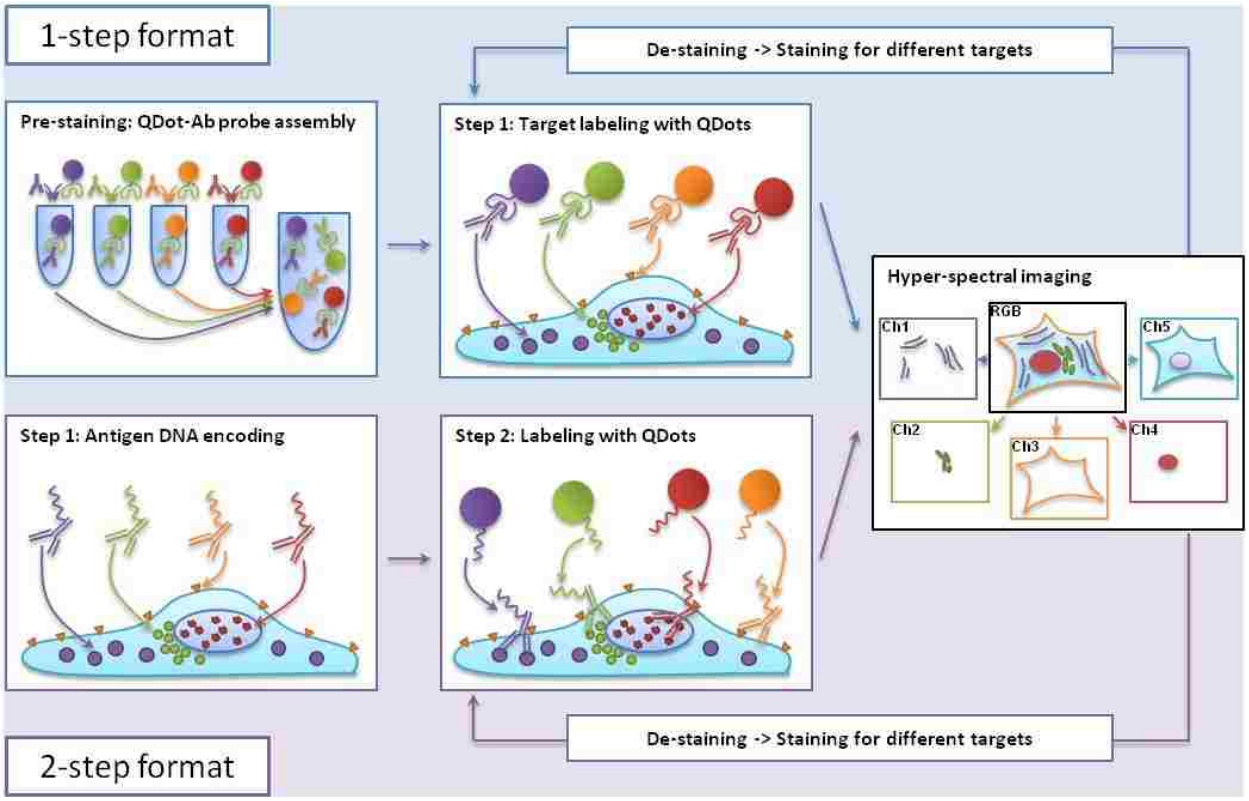

Figure 1.7 Overview of the QDot molecular profiling platform. Multiplexed target labeling is achieved either directly with self-assembled QDot-Antibody probes or in 2 steps using intermediate "encoding" DNA linkers. Hyper-spectral imaging is then utilized for unmixing and quantitative analysis of individual QDot signals. Finally, specimen re-labeling for different target sets via a cyclic staining methodology dramatically expands the multiplexing capacity of this platform to enable interrogation of 100+ molecular targets for a truly comprehensive single-cell molecular profiling.

for primary antibody) [73, 94]. Moreover, direct covalent conjugation to QDot surface often adversely affects antibody biofunctionality and provides poor control over antibody orientation, resulting in steric hindrance to target binding.

To overcome the complexity of QDot-Antibody probe preparation, we have developed a universal QDot-based nanoparticle platform that can be converted on-demand into functional QDot-Antibody probes via self-assembly with intact antibodies. Good stability of pre-assembled probes enables simple mixing of multiple probes in a cocktail for highly

multiplexed parallel staining, facilitating use of a full range of spectrally distinguishable QDots without antibody species or buffer composition limitations. Notably, this procedure requires no chemical modification of antibodies, eliminates the need for QDot-Antibody probe purification, streamlines assay development, significantly lowers cost of probe preparation, and makes QDot platform accessible to a wide range of biomedical researchers (**Table 1.2**).

Labeling of molecular targets with multi-step procedure, in turn, provides several important benefits not available through 1-step staining. Specifically, (i) individual probes are prepared using standard well-characterized bioconjugation techniques (with many QDot probes available commercially); (ii) staining conditions can be optimized for antibodies and QDot probes separately; (iii) target recognition is performed by free primary antibodies without experiencing steric hindrance; (iv) QDot probe size can be kept significantly smaller (as compared to QDot-Antibody bioconjugates); and (v) signal amplification can be incorporated within the staining methodology. The major drawback of this approach, however, is the loss of target-specific information encountered through use of poorly selective intermediate linkers (*e.g.* primary/secondary antibody or biotin/streptavidin), which renders multiplexed staining highly challenging [99, 101, 102].

To take advantage of multi-step procedure benefits while preserving the molecular information content, we have designed a QDot-based staining methodology featuring highly selective intermediate DNA links for unique assignment of probes to corresponding molecular targets. Specifically, multiplexed labeling of molecular targets with QDot probes is achieved by (i) encoding each target with a unique ssDNA tag via recognition by ssDNA-labeled primary antibodies and (ii) subsequent detection with complementary QDot-ssDNA' probes via sequence-specific hybridization. At the same time, as with 1-step staining platform, technical simplicity of probe preparation (critical for ready technology adoption by a wide range of

biomedical laboratories) is ensured by employing intuitive and straightforward covalent bioconjugation and self-assembly mechanisms. In contrast to other multi-step staining methodologies developed so far, DNA encoding approach converts molecular information between three high-content modes – molecular target antigenicity, DNA sequence code, and QDot emission signature, preserving labeling specificity and achieving multiplexed target staining in a quick, simple, and cost-effective manner (**Table 1.2**).

Table 1.2 Comparison of QDot-based staining methodologies

	Target detection	Multiplexing capacity	Method complexity/cost	1' Antibody modification	Methodology flexibility
Covalent QDot-1'Ab	direct	High	High / $$$	Moderate	Low
Self-assembled QDot-1'Ab	direct	High	Low / $	None	High
QDot-2'Ab	via 1'/2'Ab bond	Low	Low / $	None	Moderate
QDot-DNA	via DNA bond	High	Low / $$	Minor/None	High

Implementation of either 1-step or 2-step methodology described here enables straightforward simultaneous quantitative analysis of 5-10 molecular targets at sub-cellular resolution, providing a strong foundation for initial exploration of single-cell molecular profiling applications. However, further expansion of parallel multiplexing capacity necessarily requires design of higher-quality QDots and increase in complexity of staining methodology and imaging instrumentation. Instead, we have bypassed technical difficulties associated with parallel multiplexing by incorporating a cyclic staining approach within the QDot imaging platform. In its most simple form utilizing organic dyes, cyclic staining involves separate labeling and imaging of individual targets alternated by de-staining steps, during

which fluorescent labels are either quenched or completely removed from the specimen [48-50]. QDot imaging platform significantly expands the amount of molecular information obtained during each staining cycles, both in terms of target number and quantitative content, dramatically reducing specimen processing time and collecting comprehensive molecular profiles within just few cycles. At the same time, complete de-staining can be accomplished under substantially milder conditions compared to conventional techniques due to ready disassembly of semi-stable QDot-based probes. For example, elution of self-assembled QDot-Antibody probes is efficiently achieved via brief exposure to low-pH buffer, whereas partial removal of QDot-ssDNA probes can be done under physiological pH via DNA bond displacement with a competitor ssDNA.

1.6 Summary

Advancement of personalized medicine is essential for making progress towards combating such complex diseases as cancer and immune system disorders, and implementation of single-cell molecular profiling concepts will undoubtedly play a major role in this process. While conventional technologies lack the fundamental features necessary for comprehensive molecular characterization of physiological and pathological processes at a single-cell level, imaging platforms based on fluorescent nanoparticles, quantum dots, present promising tools uniquely suited for addressing this challenge. Benefiting from favorable photo-physical properties and versatile bio-functionalization capabilities, design of compact, stable, and biocompatible coatings decorated with targeting agents have already converted QDots into potent probes for labeling of molecular targets in fixed cultured cells and FFPE tissue specimens. However, such technologies have neither contributed to major biomedical discoveries nor found wide adoption within clinical diagnostics, suffering from unreliable staining methodologies, poor multiplexing capacity, and sophisticated probe preparation.

QDot imaging platform described in this dissertation represents the only technology reported to date capable of achieving comprehensive single-cell molecular profiling in specimens with preserved morphology, while featuring simple probe preparation and robust multiplexed staining methodology. This platform overcomes the fundamental limitations faced by conventional as well as nanoparticle-based methods by employing a unique combination of (i) simultaneous labeling of multiple molecular targets with QDot fluorescent probes via either a 1-step or a 2-step procedure, (ii) cyclic staining methodology for interrogation of expanded target sets, and (iii) high-content analysis of molecular profiles via hyper-spectral imaging and subsequent data processing.

CHAPTER 2: GENERAL PRINCIPLES FOR ENGINEERING OF QDOT PROBES

Chapter 1 has introduced the concept of single-cell molecular profiling, challenges faced by implementation of this concept in practice, and unique features of quantum dots that enable development of highly powerful imaging technologies for multiplexed and quantitative analysis of molecular targets within individual cells. A number of initial proof-of-concept studies performed with conventional and QDot-based methods have also been discussed, setting stage for presentation of advanced QDot imaging platform for single-cell molecular profiling described in this dissertation. However, before delving into details of experimental procedures, it is worth taking a closer look at main components that make up bio-functional QDots and outline general principles that go into design and engineering of probes for molecular profiling applications (for in-depth discussion on this topic see ref. [62]).

Strictly speaking, QDots are semiconductor nanoparticles made of hundreds to thousands of atoms of group II and VI elements (*e.g.* CdSe and CdTe) or group III and V elements (*e.g.* InP and InAs). This inorganic core yields all the unique photo-physical properties, which can be controlled by the nanoparticle chemical composition, size, and structure, and serves as a rigid foundation for the development of QDot probes. However, bare nanoparticles usually cannot interact with biological systems and do not possess any biological functionality. Careful design of coating materials that can encapsulate the QDot core and shield it from the environment yields biocompatible probes with controllable physicochemical properties. Further decoration of the QDots with biomolecules imparts the bio-functionality and enables probe interaction with biological systems. Therefore, preparation of QDot-based probes and

nanodevices represents a multi-step process, which each step being guided by unique application-specific criteria (**Figure 2.1**).

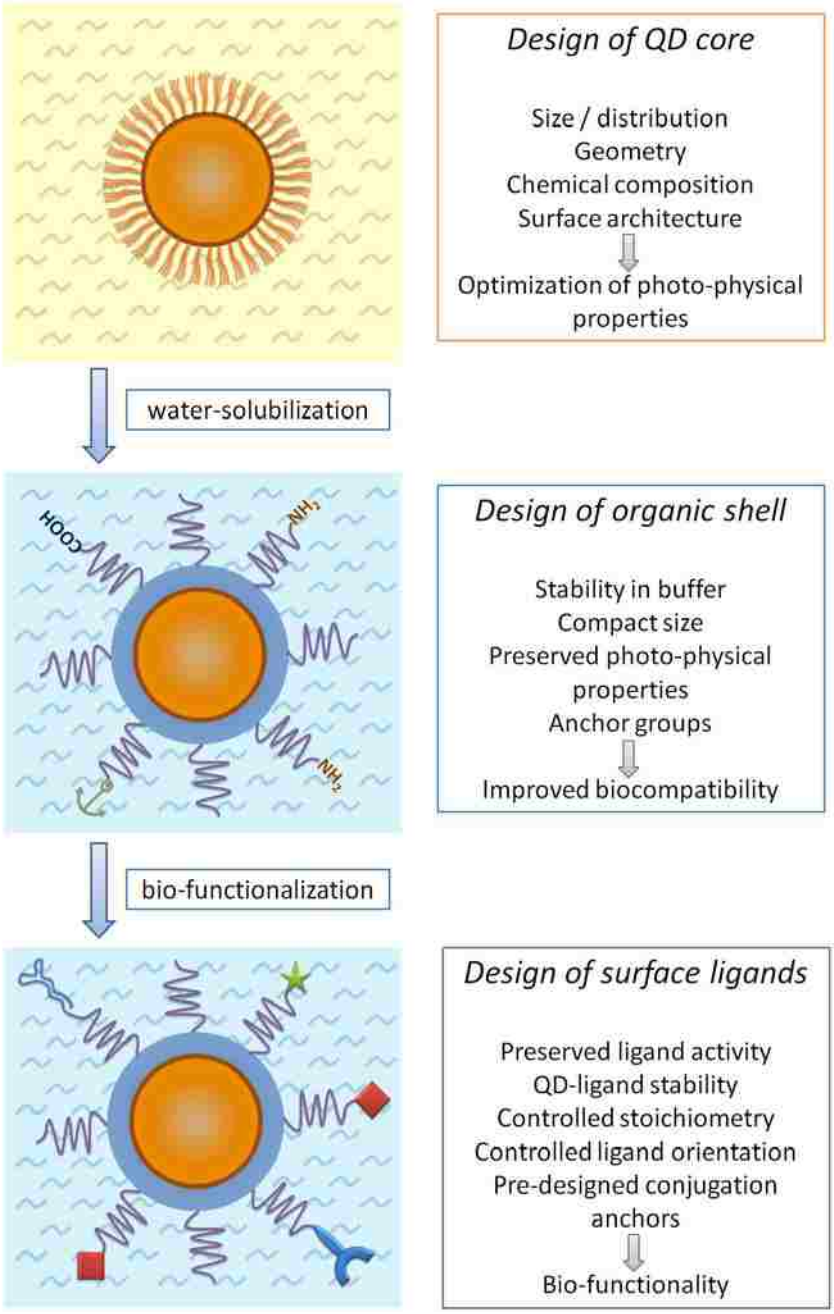

Figure 2.1 General steps and design criteria in engineering of QDot probes for molecular profiling applications. Each step is guided by individual design principles aiming at controlling optical, physical, and chemical properties of the final probe.

2.1 Design of the QDot nanocrystal core

The QDot core defines optical properties of the probe and represents a structural scaffold for engineering of nanodevices. Therefore, utilization of compact and stable QDot cores with precisely controlled nanoparticle size distribution, geometry, chemical composition, and surface chemistry is essential for engineering of high-quality QDot probes. Initial reports on preparation of semiconductor nanoparticles utilized synthesis in aqueous solutions and yielded QDots with poor fluorescence efficiencies and large size variation. Advancements in synthetic procedures and surface chemistry have enabled production of water-soluble QDots with higher quantum yield (QY, up to 40-50%) and relatively narrow size distribution (exhibiting spectral emission width at half maximum, FWHM, of about 50 nm for CdTe/CdSe particles [103] and down to 19 nm for ZnSe QDots [104]). However, aqueous synthesis still suffers from poor control over the QDot photo-physical and chemical properties.

A major leap towards synthesis of highly uniform colloidal CdSe QDots was made in 1993 by Bawendi and coworkers by developing a high-temperature organometallic procedure [105], which is now widely used for synthesis of QDots for a variety of applications. In this procedure, pyrolysis of organometallic precursors at high temperature yields nucleation and growth of nanocrystals, while coordination of trioctyl phosphine/trioctyl phosphine oxide (TOP/TOPO) base with unsaturated metal atoms on the QDot surface prevents the formation of bulk semiconductor. Yet, utilization of a highly toxic and unstable Cd precursor (dimethyl cadmium) imposes restrictions on the equipment and reaction conditions and limits flexibility in the QDot core design. A leap towards large-scale preparation of high-quality QDots has been done by Peng *et al* using alternative inexpensive precursor materials (such as CdO) [106, 107]. Relatively mild and simple reaction conditions along with slower nucleation and growth

rates offer extensive flexibility in engineering of QDot chemical composition, geometry, and photo-physical properties.

Precise kinetic control over a nanoparticle growth achieved with organometallic procedure enables preparation of QDot populations with narrow size distribution. With optimization of reaction conditions and utilization of size focusing via re-injection of precursors, an emission spectral width below 20 nm has been achieved [108-110]. Further bandgap engineering by varying the chemical composition of nanocrystals has produced QDots emitting light from the ultraviolet, throughout the visible, and into the infrared spectra (400-4,000 nm) [64, 110-116].

As discussed in Chapter 1, precise control over QDot core size, monodispersity, and chemical composition is instrumental in fine-tuning the QDot optical properties, in particular fluorescence emission profile, which are essential for highly multiplexed labeling applications. Interestingly, in addition to fluorescence-based methods, high electron density of QDots and direct correlation between the particle size/composition and emission wavelength facilitate detailed evaluation of relatively low-resolution fluorescence images with such high-resolution imaging modalities as transmission electron microscopy (TEM) [117] and electron spectroscopic imaging (ESI) [118] for multiplexed imaging based on particle size and chemical composition respectively.

While providing good control over the particle size, original organometallic procedure produces QDots with low quantum yield, compromising the utility of such particles as fluorescent probes. Moreover, TOPO-coated QDots are unstable with respect to photooxidation, resulting in effective degradation of nanocrystals [119]. Both issues arise from the relatively large number of atoms exposed on the surface of nanoparticles. In the nanoscale regime, surface atoms play a major role in determining the catalytic, electronic,

and optical properties. As the radius of a spherical particle decreases, the ratio of its surface area to volume rapidly increases placing larger number of atoms on the surface [120]. Surface atoms lack neighbors with which to form chemical bonds and thus possess unoccupied electron orbitals. Commonly referred to as dangling bonds or surface trap sites, these orbitals can trap charge carriers and either prevent or delay electron-hole recombination and subsequent photon emission, thus reducing the fluorescence quantum yield [121, 122]. Furthermore, such sites might exhibit enhanced chemical reactivity and compromise chemical stability of the nanoparticles. In order to prevent some of these undesirable characteristics, dangling bonds can be saturated by organic and inorganic capping layers.

Several groups have developed high-bandgap-energy inorganic shells (*e.g.* CdS and ZnS) several layers thick that effectively shield the photoactive core of QDots [123-125]. Wider band gap of the shell efficiently confines the exciton to the core, reducing nonradiative relaxation pathways and increasing the quantum yield [67]. At the same time, careful choice of core and shell materials as well as optimization of the shell thickness are necessary to minimize the lattice strain between the core and shell and maximize the QDot photo-physical properties. Although thin shells (1-2 monolayers) often produce the highest fluorescence yields, thicker shells (4-6 monolayers) provide more core protection from photooxidation and degradation [66]. For example, Peng *et al* have observed confinement of the hole created during excitation within the CdSe core by a higher-bandgap CdS shell [125]. As a result of such confinement, hole-dependent photo-oxidative processes that cause QDot degradation and lead to the loss of fluorescence are impeded.

A thicker shell might also significantly reduce QDot blinking (intermittence in light emission) associated with charge trapping and un-trapping at surface defects of a nanocrystals or due to charge ejection from the QDot (Auger ionization) followed by

recombination process [82, 126-128]. Since blinking might cause signal fluctuations in ultrasensitive detection and spectral jumping (change in the emission peak position), its elimination is often desirable.

Alternative approaches aim at achieving better fluorescence efficiency by optimizing the surface structure of nanocrystals and minimizing the number of surface trap sites. Some success in this direction has been observed with adjusting the precursor mixture composition and improving surface coating with multiple organic ligands (*e.g.* use of alkylamine surfactants, such as (hexa/octa/do)decylamine, along with TOPO) [113, 129-131]. In one example, Talapin *et al* have stabilized CdSe QDots with alkylamines, achieving quantum yield of 40-50% at room temperature (*vs.* 10-25% QY of as-prepared QDots) [131]. Qu and Peng have systematically studied the formation of photoluminescence bright point (presumably resulting from an optimal nanocrystal surface structure) during the QDot synthesis, obtaining red-emitting CdSe nanoparticles with quantum yield as high as 85% at room temperature without using inorganic cappling layer [113]. However, further optimization of reaction conditions for preparation of multicolor QDots is required, and evaluation of single-core QDot photo-physical properties and stability in aqueous environment is necessary in order to assess applicability of such nanoparticles for biological applications.

Advances in synthesis and surface passivation technologies made QDots appealing platforms for engineering of biological probes with the advantages of enhanced photostability, improved brightness, tunable fluorescence, and single-source multicolor excitation. Subsequent steps of probe development process focus on controlling the QDot surface properties and functionalization with biological ligands, transforming this inorganic nanoparticle platform into biologically compatible and bio-functional nanodevices.

2.2 Transition towards biologically compatible nanoparticles

Organic phase synthesis produces high quality hydrophobic QDots soluble only in nonpolar organic solvents, such as chloroform and hexane. However, in order to be useful for biological applications QDots must be made water-soluble. In general, water-solubilization procedure should yield nanocrystals soluble and stable in biological buffers, preserve the original photo-physical properties, retain relatively small particle size, and provide reactive groups for subsequent conjugation to biomolecules. Several different approaches have been developed to produce water-soluble QDots satisfying these criteria.

One approach involves replacing hydrophobic surface groups with hydrophilic ones by means of ligand exchange. This is usually accomplished by substitution of the native TOPO coating with bifunctional ligands, which present both a surface-anchoring group (*e.g.* thiol) and a hydrophilic end group (*e.g.* carboxyl or hydroxyl). Examples include utilization of negatively-charged carboxy-terminated thiols, such as mercaptoacetic (MAA) [132] and mercaptopropionic (MPA) acids (**Figure 2.2A**), and thiol-containing zwitterionic molecules, such as cysteine [133, 134], for decoration of QDot surface with hydrophilic moieties. In addition to producing ultrasmall (hydrodynamic diameter, HD, below 6 nm) and highly water-soluble nanoparticles, amine and carboxylic acid groups provide binding sites for cross-linking to proteins, peptides, and nucleic acids. Despite the simplicity of the procedure, ligand exchange with monodentate surface ligands often compromises the fluorescence efficiency, photochemical stability, and shelf life of the probes, as ligands tend to detach from the QDot surface leaving behind surface trap sites and causing nanoparticle aggregation [135, 136].

In general, crosslinking of small ligands or substitution from mono-thiol to di-thiol ligands substantially improves long-term stability. For example, Liu *et al* have utilized di-thiol ligand dihydrolipoic acid (DHLA) conjugated to poly(ethylene glycol) (PEG) to prepare small (HD of

11.4 nm) and stable QDots with some loss of fluorescence efficiency (drop in quantum yield from 65% to 43%) (**Figure 2.2B**) [137]. In an alternative approach, Sukhanova *et al* have water-solubilized QDots with DL-Cysteine and further stabilized the particles with poly(allylamine), achieving improvement in QDot colloidal stability and increase in quantum yield (from 40% to 65%) (**Figure 2.2C**) [138]. Jiang *et al* have improved the stability of mercaptoundecanoic acid shell by covalently cross-linking neighboring molecules with lysine [139]. However, the dramatic increase in nanoparticle size (from 8.7 to 20.3 nm HD) induced by shell cross-linking is undesirable, and further optimization of this procedure is required. Recently, Smith and Nie have developed a new class of multidentate polymer coatings that are only 1.5-2 nm thick (**Figure 2.2D**) [140]. Consisting of a poly(acrylic acid) backbone grafted with multiple anchors (thiol and amine groups), this coating renders CdTe QDots biocompatible and colloidally stable, while keeping the final HD between 5.6 and 9.7 nm.

A more robust ligand-exchange approach involves formation of polymerized silanol shell on the QDot surface (**Figure 2.2E**) [65, 141]. In this procedure 3-(mercaptopropyl)trimethoxysilane (MPS) is also directly absorbed onto the nanocrystals displacing the native TOPO molecules. However, upon addition of base, silanol groups are hydrolyzed and linked with each other producing stable and compact (1-5 nm thick) silica/siloxane shell and rendering particles soluble in intermediate polar solvents (*e.g.* methanol or dimethyl sulfoxide). Further reaction with bifunctional methoxy compounds renders QDots soluble in aqueous buffers. Polymerized siloxane-coated nanoparticles are highly stable against flocculation. However, residual silanol groups on the QDot surface often lead to precipitation and gel formation at neutral pH [67].

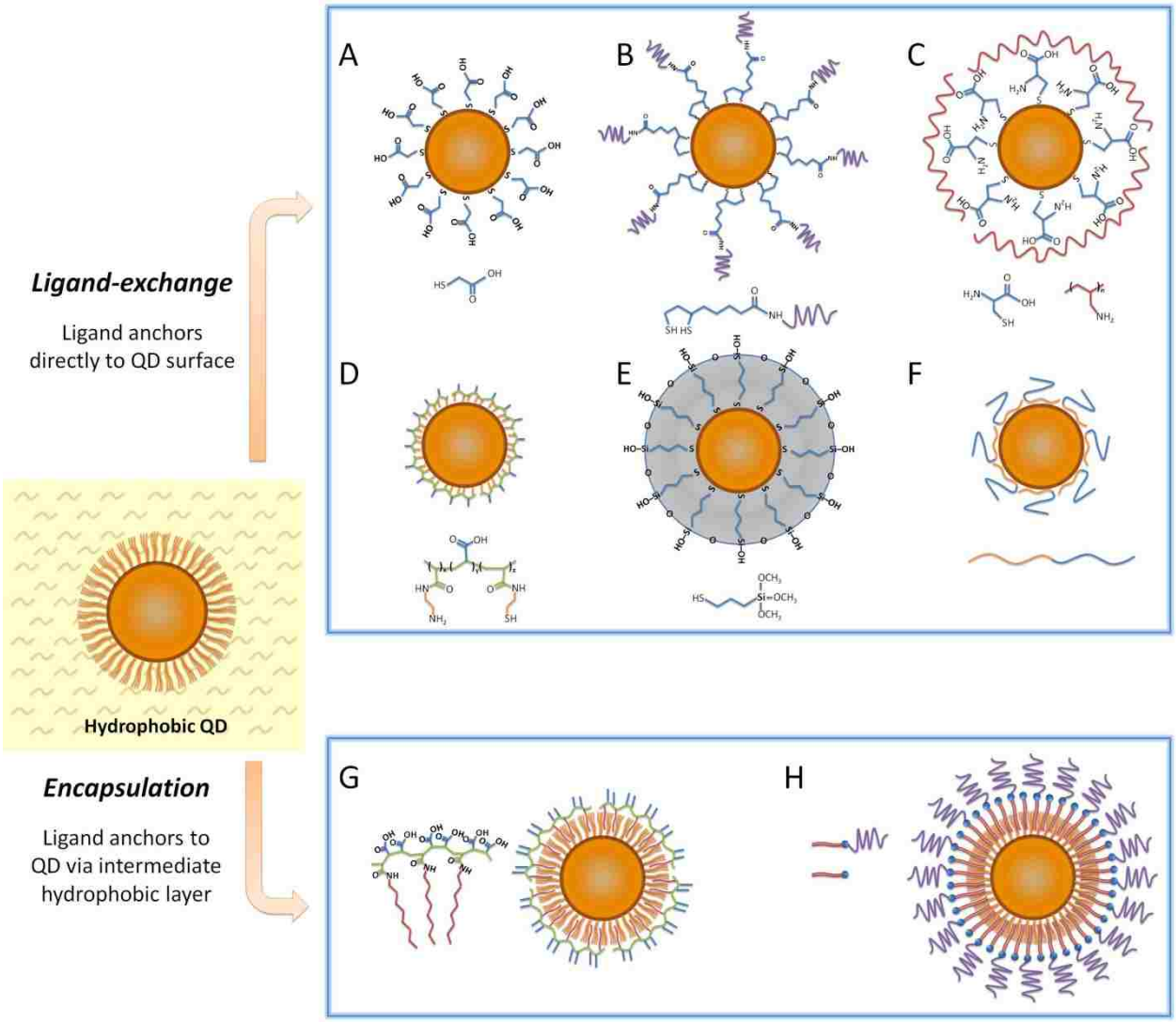

Figure 2.2 **Routes for water-solubilization of hydrophobic QDots.** Ligand-exchange procedures (A-F) involve replacing the native hydrophobic surface ligands (*e.g.* TOPO) with hydrophilic ones by direct anchoring of ligands to the QDot surface. (G-H) Encapsulation procedures preserve the native QDot surface structure and over-coat QDots with amphiphilic molecules (such as polymers or lipids) via hydrophobic interactions.

Employing native stability and biocompatibility of biomolecules, Weiss and colleagues have demonstrated preparation of compact water-soluble QDots via ligand exchange with engineered peptides (**Figure 2.2F**) [142]. With the use of phage-display libraries [143] and accelerated evolution this procedure enables selection of peptide sequences that can specifically bind to any type of QDots, thus providing a universal surface coating approach. Yet, due to relatively high complexity and inaccessibility of this technique along with lack of characterization data on peptide-coated QDots, such an approach is not widely used.

An alternative approach to QDot water-solubilization is to retain the native TOPO coating and encapsulate the hydrophobic QDots with amphiphilic molecules such as polymers (**Figure 2.2G**) [101, 144] or phospholipids (**Figure 2.2H**) [145]. The hydrophobic portion of this molecule intercalates within alkyl-chain-terminated surface ligands while the hydrophilic portion (*e.g.* charged groups, PEG, *etc.*) faces outwards, interacting with the aqueous solvent and rendering the particle water-soluble. This method produces exceptionally stable water-soluble QDots with preserved optical properties, as the coating does not directly interact with the nanocrystal surface and does not disturb the surface passivation layer [78]. However, deposition of several organic layers usually results in dramatic increase of the nanoparticle hydrodynamic size. For example, block copolymer coating increases the diameter of CdSe/ZnS QDots from ~4-8 nm before encapsulation to up to 30 nm HD [66, 146]. Since size increase might be detrimental for quantitative detection of molecular targets in a crowded biological environment and hamper intracellular penetration of the QD probes, development of encapsulation procedures yielding thinner organic shells is necessary for preparation of compact QDot probes for molecular profiling applications [82, 147, 148].

As new QDot-based applications are being explored, more stringent requirements for QDot surface coating arise. In general, the size of QDots should stay small after coating, the

surface should be biocompatible, reactive groups should be available for conjugation of biomolecules and targeting ligands, and QDot probes should show minimal non-specific interactions with the biological environment. With a variety of water-solubilization procedures developed, a number of QDot-based biological applications have already become available. However, there is no method that satisfies all the design criteria imposed by increasing demands of biomedical research. Ligand-exchange approaches often yield compact probes at an expense of reduced stability and fluorescence efficiency, whereas polymer-encapsulation produces exceptionally stable and bright particles at an expense of increased size. Therefore, engineering of novel coatings that combine the protective features of encapsulation procedures with the compactness of small ligands represents an active area of research.

2.3 Development of bio-functional QDot probes

The final step in QDot probe engineering comprises addition of bio-functionality to otherwise inert water-soluble nanoparticles. This is usually achieved by decorating QDots with proteins, peptides, nucleic acids, or other biomolecules that mediate specific interactions with biological systems. Design of such nanoparticle-biomolecule hybrids should preserve and integrate useful properties of both materials involved, *i.e.* optical properties of the nanocrystals and biological functions of ligands attached.

Several approaches can be used for conjugation of QDots and biological molecules. One of the most simple and popular bioconjugation methods is covalent bond formation between reactive functional groups (*e.g.* primary amines, carboxylic acids, alcohols, and thiols). For example, linking of proteins via primary amine groups to carboxylic acid-containing QDots can be achieved via carbodiimide-mediated amide formation (*i.e.* EDC, 1-ethyl-3-(3-

dimethylaminopropyl) carbodiimide, condensation reaction) (**Figure 2.3A**). As this reaction utilizes naturally occurring amine groups it does not require additional chemical modification of proteins, preserving their natural structure; but it lacks control over the molecular orientation of the attached proteins, thus allowing attachment at a point close to ligand's active site that might result in partial or complete loss of biological functionality of that ligand. Moreover, EDC reaction might result in QDot aggregation due to crosslinking between multiple reactive sites on QDots and proteins. Another common covalent bonding procedure involves active ester maleimide-mediated amine and sulfhydryl coupling (**Figure 2.3B**). Since free sulfhydryl groups are rare in native biomolecules, additional treatment of the ligands is often required (*e.g.* reduction of antibodies with dithiothreitol). This reaction yields stable QDot-ligand complexes with often controlled ligand orientation. However, chemical treatment might compromise the biological activity of ligands and cause reduced sensitivity and/or specificity of the probe. Nonetheless, both approaches are widely used for variety of applications, including custom production of QDot-antibody probes and preparation of QDot-streptavidin conjugates. Recently, Barat *et al* have utilized amine-sulfhydryl coupling for preparation of compact diabody-QDot probes [149]. Using small cysteine-terminated antibody variable chain domains instead of complete antibodies along with site-specific conjugation of a cysteine tag, decoration of QDots with fully functional antigen-recognition ligands has been achieved. Despite the complexity of the approach, bio-functionalization of QDots with small genetically engineered molecules carrying site-specific conjugation anchors represents a promising route for preparation of compact and highly specific QDot probes.

Besides covalent bonding to organic shell, biomolecules can be linked directly to nanocrystal surface via coordination with metal atoms of the QDot core. To achieve this, QDots coated with labile small ligands are mixed with thiolated biomolecules or biomolecules containing polyhistidine (HIS) residues (**Figure 2.3C**). As a result, small ligands are replaced on

the QDot surface by biomolecules. Yet, utilization of QDots with unstable displaceable surface coatings (such as mercapto compounds) and direct interaction with the nanocrystal surface might significantly reduce the brightness and stability of such bioconjugates in aqueous solutions. In a more robust variation of this approach, Medintz *et al* have functionalized stable DHLA-coated QDots with HIS-tagged maltose-binding protein (MBP) via coordination of oligohistidine with the QDot surface at defects in DHLA surface coating. Such binding event is accompanied by improved surface passivation and rise in quantum yield (from 16% to 39%), thus enabling direct measurement of the binding stoichiometry. Later, this approach was successfully applied for conjugation of other HIS-tagged engineered ligands, such as enzyme sensing [150] and cell penetrating [151] peptides. Bio-functionalization via coordination with QDot surface is attractive due to the simplicity of the reaction, control over the final bioconjugate assembly, and ability of using unmodified ligands with preserved native structure. However, custom design of ligands incorporating thiol groups or HIS-tags is often complex and suitable only for small biomolecules with relatively simple structures.

Non-covalent self-assembly of engineered proteins on the surface of QDots with preserved organic shell prevents direct access to inorganic nanocrystal core and exhibits minimal effect on the photo-physical properties (**Figure 2.3D**). In one example a fusion protein has been utilized as an adaptor for immunoglobulin G (IgG) coupling [152, 153]. Electrostatic interaction between the positively charged leucine zipper domain of an adaptor protein and the negatively charged QDot shell stably deposits the adaptor protein to the QDot surface, while the protein G domain specifically captures the antibody Fc region. The resulting assembly features precise control over the antibody orientation and eliminates any chemical modification of IgG, thus preserving its activity. However, this procedure is often limited to conjugation of specific classes of ligands (*e.g.* antibodies). Moreover, the size of such bioconjugates is large due to a number of thick biomolecule layers deposited onto the QDot.

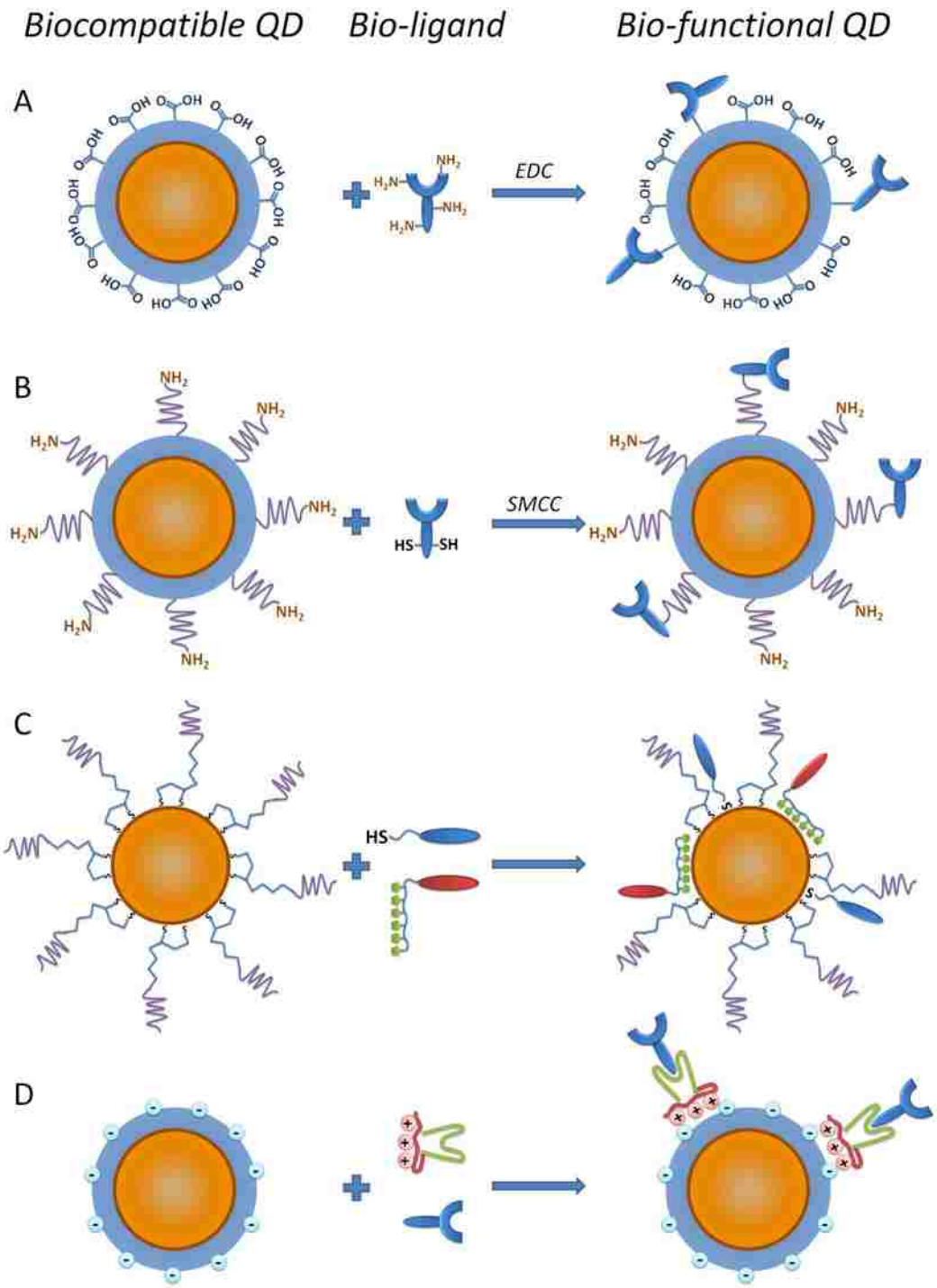

Figure 2.3 Routes for QDot bio-functionalization. Decoration of QDot surface with bio-ligands can be achieved via covalent conjugation (A, B), non-covalent coordination of thiol groups or polyhistidine tags with the QDot surface metal atoms (C), or electrostatic deposition of charged molecules on the QDot organic shell (D).

Recent achievements in merging nanoparticle encapsulation and bioconjugation steps and design of pre-functionalized surface coatings promise to provide more compact, stable, and biocompatible nanoparticles with controlled density and orientation of ligands attached. Amphiphilic polymers with a maleic anhydride backbone are being actively explored for this purpose. In organic anhydrous solvents, such polymers encapsulate TOPO-coated QDots and introduce reactive anhydride groups on the surface. In basic aqueous buffers anhydride rings are quickly hydrolyzed, yielding negatively charged carboxylic acid groups and rendering QDots water soluble [144]. More importantly, anhydride groups are highly reactive towards amine-containing molecules, thus allowing covalent conjugation of a variety of biomolecules to the polymer chains without the need for post-encapsulation modification [154, 155].

Choice of the bio-conjugation approach depends on availability of ligands with suitable functional groups and on specific application requirements. However, common design criteria involve preserved QDot photo-physical properties and ligand bio-functionality, controlled ligand orientation and binding stoichiometry, compact probe size, and good stability in physiological environment. As these criteria can be satisfied in only few specific cases, improvement of existing bioconjugation techniques and design of novel application-specific water-solubilization and bioconjugation approaches remains an active area of research [156].

2.4 QDot probe design criteria for molecular profiling applications

In the last decade, surface engineering and bio-functionalization techniques have transformed semiconductor nanocrystals into complex cellular probes capable of interaction with biomolecules and direct participation in biological processes. In 1998, two seminal *Science* papers first demonstrated that semiconductor nanoparticles could be made water-soluble and used as biological imaging probes [65, 132]. One approach utilized silica shell

encapsulation chemistry in order to produce QDots for a single-excitation dual-color cell staining [65]. When derivatized with trimethoxysilylpropyl urea and acetate groups, green QDots preferentially labeled the cell nucleus, and when derivatized with biotin, red QDots labeled F-actin filaments pre-treated with phalloidin-biotin and streptavidin. The second paper was the first to demonstrate the ligand-exchange approach to QDot water-solubilization [132]. Subsequent conjugation of transferrin produced QDot probes that were endocytosed by live HeLa cells resulting in punctate cell staining, while IgG bioconjugates were used in an aggregation-based immunoassay. Since then, a number of surface engineering techniques for QDot solubilization and bio-functionalization have been developed towards preparation of better imaging probes for molecular profiling applications. In this respect, particular attention needs to be paid to careful design of the probe size, surface properties, and specific ligand bio-functionality.

The hydrodynamic size of the QDot-ligand bioconjugate should be minimized in order to achieve good penetration of the probes within the cross-linked intracellular compartments of fixed specimens (*e.g.* formalin-fixed cultured cells or formalin-fixed paraffin-embedded, FFPE, tissue sections). Membrane-bound compartments, such as nucleus and mitochondria, represent especially difficult targets for QDot staining. For example, Wu *et al* have investigated the utility of QDot-streptavidin and QDot-antibody bioconjugates for simultaneous labeling of membrane-associated Her2 receptor and of a nuclear antigen in breast cancer cells [101]. While staining of cell surface antigens is reliable and effective, staining of cytoplasmic and nuclear markers is more variable, resulting from the relatively large size of the probes. In another example, Tholouli *et al* have employed the biotin-streptavidin linkage for preparation of QDot-oligonucleotide probes for FISH-based studies of mRNA [157]. Biotinylated DNA probes pre-incubated with QDot-Streptavidin conjugates enable detection of 3 mRNA targets in a 1-step FISH procedure. Yet, pre-conjugation of multiple

oligonucleotides to QDots significantly increases the overall size of the probe, thus requiring specimen permeabilization with proteinase K, which necessarily degrades cell and tissue architecture and destroys most of the protein-based targets useful for IHC and IF studies. Chan *et al* have resolved this issue by developing a more controlled procedure for pre-conjugation of exactly one oligonucleotide probe per QDot via biotin-streptavidin linkage [92]. Starting with QDot-Streptavidin conjugates, excess streptavidin sites are blocked with biocytin (water soluble biotin derivative), and only a few biotinylated oligonucleotides are allowed to bind. Further purification of QDot-oligo conjugates with agarose gel electrophoresis yields relatively small mono-oligonucleotide FISH probes suitable for multiplexed mRNA detection under mild specimen permeabilization. As a result, a combined QDot-based FISH-IF procedure has been developed to compare cellular distribution patterns of vesicular monoamine transporter (Vmat2) mRNA and immunoreactivity of tyrosine hydroxylase in dopaminergic neurons [92]. In general, with larger QDot probes, stronger permeabilization of specimens with detergents and/or enzymes might be required to obtain sufficient intracellular access; however, chemical treatment might damage the target molecules, thus reducing staining sensitivity and providing inaccurate quantitative information about expression levels of molecular targets. Furthermore, entrapment of larger QDot probes within specimens hampers post-staining washing of unbound probes and reduces the specificity of staining. Therefore, engineering of more compact probes is highly desirable.

QDot surface engineering is critical for minimizing the non-specific binding of QDot probes to biomolecules, a common reason of reduced staining signal-to-noise ratio and decreased sensitivity and specificity of the target detection. Majority of the non-specific binding results from the electrostatic interactions, when highly charged QDot probes are used, and from hydrophobic interactions, when QDots with exposed hydrophobic regions or partially hydrophobic ligands are used. Decoration of QDots with uncharged hydrophilic moieties (*e.g.*

PEG) and zwitterionic molecules produces highly water-soluble and stable probes while efficiently eliminating non-specific interactions. For example, QDot probes used in the majority of published research have a layer of PEG that shields the nanoparticle core from the environment and provides anchor points for ligand attachment. Popularity of QDot-PEG comes from the outstanding non-fouling properties of PEG as well as high stability of probes in a wide range of experimental conditions, which facilitates engineering of QDot probes for virtually any application. However, addition of a PEG layer often results in increased particle HD leading to the detrimental size-dependent consequences described above. Zwitterionic coatings, on the other hand, become utilized more often as smaller probes are being developed. Featuring a densely packed alternating positively and negatively charged groups, these coatings do not favor electrostatic or hydrophobic interactions, while providing an overall neutral well-hydrated surface. However, zwitterionic coatings tend to show high pH-sensitivity, thus imposing more stringent requirements on bioconjugation and staining conditions. Alternatively, the QDot surface can be completely over-coated with large biomolecules (*e.g.* proteins) shielding the QDot from the environment and mimicking the native functionality of the ligand; yet, possible dramatic increase in probe size renders this approach mainly suitable for labeling of extracellular targets.

2.5 Summary

As argued in Chapter 1, future advancements in the area of personalized medicine rely on highly multiplexed quantitative single-cell molecular profiling. Engineering of more compact and sensitive QDot probes with outstanding stability and non-fouling properties, therefore, presents the major focus of research in this area. Decreasing the band gap by tuning the QDot chemical composition, for example, might enable shifting QDot emission into deep blue [158] or far red [116] region, thus expanding the pool of available QDot colors while keeping the

particle size constant within 4-6 nm range. However, further reduction of the QDot inorganic core size below 3-4 nm might be highly challenging. Meanwhile, significant probe size reduction can be achieved via engineering of the compact organic coating layers and ligands that offer great design flexibility. Substitution of thick shells with thinner zwitterionic coatings, development of mono-valent probes, and utilization of smaller targeting ligands (*e.g.* peptides and aptamers) might prove instrumental in this regard. Finally, development of versatile and simple QDot bio-functionalization procedures is essential for translation of this powerful technology to biomedical research and clinical diagnostics. Subsequent chapters of this dissertation discuss potential solutions to some of the design criteria imposed by molecular profiling applications.

CHAPTER 3: QDOT-OPTIMIZED IMMUNOFLUORESCENCE PROTOCOL

While labeling of cell surface targets is easily achievable on intact cells with variety of QDot-antibody probes, permeabilization of fixed cells with detergents is necessary for obtaining access to intracellular molecular targets. At the same time, removal of natural lipid barriers eliminates the negative charge on the cell surface and opens access to a variety of electrostatic and hydrophobic interactions. As a result, many QDot probes, commonly featuring negatively-charged surface and stabilized via electrostatic repulsion, become inapplicable for staining of fully processed specimens. To overcome this limitation, QDot surface is often decorated with highly hydrophilic and non-fouling poly (ethylene glycol) (PEG) layer, which shields charged and hydrophobic regions on the QDot surface. Despite increasing the nanoparticle size and impeding bio-conjugation efficiency, PEG modification remains the most robust and popular approach for producing stable QDots for variety of biological assays. In particular, majority of commercially available QDot probes (*e.g.* QDots from Invitrogen, now part of Life Technologies Corporation) utilize PEG coating for particle stabilization. Therefore, we have optimized IF protocol for existing PEG-coated QDot probes (such as QDots functionalized with secondary antibodies and streptavidin) and primarily used amine-functionalized PEG-coated QDot scaffolds for engineering of new QDot probes for single-cell molecular profiling applications.

3.1 Processing of cultured cells

Proper pre-staining processing, including cell fixation, permeabilization, and blocking, is critical for accurate labeling of molecular targets with QDot probes. In particular, pre-staining processing should preserve specimen morphology and target antigenicity, while providing sufficient access to intracellular compartments and precluding non-specific interactions between QDot probes and cell components. In this regard, access to intra-nuclear targets is particularly hard to achieve due to relatively large size of QDots and antibodies. Therefore, we have screened several common cell fixation/permeabilization procedures to establish a suitable specimen processing protocol compatible with QDot probes.

All studies presented in this dissertation have been done on prostate cancer cell line, LNCaP, and cervical cancer cell line, HeLa, both representing adherent cell cultures growing primarily in a monolayer and representing suitable models for development and evaluation of the QDot molecular profiling platform. Strong attachment of these cells to a variety of surfaces, including untreated glass, has enabled performing cell culture on glass coverslides, glass-bottom 24-well plates (Greiner Bio-One), and glass-bottom flow-chambers (ibidi), all of which feature lack of autofluorescence, commonly observed with plastic plates, upon illumination with UV light. In addition, small thickness of glass coverslides facilitates sensitive high-magnification fluorescence imaging with oil-immersion objectives. In general, cells were grown on glass for 2-3 days to a density of about 70% for LNCaP and 80-90% for HeLa. Humidified atmosphere at 37^0C with 5% CO_2 was maintained. LNCaP cell were cultured in RPMI-1640 culture medium with L-Glutamine and 25mM HEPES (Lonza) supplemented with 10% Fetal Bovine Serum (PAA Laboratories) and antibiotics (60 µg/mL streptomycin and 60 U/mL penicillin). HeLa cells were cultured in MEM culture medium with L-Glutamine (Invitrogen) supplemented with 10% Fetal Bovine Serum and antibiotics (60 µg/mL streptomycin and 60

U/mL penicillin). It should be noted here, that, unlike HeLa, LNCaP cells develop strong attachments between each other. As a result, during trypsinization and subsequent seeding these cells tend to form clumps of cells that grow into three-dimensional clusters, hampering reliable cell staining and imaging. Therefore, rigorous pipetting or vortexing should be employed during trypsinization step to break apart cell clumps and ensure growth of cells in a single layer. Being sturdy, fast-growing, and well-characterized, properly grown LNCaP and HeLa cultures have proven instrumental in developing QDot-optimized cell processing and immunofluorescence protocols.

Considering relatively large QDot size (comparable to antibodies and other large proteins), achieving proper intracellular penetration and labeling of tightly packed molecular targets with QDot probes presents a challenge. We have evaluated several common pre-staining cell processing procedures and established that only fixation with 10% formalin (4% formaldehyde prepared from methanol-free 16% stock, Thermo Scientific) in TBS (Tris buffered saline) for at least 20-30 minutes followed by permeabilization with 2% DTAC (Dodecyltrimethylammonium chloride, Sigma-Aldrich) for another 20 minutes ensures reliable staining of intra-nuclear targets even with larger red-emitting QDots (**Figure 3.1, top**). Additional brief treatment with non-ionic surfactants (such as 0.25% TritonX-100 and 0.5% Tween-20, Thermo Scientific) helps in reducing non-specific QDot binding. It should be noted, in contrast, that common pre-staining cell processing procedures, such as fixation with 4% formaldehyde in PBS followed by permeabilization with 0.1% TritonX-100, yield reduced and inconsistent intra-nuclear staining (**Figure 3.1, bottom).**

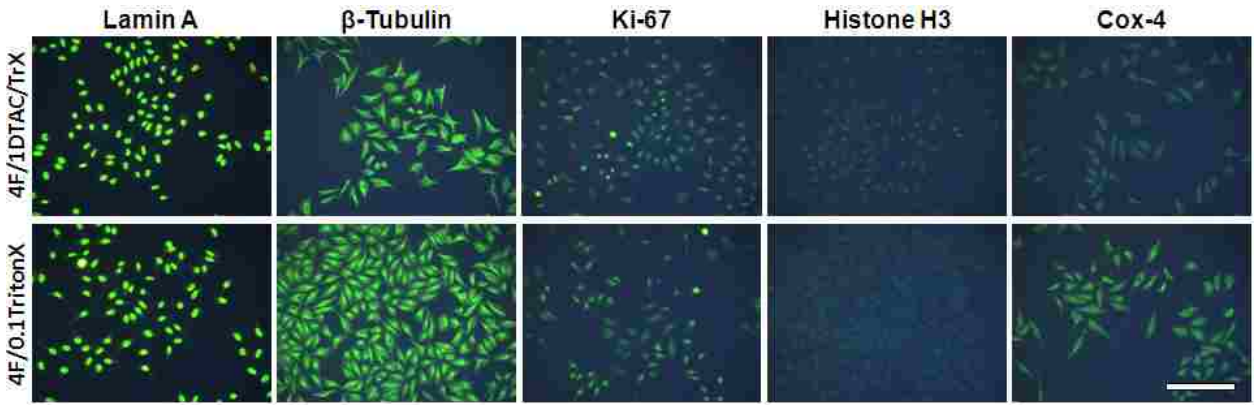

Figure 3.1 Effect of pre-staining cell processing on QDot labeling of intracellular targets. Optimized cell processing procedure (top) yields reliable staining of intra-nuclear (*e.g.* Ki-67, Histone H3) as well as cytoplasmic (*e.g.* ß-Tubulin) targets in LNCaP cells. At the same time, conventional fixation in PBS with TritonX-100 permeabilization (bottom) often hampers intra-nuclear access for QDot probes. Scale bar, 250μm.

One approach to overcoming limited probe penetration in this case is to treat cells with Proteinase K. However, along with improving intra-nuclear access, protein digestion results in degradation of cell-surface and cytoplasmic targets (**Figure 3.2**). Alternative methods of cell fixation with ice-cold methanol or acetone, in our experience, deteriorate cell morphology and lead to enhanced non-specific binding by QDot probes. Instead, 20-minute fixation with 4% Formaldehyde in PBS/0.05% TritonX-100 followed by 10-minute permeabilization with 0.5% TritonX-100 can be successfully employed for proper cell processing, should optimized procedure described above prove incompatible with certain targets. Note, however, that such specimens are highly susceptible to degradation with ionic surfactants (*e.g.* DTAC and SDS) and acidic buffers.

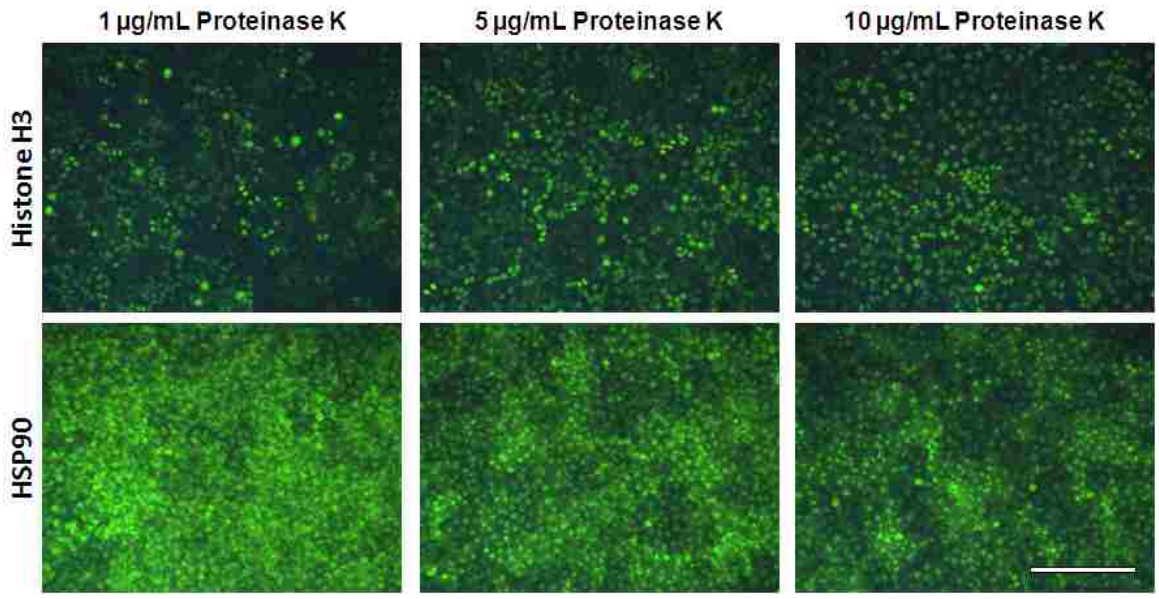

Figure 3.2 Achieving QDot probe intra-nuclear access with Proteinase K digestion. Greater degree of specimen digestion with Proteinase K (as indicated by the increasing amount of enzyme used) leads to substantially improved staining of nuclear Histone H3 with green QDot565 probes (top). However, enzyme digestion also leads to undesirable damage to cytoplasmic targets (such as HSP90, bottom). Therefore, such procedure might be incompatible with multiplexed staining studies when a mix of cell-surface, cytoplasmic, and nuclear targets are labeled. Scale bar, 500µm.

3.2 General considerations for specimen blocking and staining conditions

While producing minimal to no non-specific specimen staining upon proper blocking with bovine serum albumin (BSA), commercial PEG-coated QDots exhibit disparity in quality (and thus in levels of non-specific staining) between different lots, presumably due to variations in QDot surface coverage with PEG. To compensate for this effect, in addition to commonly used BSA we have routinely included 0.1% casein in a blocking step considering that, being more negatively charged and hydrophobic than BSA, casein might serve as a more stable blocking reagent for QDots (which also carry a net negative charge despite the PEG coating). In fact,

this modification of blocking step has helped to considerably reduce non-specific staining, especially nuclear staining, for variety of PEG-coated QDot probes. However, since use of higher casein content during blocking step or incorporation of casein in staining buffer often results in decreased staining intensity, it is advisable to keep utilization of this blocking reagent to a minimum.

Overall, we have determined the composition of blocking buffer consisting of 2% BSA (from Bovine Serum Albumin powder, Sigma-Aldrich), 0.1% casein (from 5% solution, Novagen), and 1x TBS to be optimal for most QDot staining applications. Optimized QDot staining buffer composition is 6% BSA in 1x TBS. Blocking is always performed for 30-60 minutes immediately prior to staining followed by a rinse with 1x TBS. Staining can be performed in either 1-step or 2-step format, each step taking 1.5-2 hours at room temperature. While shorter incubation also produces clearly detectable staining, at least 2 hours are usually required for complete labeling of all targets due to slightly slower diffusion of QDot probes. Longer incubation, in turn, might lead to increased non-specific binding, while producing no improvement in target staining intensity. All staining steps are performed directly inside the wells of glass-bottom 24-well plate (commonly requiring 300µL 1µg/mL primary antibodies and 4-10nM QDot probes), inside ibidi flow-chambers (50µL of reagents at same concentrations), or on glass slides with tissue sections in a humid chamber (100-200µL of reagents at same concentrations). Extra fluorescent labels are efficiently removed by rinsing specimens with 1%BSA/0.1%casein/TBS twice and washing with TBS 3 times. Fluorescence imaging should be done immediately following staining when cells are immersed in non-solidifying buffers, especially when probe dissociation is of concern. Yet, we have observed virtually no loss of staining intensity within 24 hours of specimen incubation in TBS with all procedures described in this dissertation. Importantly, for fluorescence imaging TBS should be substituted with 70% Glycerol in TBS, as substantial mismatch in refractive index

between glass, cells, and TBS leads to light reflection within the solution creating glare (thus blurring images) and damages cells upon extended exposure to UV light (*e.g.* continuous spot illumination for 5 minutes with 100x oil-immersion objective). Addition of glycerol conveniently resolves this issue, preventing specimen damage and producing crisp images, while still allowing for further exchange to TBS buffer.

3.3 Hyper-spectral imaging as a tool for multiplexed QDot analysis

Specimen processing and staining using QDot-optimized protocols enables reliable labeling of extracellular, cell-surface, and intracellular molecular targets with QDot probes. However, accurate quantitative analysis of multiple targets based on QDot labeling, in addition, demands standardization of image acquisition and processing algorithms. Narrow symmetrical emission profiles facilitate spectral isolation of individual QDot signals from a multiplexed specimen. For example, careful choice of band-pass emission filters might enable imaging of 3-4 QDot colors with conventional fluorescence microscope equipped with CCD camera. Quantitative analysis of a larger number of targets, nonetheless, might be compromised by spectral cross-talk between probes with closely spaced emission peaks and non-linear response of the detector. Hyper-spectral imaging (HSI) overcomes these limitations to a great extent, enabling extraction of high-content information from a narrow visible spectral window [5, 159, 160].

Generally, HSI systems incrementally apply narrow band-pass filters and collect a series of images for each wavelength band over a specified spectrum, thus producing an "image cube" providing spectral information for each pixel of an image. Deconvolution of known emission profiles from the resulting image cube separates different probe signals from each other and

from the background fluorescence, enabling qualitative target co-localization studies and quantitative analysis of molecular expression profiles (**Figure 3.3**).

A number of HSI systems for variety of imaging applications are commercially available. We have tested HSI camera (Nuance) from Cambridge Research & Instrumentation (CRI, now Advanced Molecular Vision), one of the leading providers of liquid crystal-based imaging and optical processing instrumentation for life science research. CRI camera is able to identify multiple fluorescent tags based on small but meaningful spectral differences by scanning

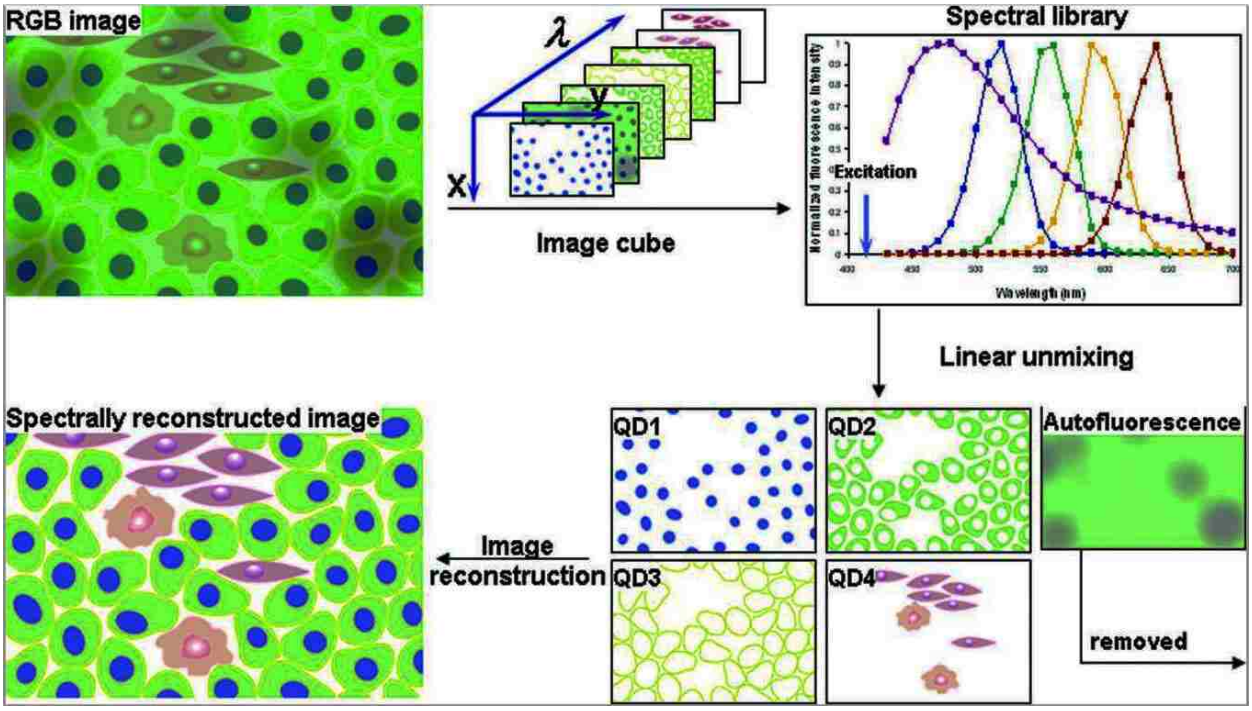

Figure 3.3 Schematic illustration of hyper-spectral imaging of tissue specimens labeled with multicolor QDots. Conventional RGB cameras display images in three color channels (red, green, and blue) and thus cannot distinguish spectrally overlapping fluorophores. In contrast, HSI works in a way similar to spectroscopy in that it samples the emission spectra of every pixel at a series of wavelengths (thus creating an image cube). Based on the spectral information obtained for each pixel, the fluorescent components (multicolor QDots and autofluorescence) can be unmixed into separate images for quantification or merged together with the autofluorescence removed. Adapted from: True, L.D. and X. Gao. J. Mol. Diagn., 2007. **9**(1): p.7.

wavelength range of 420-720 nm with a built-in liquid crystal tunable filter at step increments as small as 1 nm. Furthermore, the camera captures images at each wavelength with constant exposure, and the software mathematically separates the color components based on reference spectra, thus enabling accurate quantitative analysis (**Figure 3.4**). Importantly, CRI camera can be mounted on any fluorescence microscope and controlled by a standard PC with Nuance image analysis software, offering a straightforward and cost-effective solution to high-resolution hyper-spectral imaging that can be easily adopted by a range of research and clinical laboratories.

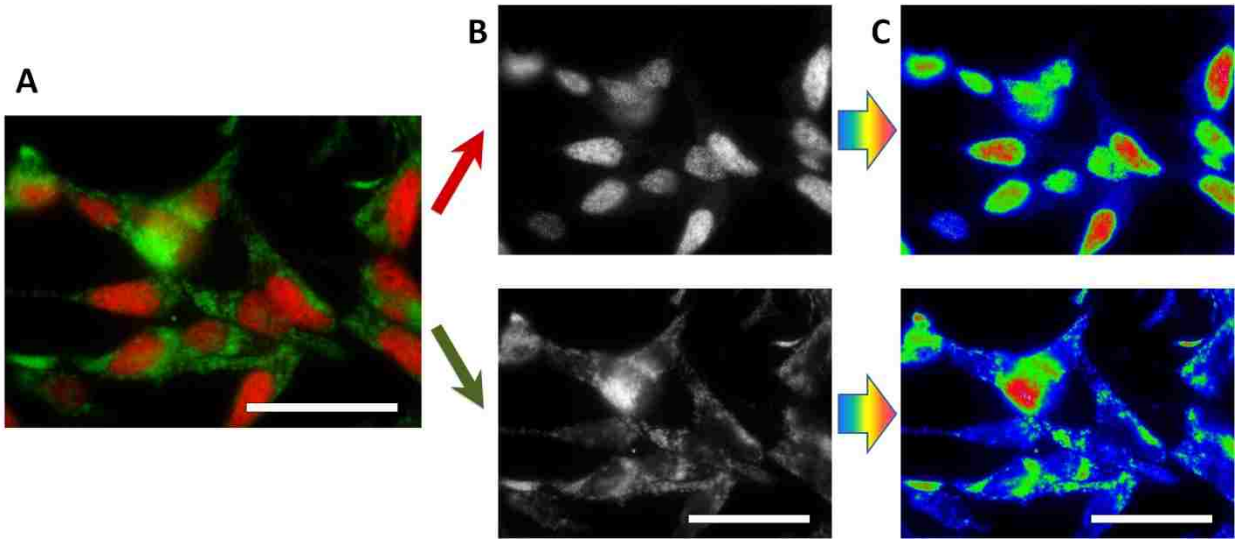

Figure 3.4 Multiplexed quantitative evaluation of molecular profiles with HSI. Hyper-spectral imaging camera acquires spectral information for each pixel of composite multicolor image (A) and uses reference QDot spectra for deconvolution of QDot signals into individual channels (B), enabling quantitative analysis of fluorescence signal intensity produced by each probe (highlighted with a heat map here) (C). Specifically, nuclear target AR (androgen receptor) and mitochondrial target MAOA (monoamine oxidase A) are simultaneously labeled with red and green QDots in fixed LNCaP cells. Notably, unmixed images provide staining intensity information for each pixel, facilitating detailed assessment of target abundance and distribution at sub-cellular resolution. Scale bar, 50μm.

Specifically, we have employed IX-71 inverted fluorescence microscope (Olympus) equipped with Nuance HSI camera and Wide UV filter cube (330-385 nm band-pass excitation, 420 nm long-pass emission, Olympus) for simultaneous imaging and spectral unmixing of up to 10 QDot colors (currently limited by the software) with emission peak separation as small as 20 nm (**Figure 3.5**). For example, with single-cell molecular profiling platforms described in subsequent chapters we have achieved simultaneous imaging and quantitative analysis of up to 5 molecular targets. Nuance image analysis software was used for unmixing image cubes based on the reference spectra of each QDot component (along with an extra channel for background fluorescence when biological specimens with high autofluorescence were studied). For qualitative evaluation of target distribution, brightness and contrast of each channel was automatically adjusted to achieve optimal visual representation. For quantitative analysis, average signal intensity within automatically selected regions of interest (ROIs) that included QDot staining and excluded "blank" non-stained areas within each QDot channel was measured. We have routinely performed identical analysis on 3-5 image cubes taken from different fields of view of the same specimen to obtain an overall average cell staining intensity and assess variability of signal intensity throughout the specimen (reported as error bars equal to standard deviation of average signal intensities between 3-5 areas imaged). Low-magnification images obtained with 20x dry objective (NA 0.75, Olympus) and containing at least 400 cells per field of view were used for quantitative analysis, whereas high-magnification images obtained with 100x oil-immersion objective (NA 1.40, Olympus) were used for qualitative evaluation of intracellular distribution of molecular targets. Additionally, true-color CCD camera (QColor5, Olympus) was used for evaluation of 1-color and 2-color reference stains performed with either QDot-based or organic dye-based labels.

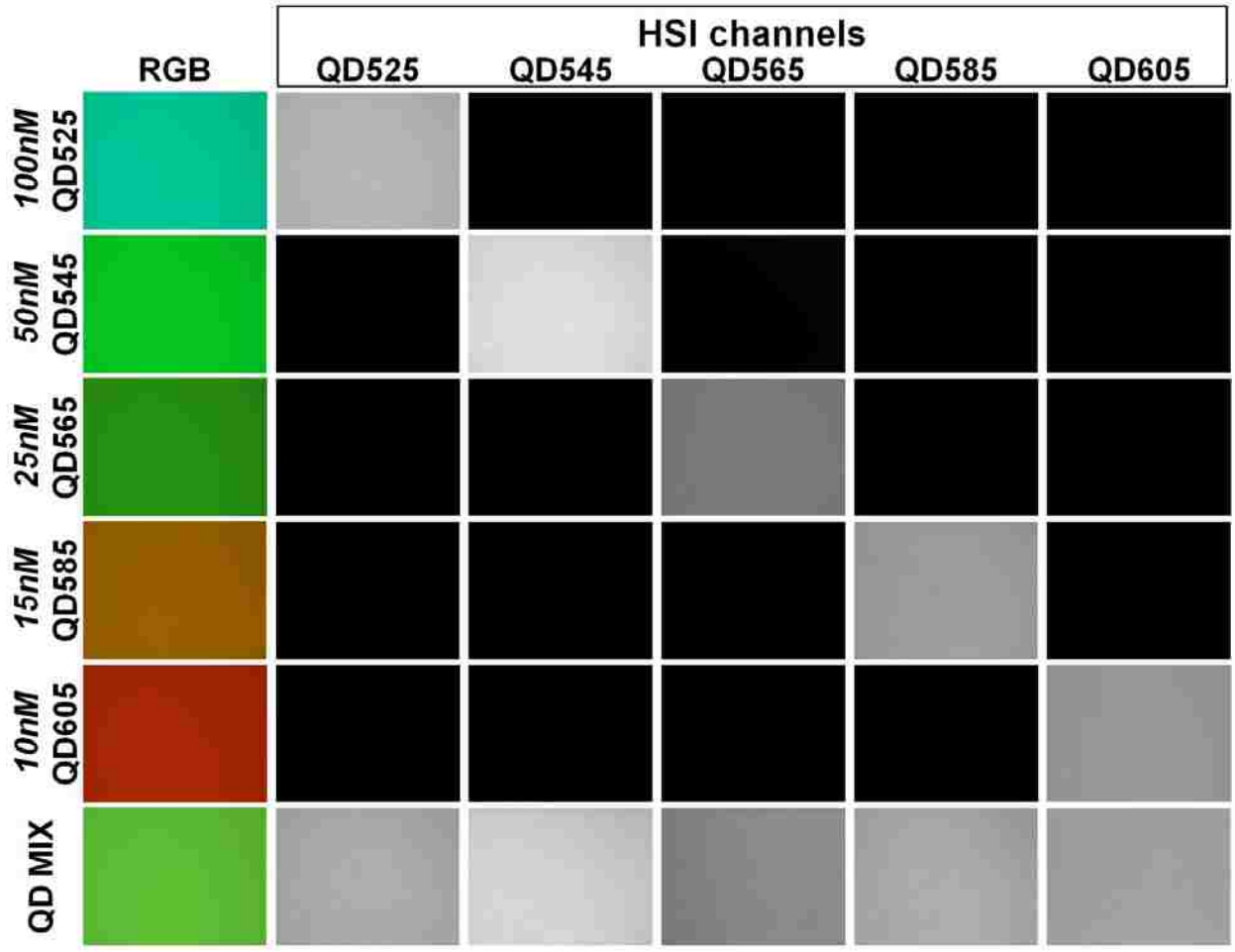

Figure 3.5 Unmixing of multiple QDot colors with HSI. Narrow symmetrical QDot emission profiles enable reliable unmixing of individual QDot signals with emission peaks spaced as close as 20nm apart, yielding lack of spectral crosstalk between QDot channels and enabling accurate quantitative measurement of individual QDot probe intensities. All QDot channels have been normalized for direct comparison of signal intensity.

Despite extensive analytical capabilities of HSI, quantitative analysis of target expression with multiplexed staining might be complicated by the differential brightness of multicolor QDot probes. In fact, sensitivity of detection achieved with larger (red) QDots if often greater compared to smaller (green-blue) QDots [73, 161]. For example, Ghazani and coworkers have demonstrated three-color staining of lung carcinoma xenografts for epidermal growth factor receptor, E-cadherin, and cytokeratin with 655, 605, and 565 nm QDot-based assays and

noticed significant enhancement of 655 nm signal over 565 nm one [42]. In most cases the discordance in fluorescence intensity of individual probes originates from differential light absorption properties of QDots, as larger particles possess larger absorption cross-sections and thus collect light more efficiently. To account for this effect, differences in photo-physical properties of individual probes can be readily characterized in advance and incorporated into signal analysis algorithms. In one study exemplifying such analysis, Yezhelyev *et al* have demonstrated the multiplexed labeling and quantification of three clinically significant breast cancer markers – Her2, ER, and PR – on FFPE breast cancer cells as well as 5-biomarker profiling on FFPE breast cancer tissue biopsies [69]. In order to account for signal enhancement of red QDots and compare expression levels of biomarkers within one sample, acquired data was normalized according to the relative QDot intensities (QDot655:QDot605:QDot565 = 8:4:1 as measured in a separate experiment for equal QDot concentrations), yielding relative biomarker abundance consistent to that obtained with conventional techniques (IHC, Western blot, and FISH).

At the same time, it should be noted that normalization for differential QDot photo-physical properties might not be sufficient for accurate analysis of multicolor stains, as imaging instrumentation parameters might also introduce bias in signal recording. Therefore, in our studies we have evaluated brightness of all QDot probes with exactly same imaging setup and parameters as used for studies performed on cell and tissue specimens. Specifically, equal volumes of QDot solutions were placed in separate wells of a 96-well plate, and each well was imaged on IX-71 inverted fluorescence microscope using 20x objective and Wide UV filter cube. Measurements were done with Nuance HSI camera and true-color QColor5 camera (Table 3.1). Quantitative analysis of signal intensities was performed with Nuance image analysis software and ImageJ respectively. Correction factors obtained in this manner can be applied during processing of multiplexed images for direct comparison of

target abundance labeled with different QDot probes. In should be noted, however, that different QDot stocks often exhibit disparity in optical properties (such as fluorescence peak position and quantum yield). Therefore, it is advisable to perform evaluation of QDot apparent brightness for each new preparation of QDot probes as well as with changes in imaging instrumentation. Differential QDot brightness is also important to take into account when performing multiplexed staining of targets with varying abundance levels and intracellular distribution. In particular, brighter red QDot probes should be used for less abundant (or more diffusely distributed) targets, while dimmer green QDots should be reserved for more abundant (or more densely packed) targets to achieve a relatively uniform apparent staining intensity throughout all targets and avoid camera saturation by any one exceptionally bright signal.

Table 3.1 Differential QDot brightness measured with HSI and true-color cameras

	QDot525	QDot545	QDot565	QDot585	QDot605
Nuance HSI	1.0	2.5	3.0	6.6	9.7
QColor5	1.0	1.3	1.9	4.9	5.4

3.4 Summary

QDots are commonly presented as “better fluorescent probes” fully compatible with conventional immunofluorescence methodologies, capable to demonstrate superior performance in comparison to organic fluorophore-based probes under identical experimental conditions. However, such a notion is misleading. While featuring unique beneficial optical properties, QDots also impose a number of limitations on specimen processing and staining conditions, occasionally being incompatible with labeling of certain targets. In addition,

parallel labeling of multiple targets requires complete preservation of antigenicity and sufficient QDot accessibility for the whole set of targets, thus limiting specimen processing options. Therefore, careful optimization of specimen processing and staining conditions tailored to QDot probes should be done. We have identified one set of conditions that offers robust staining of various targets with QDots in fixed adherent cell lines. Yet, modifications to this procedure might be introduced to satisfy unique criteria of molecular profiling applications of interest.

We have carefully explored the capabilities of hyper-spectral imaging with CRI Nuance camera and established great utility of this imaging technology for simultaneous detection, accurate unmixing, and quantitative analysis of signal intensity of at least 5 QDot probes with emission peaks spaced 20 nm apart through the visible spectrum. We note that apparent differential brightness of multicolor QDots, originating from the differences in QDot optical properties and imaging instrumentation, must be taken into account during quantitative assessment of multiplexed stains. Importantly, calibration for differential brightness should be performed with each QDot stock and each imaging setup (including changes in excitation source, filter cubes, and camera). With these technical concerns properly addressed, HSI perfectly complements the multiplexing capabilities of QDot probes and offers a straightforward, yet analytically powerful, approach for implementation of QDot imaging platform for single-cell molecular profiling.

CHAPTER 4: PREPARATION OF POLYMER-ENCAPSULATED QDOT SCAFFOLDS

Success of QDot probe engineering depends on the quality of the QDot platform used for implementation of a particular design. A number of water-soluble QDots currently available from commercial sources cover basic imaging and detection applications and offer some room for further probe design and method development. However, many design strategies require incorporation of features or processes incompatible with commercial water-soluble QDot platforms. In this regard, organic QDots provide more flexibility, as custom hydrophilic coatings can be tailored to specific parameters. To gain better control over QDot probe structure and properties, we have explored polymer encapsulation strategy for preparation of versatile water-soluble scaffolds and developed a set of procedures for QDot purification, characterization, and surface modification tailored to preparation of probes for molecular profiling applications.

4.1 QDot encapsulation with amphiphilic polymer

Water-solubilization of organic QDots via encapsulation with amphiphilic polymer represents one of the most robust methods for preparation of stable imaging probes. This reaction is mainly driven by absorption of an amphiphilic polymer onto the nanoparticles via hydrophobic interactions. At the same time, hydrophilic functional groups exposed to the solution render QDots water soluble and amenable for further bioconjugation. Since intact organic coating on the QDot surface is preserved with this procedure, optical properties are

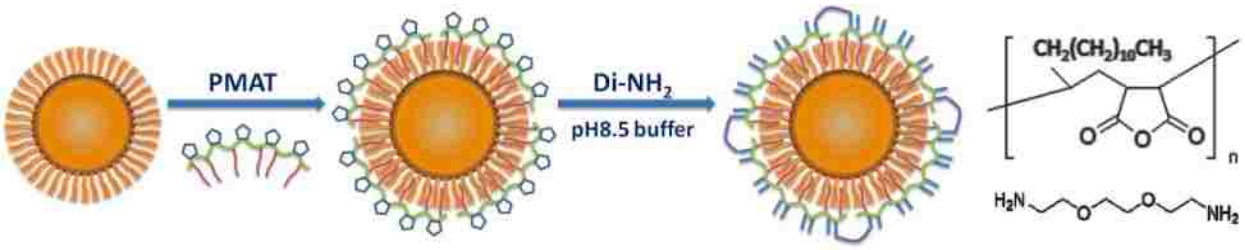

Figure 4.1 QDot encapsulation with amphiphilic polymer. First, PMAT is deposited onto the surface of hydrophobic QDots. Then neighbor polymer chains are cross-linked with short di-amine molecules by spontaneous reaction with maleic anhydride rings. Resuspension in basic buffer promotes hydrolysis of anhydrides and produces negatively-charged surface, which stabilizes QDots in aqueous solutions.

not affected, and good shielding of the nanocrystals core from contact with the outside environment is achieved. Therefore, we have utilized polymer encapsulation strategy towards developing stable water-soluble QDot scaffold for engineering of imaging probes satisfying design criteria of molecular profiling applications.

Preparation of QDot scaffolds was based on high-quality hydrophobic nanoparticles obtained from a commercial source, Ocean Nanotech. To render nanoparticles hydrophilic and suitable for further bioconjugation, QDots were coated with an amphiphilic polymer poly(maleic anhydride-*alt*-1-tetradecene) (PMAT, MW=9,000 Da, Sigma-Aldrich). Consisting of alternating hydrophobic chains on a maleic anhydride backbone, this polymer self-assembled onto the hydrophobic QDot core and introduced reactive anhydride groups on the surface for further cross-linking (**Figure 4.1**). To achieve uniform and stable encapsulation, QDot powder was dissolved in chloroform to a final concentration of 1-5 μM and mixed with 500-1000 molar excess of polymer. Few drops of methanol were added to aid in dissolution of the anhydride groups and promote QDot-PMAT self-assembly. After thorough mixing, chloroform was evaporated overnight in the chemical hood or under mild vacuum to deposit PMAT molecules on the QDot surface. It is important to avoid sonication at this step, as it leads to severe loss

of QDot fluorescence, likely due to disruption of organic passivation layer on the nanocrystal surface and exposure of surface trap sites. As discussed in Chapter 1, hydrophobic QDots are coated with a layer of labile small surface ligands (easily dislodged with sonication) that shield the nanoparticle surface and preserve unique photo-physical properties of the core. It is also important to ensure complete evaporation of the solvent (indicated by deposition of a thin dry QDot/PMAT film on the walls of glass vial), as minor amounts of organic solvents might facilitate dissociation of PMAT from the nanoparticle surface, leading to QDot aggregation in aqueous buffers. At the same time, forcing quick drying (*e.g.* with rotary evaporator) should be avoided, as it does not allow sufficient time for proper arrangement of the linear polymer on the nanoparticle surface, also leading to QDot aggregation.

Further cross-linking of the polymer shell was done in chloroform in presence of excess diamine. We have found cross-linking to be an essential step for preparation of stable QDots amenable to a wide range of conditions used for further bioconjugation. While polymer encapsulation of QDots without cross-linking produced water-soluble particles, chemical modification of such particles often resulted in severe aggregation due to exposure of hydrophobic patches or unbound PMAT on the QDot surface. Proper cross-linking was achieved by re-suspending dry QDot/PMAT film in chloroform/methanol (hexane represents another suitable solvent for this step), incubating with 500-1000 molar excess of cross-linker (2,2'-(Ethylenedioxy)bis(ethylamine), Sigma Aldrich) for 30-60 minutes, and completely evaporating solvent under mild vacuum overnight.

Rendering of polymer-coated particles water-soluble was achieved by re-suspension of QDot/PMAT powder in an aqueous buffer with basic pH. Specifically, 50 mM Borate buffer (pH 8.5) was added to a vial containing QDot/PMAT film. Basic buffer promotes hydrolysis of anhydride rings into carboxylic acid groups, which yield particles highly negatively charged

and water-soluble at neutral or basic pH. Buffers with neutral and acidic pH failed to provide sufficient rate of hydrolysis, forcing slow dissolution of QDots with hydrophobic surface patches into aqueous environment, which eventually led to QDot aggregation. Similar effect can be observed even with highly basic buffers when quick dissolution of polymer-coated QDots is forced by rigorous vortexing or sonication, as insufficient time is allowed for hydrolysis of anhydride group and proper arrangement of the polymer. Therefore, only mild shaking can be used to facilitate slow dissolution of well-stabilized single QDots. Notably, following complete dissolution, polymer-coated QDots can be successfully transferred to buffers with neutral or even mildly acidic (pH 4-5) buffers, should this be required by specific bio-conjugation procedures.

4.2 QDot purification, purity control, and characterization

QDot probe engineering often involves further surface modification and bio-conjugation. Therefore, polymer-coated QDots have to be completely purified of excess polymer and cross-linker. Out of several methods tested, ultra-centrifugation has proven to be most suitable for preparation of highly pure QDot-PMAT samples, despite offering at most 50% purification yield. Substantially higher density of the nanoparticle inorganic core leads to efficient segregation of QDots into a pellet, leaving excess polymer and cross-linker in the supernatant. Specifically, polymer-coated QDots were purified by 2-3 rounds of ultra-centrifugation at 45000 rpm for 45-60 minutes each using Beckman Coulter Optima TLX ultracentrifuge and TLA110 rotor. Soft pellet (100-150 µL) was collected each time and re-suspended in Borate buffer, while supernatant was discarded. Surprisingly, purification methods based on separation by size (rather than weight), such as fractionation with Superdex-75 gel column and ultrafiltration with 100 kDa molecular weight cut-off concentrators, fail to remove excess polymer from solution, even though such methods are expected to be suitable for removing

single polymer molecules with molecular weight of only 9 kDa. Therefore, it appears that in aqueous buffers PMAT forms high-MW micelles comparable in size to QDot-PMAT particles, thus hampering separation of free polymer by size-exclusion methods. Further purity control studies discussed below corroborate this conclusion.

Considering the chemical similarity between polymer-coated QDots and empty polymer micelles and realizing importance of the QDot purity for success of downstream bio-conjugation, we have developed 3 independent methods for purity control: detection of polymer micelles with dynamic light scattering (DLS using Zetasizer NanoZS from Malvern Instruments), staining of the polymer band on agarose gel, and measurement of polymer fluorescence (using Fluoromax4 fluorometer from Horiba Jobin Yvon) (**Figure 4.2**). DLS is the least sensitive method capable of only detecting a large population of PMAT micelles within a non-purified sample. Solution of PMAT alone in Borate buffer shows distinct population of nanoparticles with hydrodynamic diameter of 6-7 nm, which is slightly smaller than the size of pure QDot-PMAT (10-13 nm). Therefore, shift of the size distribution towards smaller HD can be used as an indicator of severe contamination with polymer micelles. In fact, DLS analysis of as-prepared non-purified QDot-PMAT mixture fails to resolve true QDot HD, indicating prevalence of 6-8 nm nanoparticles.

Detection of the polymer with agarose gel electrophoresis offers higher sensitivity, as PMAT and QD-PMAT particles are expected to form sharp distinct bands on the gel. Considering that PMAT micelles have hydrodynamic size slightly smaller than that of QDot-PMAT while providing similar surface charge density, PMAT micelles are expected to move slightly faster during agarose gel electrophoresis. Despite having no PMAT-specific detection reagent, we have identified SYBR-Gold dye, commonly used for DNA detection, as a suitable reporter for this purpose. Similarly to DNA labeling, SYBR-Gold shows bright staining of

hydrolyzed PMAT, presumably due to electrostatic interaction with negatively-charged polymer backbone. Using such staining we were able to confirm slightly faster gel motility of PMAT and detect excess polymer in non-pure samples (*e.g.* after Superdex-75 column purification or 100KDa MWCO concentrator ultrafiltration), while observing no free polymer in purified QDot-PMAT sample after ultracentrifugation (**Figure 4.2, middle panel**).

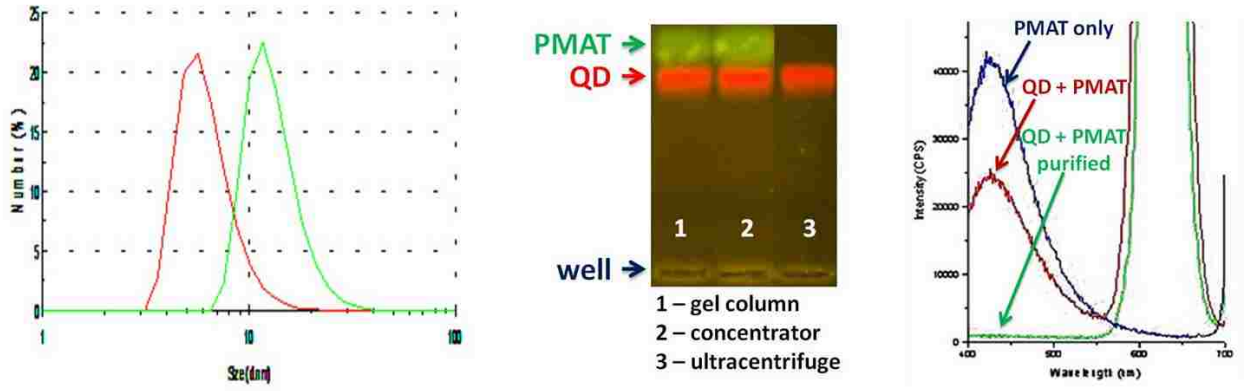

Figure 4.2 Strategies for purity control of PMAT-encapsulated QDot scaffolds. Presence of free PMAT in solution can be detected by DLS (left, red curve), gel electrophoresis with SYBR-Gold staining (middle), and fluorimetry (right, 420nm peak) in unpurified samples. Surprisingly, purification methods based on size exclusion, such as Supredex-75 column chromatography and ultrafiltration with 100KDa MWCO centrifugal filter, failed in removing excess PMAT. Only ultracentrifugation yielded pure QDots with sole single-QDot population on DLS (green curve), sharp QDot band on agarose gel, and absence of polymer fluorescence peak.

Measurement of polymer fluorescence has proven to be the most straightforward and sensitive method for purity control. When excited by a 350 nm source, free PMAT shows strong fluorescence peak at about 420 nm. At the same time, upon coating onto QDots, polymer fluorescence is quenched. Therefore, detection of only free contaminating polymer

with high sensitivity is possible using fluorescence measurements. Specifically, we first obtained reference polymer and QDot spectra by measuring bulk fluorescence of pure solutions of (i) hydrolyzed PMAT in Borate buffer and (ii) hydrophobic QDots in chloroform. Then we tested as-prepared non-purified QDot-PMAT sample as well as samples processed with different purification routes and compared fluorescence profiles to reference spectra. Consistent with DLS and gel electrophoresis results, QDot-PMAT sample successfully purified with ultracentrifugation exhibited no 420 nm fluorescence and produced only a strong QDot fluorescence peak, whereas non-purified or poorly purified samples yielded distinct polymer fluorescence (**Figure 4.2, right panel**). It should be noted that QDot fluorescence intensity at its peak is substantially higher compared to polymer fluorescence. However, having narrow symmetrical emission profile, even green-emitting particles (*e.g.* having emission peak at 510 nm) produce no contribution in the spectral range of polymer emission, thus enabling sensitive detection of the weak PMAT fluorescence.

Aside from purity control, same analytical methods, complemented by spectrophotometry and fluorescence microscopy, can be used for comprehensive characterization of purified PMAT-coated QDots. Particular attention should be paid to verification of optical properties, surface chemistry, and colloidal stability after polymer encapsulation. In particular, with DLS analysis of 100-500 nM nanoparticle solutions in Borate buffer we established QDot hydrodynamic diameter to be 10-13 nm (depending on the core size), with each QDot specimen yielding narrow size distribution and lack of aggregates. Gel electrophoresis, in turn, corroborated DLS results and confirmed the highly negative surface charge. When run on 1% agarose gel at 100V in TBE buffer, QDots formed sharp band moving towards anode, indicating monodisperse population of negatively-charged particles. Light absorption properties (measured by spectrophotometry) and fluorescence emission profile (measured by fluorometry) remained unperturbed, confirming preservation of the intact nanocrystal core.

Notably, PMAT-coated QDots featured nearly unchanged quantum yield of 50-55%, just slightly lower than 60% QY recorded with hydrophobic QDots in chloroform. High-magnification fluorescence microscopy was employed to verify the absence of QDot aggregation, as single QDots can be clearly identified by their characteristic "blinking" behavior (*i.e.* single QDots exhibit intermittency in fluorescence emission upon continuous illumination, while QDot aggregates on average stay always "on"). Finally, we examined QDot-PMAT behavior in a range of aqueous buffers employed for bio-conjugation and staining applications, such as pH5 MES, pH7 PBS, and pH9 Borate, and verified good colloidal stability and preservation of optical properties under those conditions. At the same time, being primarily stabilized by electrostatic repulsion of negatively-charged groups on the nanoparticle surface, PMAT-coated QDots completely lose stability in such polar solvents and DMF and DMSO, thus confining further surface modifications to aqueous-phase procedures.

4.3 Surface modification for reducing QDot non-specific interactions

Single-cell molecular profiling applications often involve labeling of molecular targets in fixed specimens and require access to intracellular as well as cell-surface targets. Such access can be achieved by permeabilization of fixed specimens with charged (*e.g.* DTAC and SDS) and neutral (*e.g.* Triton X-100 and Tween-20) detergents. However, removal of natural lipid barriers eliminates the negative charge on the cell surface and opens access to a variety of electrostatic and hydrophobic interactions. As a result, negatively-charged particles, quite suitable for imaging of intact cells (*e.g.* live cells or fixed non-permeabilized cells), become inapplicable for staining of fully processed specimens (**Figure 4.3A**). One common approach to resolving this issue is to deposit a thick layer of non-fouling material (most often PEG) for shielding of the negatively-charged QDot scaffolds (**Figure 4.3D**), which, however, results in the increased nanoparticle size and impeded bio-conjugation efficiency. In contrast, we have

found that non-specific interactions can be efficiently eliminated by introducing positively-charged moieties to the QDot surface, thus converting negatively-charged surface to a zwitterionic one. By creating a richly hydrated shell, zwitterionic coating stabilizes QDots in a range of buffers and impedes non-specific interactions, while retaining small particle size.

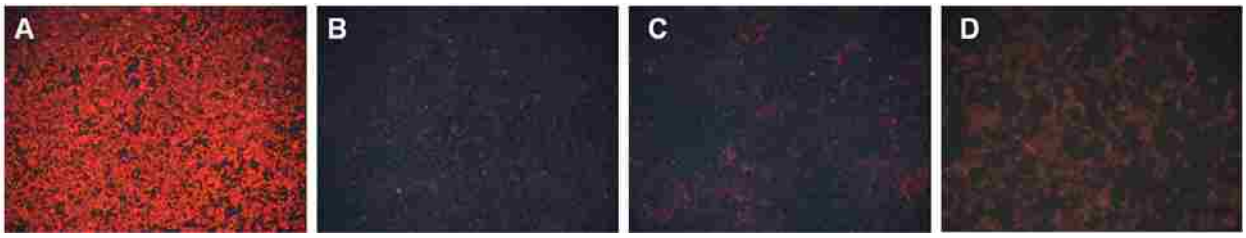

Figure 4.3 Strategies for reducing QDot non-specific cell staining. A) PMAT-coated QDots show very high non-specific binding to fixed cells, precluding from utilization of such particles in staining applications. Zwitterionic (PMAL-coated (B) and PMAT-coated and modified with 4' amines (C)) and PEG-coated QDots (D), on the other hand, show minimal non-specific interaction, providing suitable platform for engineering of probes for cell staining.

To produce QDots with zwitterionic surface we have adapted PMAT-encapsulation procedure to a similar polymer pre-modified with tertiary amines. In particular, PMAL-C8 (poly(maleic anhydride-*alt*-1-decene substituted with 3-(dimethylamino)propylamine, Anatrace), which features not only zwitterionic surface neutrally charged at slightly basic pH, but also shorter C8 hydrophobic side-chains, yields compact deposition of the polymer on the QDot surface and produces stable coating even without further cross-linking. Following procedure developed for PMAT encapsulation, QDots were coated with PMAL-C8 by mixing nanoparticles and polymer in chloroform and evaporating solvent under mild vacuum. Resulting powder was dissolved in 50 mM Borate buffer, filtered through 0.22 μm syringe filter, and purified by 2-3 rounds of ultracentrifugation. PMAL-coated QDots had smaller hydrodynamic diameter from 7 nm (for green QDot513) to 12 nm (for red QDot622), preserved

quantum yield, and no electrophoretic motility due to neutral surface charge. Interestingly, such QDots exhibited outstanding colloidal stability even in 100% DMF and DMSO, enabling exploration of more efficient bio-conjugation procedures in water-free environment. Yet most notably, zwitterionic QDots showed minimal non-specific interaction with fixed cells (**Figure 4.3B**), thus providing a suitable platform for further preparation of probes for cell and tissue staining. However, utilization of a pre-modified polymer limits the flexibility in tuning QDot surface properties, conjugation strategies, and overall robustness of the system (especially considering noticeable differences in modification degree between different lots of PMAL). To gain better control over QDot properties, we have developed a procedure for preparation of zwitterionic particles based on a more versatile QDot-PMAT platform.

QDot-PMAT features high density of carboxylic acid groups on the nanoparticle surface, thus enabling covalent conjugation of a number of ligands containing primary amines. Therefore, to convert a negatively-charged surface into a zwitterionic one, we modified part of carboxylic acid groups with either tertiary (2-(Dimethylamino) ethylamine, Sigma-Aldrich) or quaternary ((2-Aminoethyl) trimethylammonium chloride, Sigma-Aldrich) amines via EDC-mediated conjugation in Borate buffer, yielding nanoparticles with overall neutral charge at slightly basic pH. Due to excellent stability of QDot-PMAT particles, high excess of ligands and EDC could be added to improve the yield of modification. In contrast, non-crosslinked PMAT-coated QDots and commercial negatively-charged hydrophilic QDots exhibited severe aggregation when reacted under identical conditions, probably due to lack of crosslinking stabilization of the organic shell. Specifically, 100μL 1μM PMAT-coated QDots in 50mM Borate buffer were incubated overnight with 100,000 molar excess of EDC and 100,000 molar excess of quaternary amine ligands, yielding stable neutrally-charged particles. Over-modification with charge inversion was observed only in rare cases, indicating that the reaction could self-terminate upon reaching a certain level of modification (likely due to electrostatic repulsion

of positively-charged 3' and 4' amines and shielding of the carboxylic acid groups). Similar to PMAL-coated QDots, zwitterionic particles prepared in this manner showed lack of non-specific interactions with cells at optimal conditions (**Figure 4.3C**). However, significant pH sensitivity of the coating necessitated careful optimization of staining buffer pH and composition. Specifically, in our experiments with formalin-fixed cells, slight negative QDot charge induced non-specific nuclear binding, whereas slight positive charge resulted in patchy membrane staining.

4.4 Summary

Availability of a stable and versatile QDot scaffold is essential for successful probe development satisfying design criteria of molecular profiling applications. We have developed one version of such a scaffold by employing a polymer-encapsulation strategy supplemented by surface stabilization and modification. In order to obtain highly pure polymer-coated QDots we have evaluated several purification strategies, identifying ultracentrifugation as most efficient method for nanoparticle purification and dismissing commonly used size-exclusion approaches. Concurrently, we have developed three independent strategies for purity control and established a common framework for QDot characterization. Finally, we have demonstrated the utility of zwitterionic surface coating for nanoparticle stabilization in a range of aqueous buffers and polar anhydrous solvents along with efficient shielding from non-specific interactions. As a result, high stability, good control over QDot interaction with biological specimens, and capacity for further application-specific bio-functionalization offer a versatile platform for engineering of superior fluorescent probes (Table 4.1).

Table 4.1 Beneficial features of polymer-encapsulated QDot scaffolds

Design criteria	Organic fluorophore	Commercial QDot scaffolds	Our QDot scaffolds
Stability in aqueous buffers	Varies	YES	YES
Tunable physicochemical properties	NO	NO	YES
Amenability for bio-conjugation	YES	YES	YES
Brightness and photostability	NO	YES	YES
Multiplexing capacity	Poor	YES	YES
Control over probe architecture	YES	NO	YES
Consistent quality	YES	NO	YES

CHAPTER 5: DIRECT ANTIGEN LABELING WITH QDOT-ANTIBODY PROBES

Single-cell molecular profiling applications critically rely on interrogation of a number of molecular targets on the same specimen. In this regard, QDot-based probes have become a promising tool for quantitative multiplexed studies, enabling simultaneous detection and analysis of multiple targets. Advances in QDot synthesis and surface modification achieved during the last decade have produced multicolor QDot-1'Antibody bioconjugates aiming to expand multiplexing capabilities of IF staining through direct target labeling with QDots in a 1-step procedure (**Figure 5.1**). However, chemical modification and purification steps involved in the direct conjugation process are not only highly complex and prohibitively expensive, but also often result in reduction in antibody avidity. Lack of flexible, simple, and cost-effective route for QDot-Antibody probe preparation represents a major roadblock on the way toward implementation of this otherwise attractive approach for single-cell molecular profiling. To address this challenge we have stepped away from the mainstream procedure of tedious low-yield synthesis of custom-designed probes through covalent QDot-Antibody conjugation and developed a novel simple strategy of on-demand probe preparation via non-covalent self-

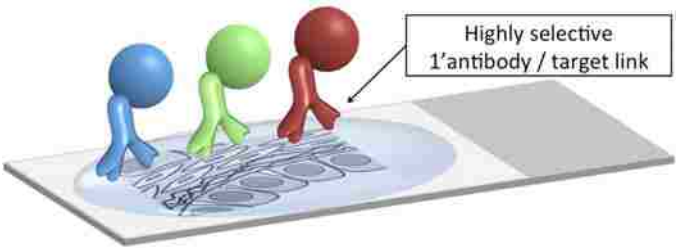

Figure 5.1 Direct antigen labeling for multiplexed staining with QDot probes. Covalent QDot-1'Antibody bioconjugates have been developed for simultaneous labeling of multiple targets. Complexity of probe preparation, however, hampers wide adoption of this technology.

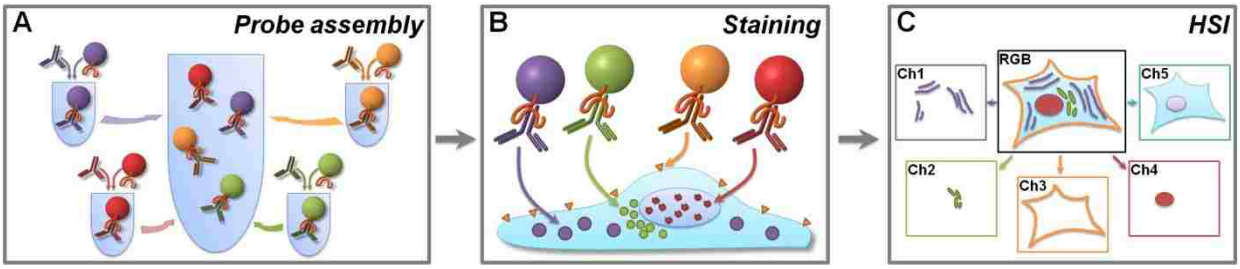

Figure 5.2 Schematic illustration of direct antigen labeling with self-assembled QDot-Antibody probes. (A) A universal QDot platform is used for 1-step purification-free assembly of functional QDot-Antibody probes via capture of free antibodies from solution. Once bound, antibodies are not exchanged with other QDot-SpA probes, thus enabling mixing of multicolor probes within a single cocktail. (B) The QDot-SpA-Antibody cocktail is used for 1-step parallel multiplexed staining. (C) Spectral imaging is performed for unmixing individual QDot colors, quantitative analysis of target expression, and depiction of relative target distribution within the specimen.

assembly between the universal QDot platform and a variety of intact primary antibodies [162]. With such QDot platform, multiplexed quantitative characterization of molecular targets can be achieved with a few simple steps. First, universal QDot bioconjugates are used to capture intact primary antibodies in solution during a pre-staining step to form functional QDot-Antibody fluorescent probes. Once formed, different probes are pooled in a single cocktail (**Figure 5.2A**) and incubated with cells for parallel multiplexed staining (**Figure 5.2B**). Then, fluorescence microscopy with HSI capability is utilized to acquire and unmix signals from each QDot color to generate quantitative expression profiles of molecular targets in separate channels and depict the relative target distribution in a merged image (**Figure 5.2C**).

5.1 Engineering of a universal QDot platform

In designing a universal QDot platform we have focused on achieving a straightforward method for on-demand QDot-Antibody probe preparation requiring no specialized expertise or instrumentation. Specifically, we have ensured that such a platform 1) binds the wide range

of primary antibody types; 2) requires no chemical modification to the antibody; 3) requires no probe purification, conserving precious antibodies; 4) provides control over the antibody orientation on the QDot surface; 5) remains stable for the duration of the staining procedure, resisting probe disassembly and/or aggregation; and 6) features high labeling specificity while suppressing non-specific interactions with biological specimens. Self-assembly between an antibody and adaptor proteins (*e.g.* bacterial protein A and protein G) has provided a suitable route for implementation of our design (**Figure 5.3**).

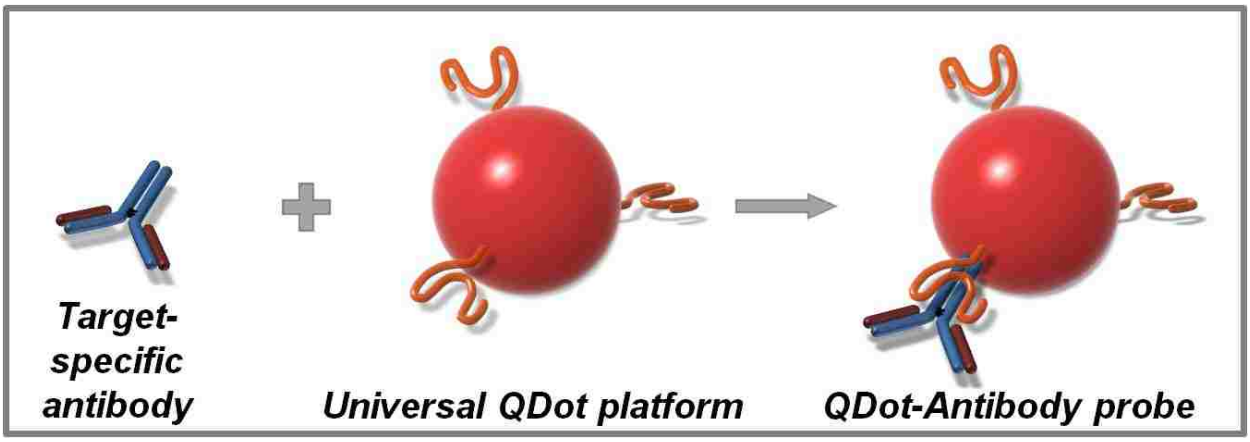

Figure 5.3 On-demand preparation of QDot-Antibody probes. Self-assembly between target-specific antibodies and the universal QDot platform is achieved via non-covalent binding of an adaptor protein (e.g. Protein G or Protein A) to an Fc region of intact IgG antibodies.

Adaptor proteins have been extensively studied and used for a variety of applications, including routine antibody isolation and purification. At the same time, novel immunoassays and live cell imaging methods have been developed based on QDot-adaptor protein conjugates, in part due to sufficiently high stability and specificity of antibody binding and compatibility with antibodies from a range of host species [87, 88, 163, 164]. However, utilization of highly charged components for probe preparation (QDots are often highly negatively charged, whereas avidin and genetically engineered protein G are highly positively

charged) leads to significant contribution of electrostatic interactions to an overall probe behavior, resulting in extremely high non-specific binding to fixed cells and tissue specimens and unpredictable probe assembly and stability. For example, we have developed a protein G functionalized QDot platform based on negatively-charged PMAT-coated QDots for direct labeling of cell-surface targets in fixed non-permeabilized cells (see section 5.1.1). Yet, high negative charge of such probes prohibits multiplexed IF on fixed and permeabilized cells and tissue specimens. To avoid this problem and render QDot probes suitable for labeling of intracellular targets, we have built the universal QDot platform based on a stable QDot-PEG scaffold, which resists non-specific binding even after bioconjugation with adaptor proteins and antibodies (see section 5.1.2).

It should be noted that, while variety of adaptor proteins, such as Protein A, Protein G, Protein A/G, and streptavidin, may be used for preparation of a universal QDot platform, it must be assured that there are no sterically accessible binding sites left on antibodies after QDot-Antibody complex formation to prevent cross-linking of different QDots via antibodies. For example, Protein A from *Staphylococcus aureus* (SpA) possesses five IgG binding sites [165], two of which are accessible simultaneously, while compatible IgG has two SpA binding sites on its Fc region, making formation of polymeric SpA-IgG complexes possible [166-169]. Indeed, complex SpA-IgG oligomer structures in solution have been previously described [167, 168]. In despite of these observations, we have successfully used SpA for preparation of a stable QDot-SpA platform (see section 5.1.2) by employing unique features of surface-bound SpA. Specifically, a divalent binding of both sites on IgG by the same or neighbor SpA molecules attached to QDot surface might be possible, thus blocking access for SpA bound to a different QDot. In solution, such a strong interaction is favored when the molar ratio of free SpA to IgG is relatively high [168]. Therefore, it is important to keep the concentration of QDot-SpA 3-5 times higher than that of IgG during the probe assembly, yielding yet greater

SpA-to-IgG excess (as multiple SpA molecules are likely present on individual QDots) and circumventing QDot surface saturation with antibodies. Furthermore, covalent attachment of SpA to nanoparticle surface might hamper formation of the aforementioned SpA-IgG oligomer structure due to steric hindrance, thus offering an additional mechanism in preventing probe cross-linking. Considering the similarity in structure and IgG binding route between SpA and protein G employed with PMAT-coated QDots (see section 5.1.1), we attribute stability of probes based on QDot-PMAT-PrG platform to the same mechanism, in addition to electrostatic stabilization via repulsion of negatively-charged particles.

5.1.1 Engineering of a universal QDot platform based on QDot-PMAT scaffold

PMAT-coated QDots represent a stable and flexible platform for preparation of bio-functional probes via direct covalent conjugation of amine-containing ligands to carboxylic acid groups. Crosslinked polymer coating provides outstanding nanoparticle stability in a variety of biologically-relevant buffers, resisting aggregation and preserving optical properties (see section 4.1), while large abundance of readily accessible reactive groups on the QDot surface facilitates covalent conjugation of biomolecules with high efficiency. At the same time, polymer encapsulation approach is quite versatile, offering efficient coating and water-solubilization of a wide range of hydrophobic nanoparticles and, thus, permitting incorporation of the newly developed QDots within our molecular profiling platform.

We have produced universal QDot probes by covalently linking adaptor protein G (recombinant PrG expressed in *E. coli*, Sigma-Aldrich) to the QDot surface at various PrG-to-QDot ratios (**Figure 5.4A**). Specifically, QDots were briefly activated with 5,000-10,000 molar excess of EDC and incubated with 5-10 molar excess PrG in 50mM Borate buffer overnight. Increasing molar excess of PrG in reaction mixture directly translated into increased number of PrG molecules conjugated to each QDot, as could be observed from the increasing

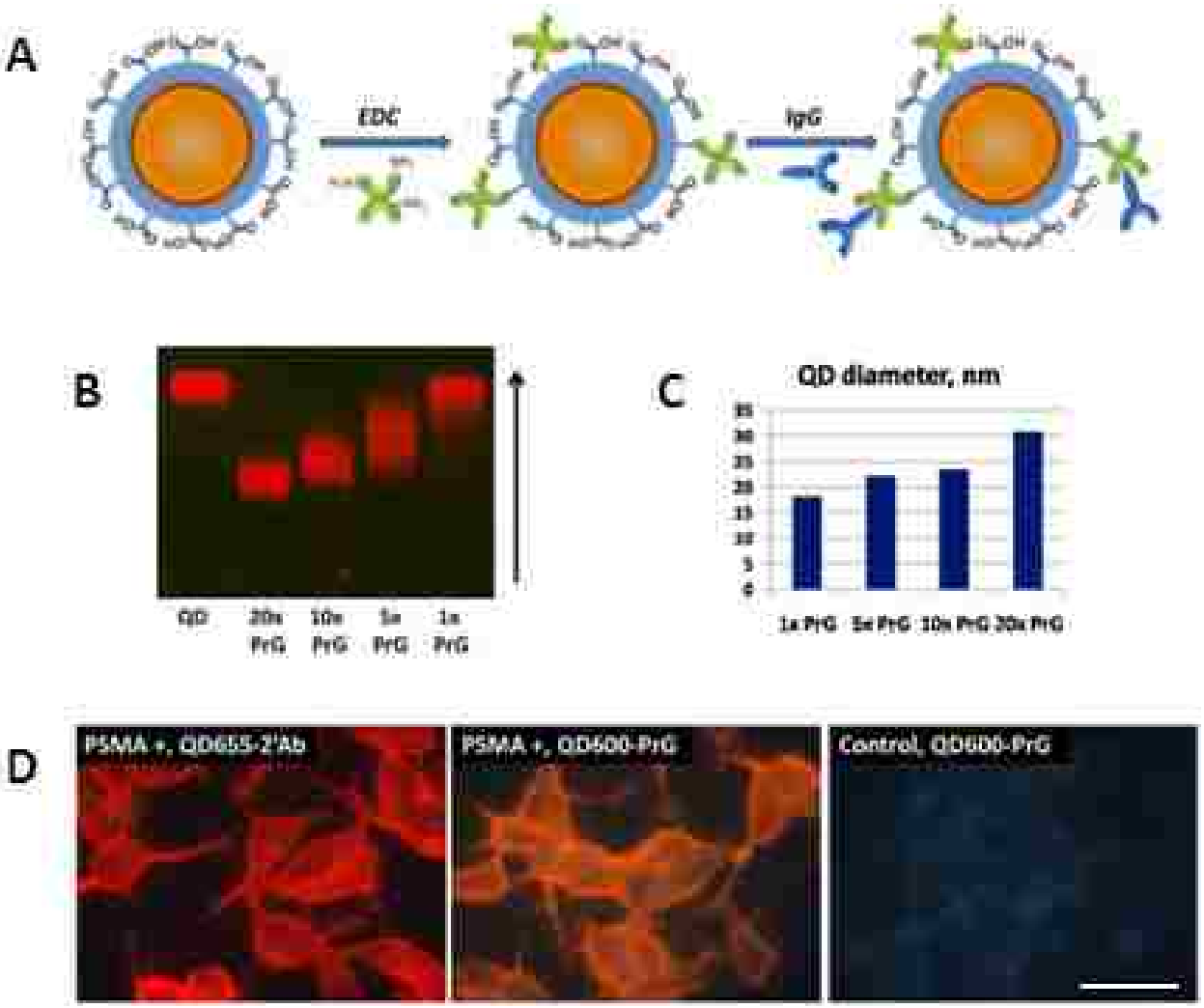

Figure 5.4 Universal QDot-PrG probe on a QDot-PMAT scaffold. (A) Adaptor protein G was covalently conjugated to QDot surface. Further mixing and incubation with IgG resulted in antibody capture by PrG, producing QDot-Antibody probes. Increasing excess of PrG to QDot during conjugation reaction resulted in higher conjugation reaction yield – QDots with higher PrG load showed slower motility in agarose gel (B) and larger hydrodynamic size (C). (D) 1-step staining with QDot-PrG-Antibody probes produced clear PSMA staining pattern on fixed LNCaP cells (middle) identical to that obtained with 2-step procedure using QDot-2'Antibody probes (left), while showing no non-specific binding to non-permeabilized cells (right). Scale bar, 50μm.

retardation of QDot-PrG motility in agarose gel (**Figure 5.4B**). At the same time, hydrodynamic size of QDot-PrG probes increased 2-3 times (up to 30 nm in diameter) upon conjugation of excessive amount of PrG (**Figure 5.4C**). Despite nearly complete shielding of the QDot surface by a layer of PrG molecules, significantly high negative charge is retained to promote the undesirable non-specific binding to permeabilized cells. Therefore, QDot-PMAT-PrG platform is limited to staining of surface targets on fixed non-permeabilized cells. In particular, we have demonstrated that staining pattern of prostate-specific membrane antigen (PSMA) on formalin-fixed prostate cancer cells (LNCaP) obtained with QDot-PMAT-PrG-Antibody probes in a 1-step staining procedure is identical to that obtained with standard 2-step staining procedure using commercial QDots functionalized with secondary antibodies (**Figure 5.4D**). At the same time, QDot-PrG probes without 1' antibodies produced no detectable non-specific staining on non-permeabilized cells, ensuring high staining specificity.

5.1.2 Engineering of a universal QDot platform based on QDot-PEG scaffold

Sensitive detection and imaging of intracellular targets with QDot-based probes require neutralization of the particle surface charge for suppression of non-specific staining in permeabilized cell and tissue specimens [77, 170, 171]. Therefore, in addition to polymer encapsulation, we have employed coating with a non-fouling layer of polyethylene glycol (PEG) and used QDot-PEG scaffolds for engineering of a universal QDot platform. As described in section 3.3, with proper specimen blocking, these particles produce no detectable non-specific specimen staining. At the same time, PEG shell can feature primary amine groups for covalent conjugation with adaptor protein. While PEG coating of QDot-PMAT scaffolds is straightforward, a number of commercial sources conveniently provide high-quality purified PEG-coated QDots for probe development. Hence, we have utilized amine-functionalized PEG-coated QDots (Qdot ITK amino (PEG) quantum dots) from Invitrogen (now part of Life

Technologies Corporation) with emission peaks centered at 525, 545, 565, 585, and 605 nm for preparation of the universal QDot platform.

Aiming at achieving straightforward orientation-controlled antibody immobilization on the QDot surface, we have built our platform with the most widely used and well-characterized adaptor protein, Protein A from *Staphylococcus aureus* (SpA, Sigma-Aldrich), which binds variety of IgG antibodies via selective non-covalent interaction with Fc region. Specifically, SpA was covalently conjugated to the QDot surface by amine-amine cross-linking. QDots were first activated with bifunctional cross-linker BS3 (Bis[sulfosuccinimidyl] suberate, Thermo Scientific). 100 µL 2 µM QDot solution in PBS was mixed with 1000 molar excess of BS3 (dissolved in deionized water at a concentration of 50 mM immediately prior to reaction) and incubated for 30 minutes at room temperature. Longer incubation time might reduce conjugation efficiency, as sulfo-NHS groups on BS3 slowly hydrolyze in aqueous buffer, thus irreversibly losing activity. Excess crosslinker was removed by passing the QDot-BS3 mixture through a NAP-5 column (GE Healthcare) pre-equilibrated with PBS. Handheld UV lamp was used to aid in the collection of activated QDots. Eluted QDots (~500 µL) were concentrated down to 50 µL with 100KDa MWCO concentrator (GE Healthcare), and 100 µL of 100 µM SpA solution in PBS (prepared from pure salt-free lyophilized SpA) was added. Concentration step is essential for achieving acceptable conjugation yield, as dilute solutions routinely fail to produce QDot-SpA bioconjugates with PEG-coated QDots. At the same time, it is important to use pure SpA stocks in amine-free buffer to preclude undesirable side-reactions and quenching of BS3. The reaction was incubated overnight at room temperature and purified by ultrafiltration for at least 6 times with Amicon Ultra 100KDa MWCO centrifugal filter (Millipore). Shorter reaction time (*e.g.* 4 hours at room temperature) can be used as well; however, additional quenching of unreacted BS3 groups with ethanolamine is advisable in this case. Continuous vortexing or other mechanical agitation should be avoided during all steps,

as it leads to QDot aggregation. Solution mixing, instead, can be achieved by pipetting or brief mild vortexing. Purified QDot-SpA probes can be stored in PBS solution at 4^0C for several months. Sodium azide might be added to a final concentration of 0.03% w/v to suppress microbial growth.

5.2 QDot-SpA-Antibody probe characterization

According to features of individual components, a universal QDot-SpA platform prepared with stable non-fouling QDot-PEG scaffold should be compatible with a range of biomedical assays, especially with labeling of molecular targets in fixed and permeabilized specimens. Therefore, all steps of molecular profiling technology development have been implemented with QDot-PEG-SpA. In assessing the utility of this platform for single-cell molecular profiling we have first validated that QDot-bound SpA preserves capacity for selective binding of IgG, while exhibiting no non-specific interaction with the specimen. Further studies have been focused on evaluating (i) staining specificity and stoichiometry of QDot-Antibody probes, (ii) probe size and staining kinetics, and (iii) probe stability and potential for crosstalk. Finally, the accuracy of HSI calibration for QDot differential brightness has been confirmed via staining of 3 different targets with all 5 QDot colors and comparing apparent staining brightness obtained with each probe.

5.2.1 Validation of preserved IgG capture by QDot-bound SpA

Capacity of the QDot-SpA platform for selective binding of IgG has been validated by labeling cytoplasmic heat shock protein 90 (HSP90) in HeLa cells with all 5 QDot colors (emission maxima at 525, 545, 565, 585, and 605 nm) in a 2-step procedure. Specifically, cells were first incubated with 300μL 1μg/mL primary mouse anti-HSP90 IgG2a for 1.5 hours, followed by washing and incubation with 300μL 20nM QDot-SpA for 1.5 hours. Characteristic

cytoplasmic staining of HSP90 achieved with this procedure (**Figure 5.5A**) indicates specific recognition of target-bound IgG with QDot-bound SpA. At the same time, control study performed by skipping the 1st step (incubation with primary anti-HSP90 antibody) yielded virtually no labeling, thus confirming the overall lack of non-specific binding by the QDot-SpA platform (**Figure 5.5C**). Taken together, preserved SpA-IgG binding capacity and resistance to non-specific interactions have enabled equally bright and specific HSP90 staining with pre-assembled QDot-SpA-Antibody probes in a 1-step procedure (**Figure 5.5B**). Specifically, probes were prepared by mixing 6μL 1μM QDot-SpA with 1.5μL 0.2mg/mL anti-HSP90 IgG2a and 0.5μL 6% BSA in TBS and incubating for 1 hour at room temperature. Following self-assembly, probes were diluted to 300μL with staining buffer and incubated with cells for 1.5 hours. Notably, since at most one QDot-SpA can bind to a target-bound antibody in a 2-step procedure, and consistent staining intensity is obtained with both 1-step and 2-step procedures (as measured by HSI, **Figure 5.5D**), these results indicate that QDot-SpA-Antibody probes produce cell staining in a stoichiometric manner, thus ensuring linearity between target abundance and measured signal intensity.

5.2.2 Evaluation of staining specificity with QDot-SpA-Antibody probes

Performance of self-assembled QDot-Antibody probes in 1-step labeling of various intracellular targets has been further assessed by staining five molecular targets separately in formalin-fixed LNCaP and HeLa cells (**Figure 5.6 and Figure 5.7 top panels**) and comparing the relative target distribution patterns with those obtained by conventional 2-step IF using commercially available QDot-labeled 2' antibodies (at 5nM final concentration) (**Figure 5.6 and Figure 5.7 middle panels**) and Alexa Fluor 568-labeled 2' antibodies (at 5μg/mL final concentration) (**Figure 5.6 and Figure 5.7 bottom panels**). The 5-target model panels used in this study (HSP90, MAOA, AR, pAkt, and ß-tubulin for LNCaP cells and Ki-67, HSP90, Lamin A, Cox-4, and ß-tubulin for HeLa cells) represent a spectrum of cell compartment localizations

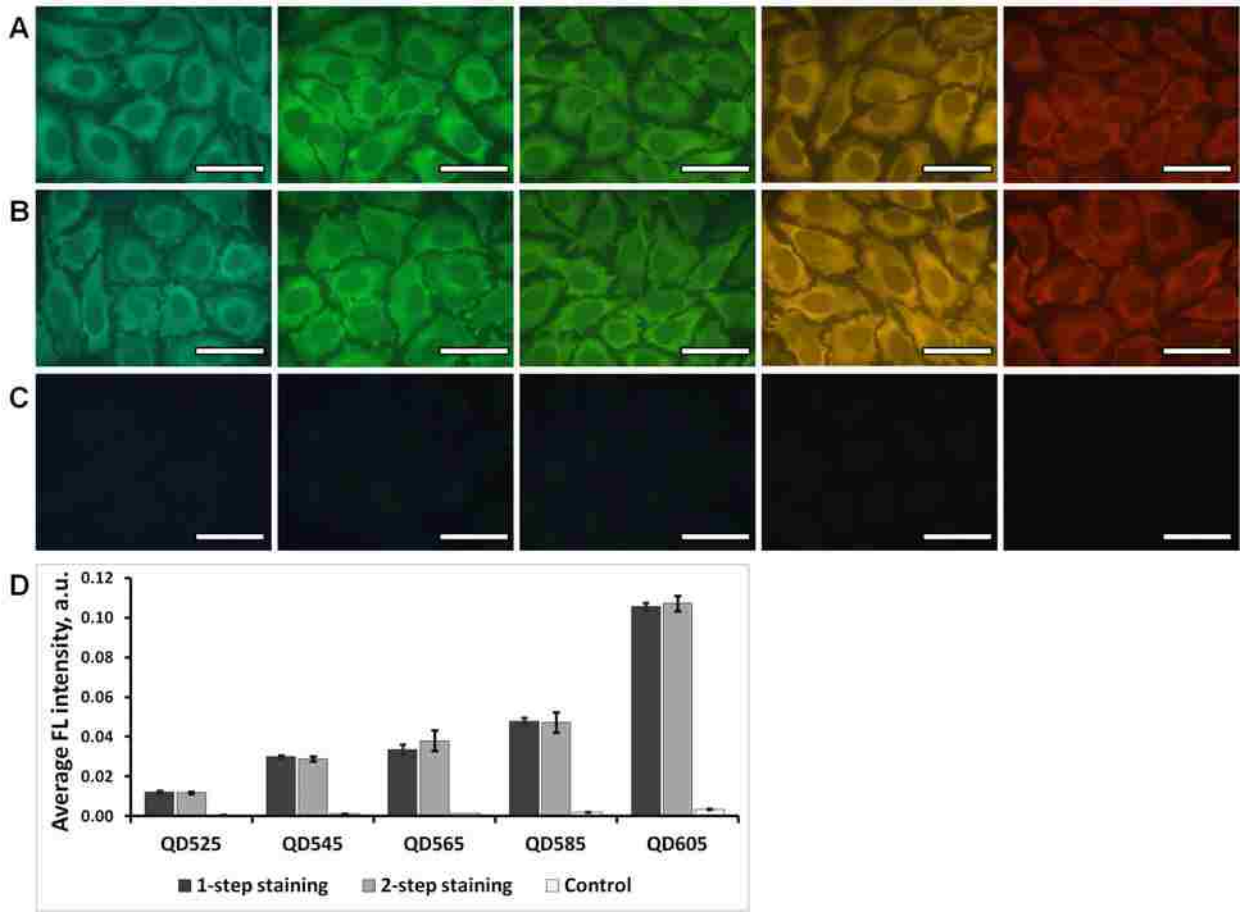

Figure 5.5 Validation of SpA-mediated QDot-Antibody probe assembly and staining stoichiometry. (A) 2-step HSP90 staining performed by first incubating cells with 1' antibody targeting HSP90, then labeling with QDot-SpA yields characteristic cytoplasmic staining, thus confirming that QDot-SpA probes recognize target-bound 1' antibodies inside cells. (B) Similarly, single-step labeling with pre-assembled QDot-SpA-Antibody probes also produces cytoplasmic staining with similar signal intensity. (C) Control staining with QDot-SpA probes (no antibodies) shows virtually no non-specific labeling. (D) Quantitative analysis of staining intensity shows identical levels of HSP90 labeling achieved via 1-step and 2-step routes, indicating stoichiometric nature of staining. Consistent imaging parameters were used for each QDot color to aid in direct comparison of staining intensity. Error bars represent standard deviation of the average staining intensity between 3 different fields of view imaged on the same specimen. Scale bar, 50μm.

and expression levels. In line with the initial evaluation, QDot-SpA-Antibody probes have produced staining results consistent with QDot-based and dye-based 2-step IF for all targets studied, indicating preserved specificity and affinity of antibodies in the QDot-SpA-Antibody complex. Importantly, despite a relatively large size, these probes have demonstrated reliable labeling of targets confined to intracellular compartments, such as nuclear AR and Ki67 and mitochondrial MAOA and Cox-4. Use of the QDot-optimized protocol described in section 3.1 has proven essential for achieving a sufficient intracellular penetration.

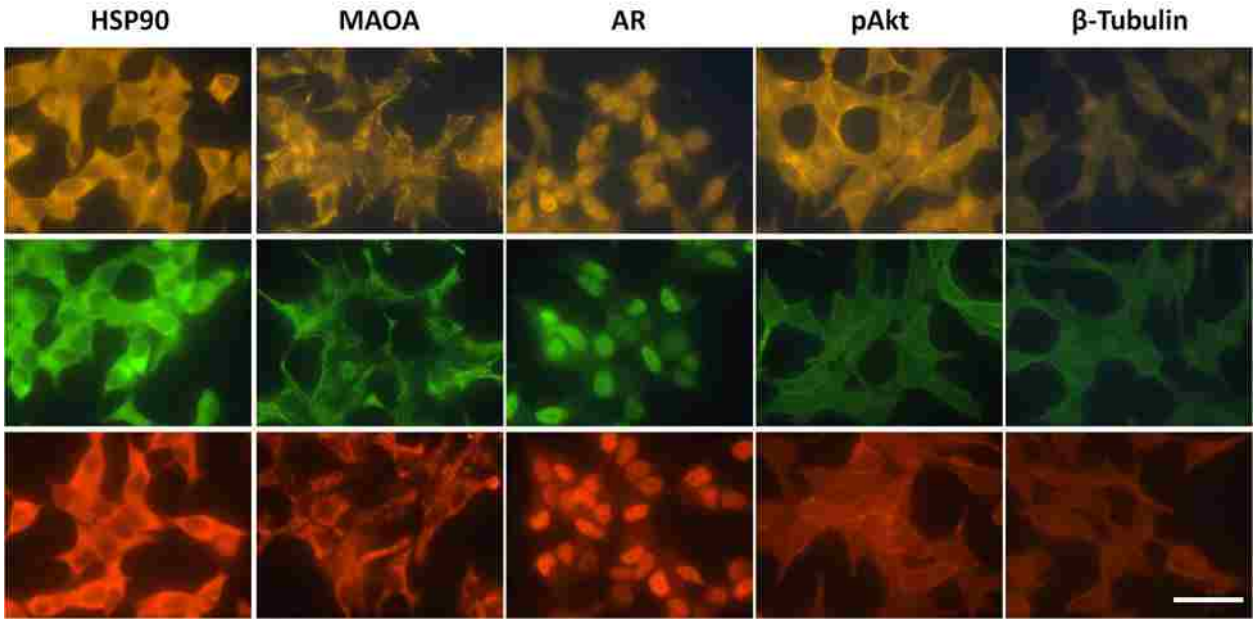

Figure 5.6 Characterization of QDot-Antibody probe specificity for staining of LNCaP cells. Five model targets (HSP90, MAOA, AR, pAkt, and ß-tubulin) are labeled with QDot585-SpA-Antibody probes in a 1-step procedure (top), producing staining patterns consistent with those obtained with either QDot565-labeled (middle) or Alexa Fluor 568-labeled (bottom) 2' antibodies in a conventional 2-step staining. Scale bar, 50µm.

5.2.3 Measurement of staining kinetics with multicolor QDot probes

Consistent kinetics of staining with different QDot probes, necessary for achieving the same degree of target labeling regardless of the QDot probe used, has been verified for QDots

emitting at 525 and 605 nm, which represent nanocrystals with smallest and largest inorganic cores respectively. HSP90 was stained in 12 separate specimens (12 wells of a glass-bottom 24-well plate) by either QDot525-SpA-IgG or QDot605-SpA-IgG probes. Staining was allowed to proceed for 30, 60, 90, 120, 150, or 180 minutes before specimens were washed and imaged.

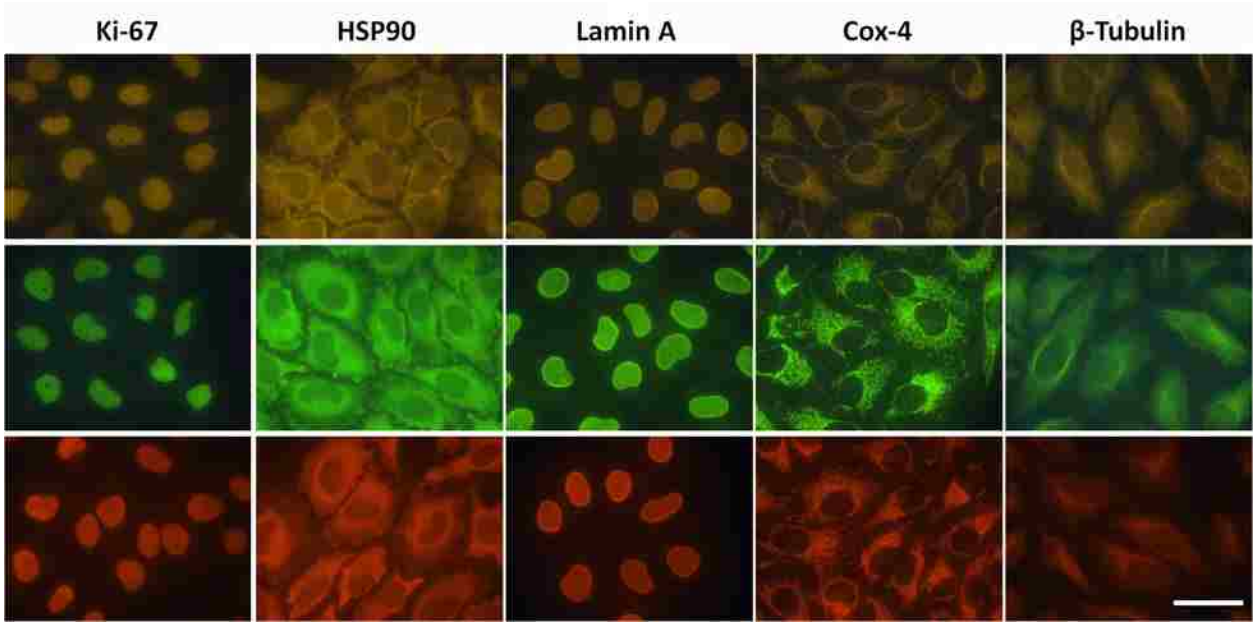

Figure 5.7 Characterization of QDot-Antibody probe specificity for staining of HeLa cells. Five model targets (Ki-67, HSP90, Lamin A, Cox-4, and β-tubulin) are labeled with QDot585-SpA-Antibody probes in a 1-step procedure (top), producing staining patterns consistent with those obtained with either QDot565-labeled (middle) or Alexa Fluor 568-labeled (bottom) 2' antibodies in a conventional 2-step staining. Scale bar, 50μm.

As shown in **Figure 5.8**, both probes demonstrate comparable staining specificity and evolution of signal intensity with increasing incubation time. HSI-based quantitative analysis shows steady increase in staining intensity through the first 2 hours of incubation, mostly reaching a plateau at longer time (**Figure 5.8B**). Importantly, regardless of staining duration both probes produce nearly identical signal intensity, yielding consistent staining kinetics (note, QDot525 signal is adjusted by a correction factor of 9.7 for direct comparison with QDot605, as indicated in Table 3.1). To explain such behavior we have performed

hydrodynamic size (diameter) measurements with dynamic light scattering on 1μM QDot-SpA solutions in TBS. Interestingly, while inorganic core size of different QDots varies substantially, overall hydrodynamic size of PEG-coated water-soluble QDots, being mostly defined by organic coatings rather than by the core size, remains similar (**Figure 5.8C, dark bars**). Further functionalization with SpA results in slight QDot size increase, but does not introduce disparity in sizes of different QDot-SpA probes, offering uniform diffusion, and thus staining, kinetics throughout all QDot probes used (**Figure 5.8C, light bars**).

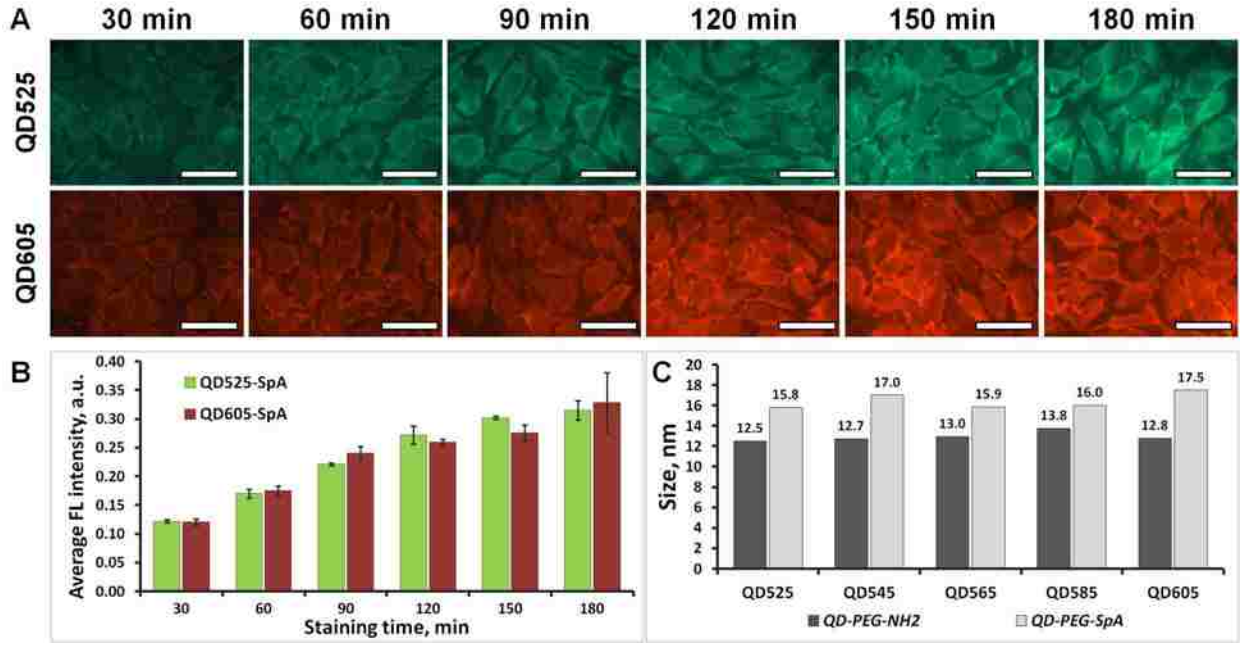

Figure 5.8 Evaluation of staining kinetics with QDot-SpA-Ab probes. (A) HSP90 is stained by either QDot525-SpA-Antibody (smallest inorganic core) or QDot605-SpA-Antibody (largest inorganic core) probes for various amounts of time (30-180 minutes), exhibiting continuous increase of staining intensity with both probes. (B) HSI-based analysis is utilized for quantitative assessment of staining kinetics. QDot525 signal is adjusted by a correction factor of 9.7 for direct comparison with QDot605. (C) DLS measurements reveal lack of variability in the size of PEG-coated QDots (dark bars). Functionalization with SpA results in slight QDot size increase, but does not introduce size disparity (light bars). Error bars represent standard deviation of the average staining intensity between 3 different fields of view imaged on the same specimen. Scale bar, 50μm.

5.2.4 Characterization of the QDot-SpA-Antibody probe stability

Particular attention has been dedicated to systematic characterization of the QDot-SpA-Antibody probe stability, as it is critical for preventing probe crosstalk and achieving accurate target labeling with a multiplexed 1-step staining procedure. In particular, we have employed non-covalent self-assembly between SpA and IgG to satisfy technology design criterion of simple and quick probe preparation. Since SpA binds a wide range of antibodies with an intermediate affinity (Kd ~10^{-8}-10^{-10} M), simple mixing of QDot-SpA platforms with primary antibodies at a slight excess should yield a nearly complete capture of antibodies, thus preventing binding of free IgG to vacant SpA sites on different QDot-SpA probes in a multicolor cocktail. However, considering that all QDot-SpA-Antibody probes form via the same non-covalent SpA-IgG bond, spontaneous probe dissociation, antibody exchange, and crosstalk between different probes (*i.e.* labeling of a wrong target by QDot-SpA due to capture of free or specimen-bound IgG during multiplexed staining procedure) cannot be completely ruled out. To evaluate this important parameter, we have studied the SpA-IgG dissociation kinetics using SPR (surface plasmon resonance)-based real-time analysis and assessed QDot-SpA-Antibody probe stability and potential for crosstalk experimentally with dual-color staining.

For SPR studies, SpA was immobilized on dextran-coated chip, and binding of excess rabbit anti-mouse IgG to immobilized SpA in reference to control unmodified surface was recorded. Interestingly, we have observed an overall lower binding affinity when analyte is injected at high concentration (250nM – 4μM) with a Kd up to 100 times higher than that for low-concentration (10nM – 250nM) analyte. Furthermore, measurements of binding and dissociation kinetics have shown a non-linear behavior, which is especially pronounced for the high-concentration analyte. This observation is consistent with early reports suggesting that

slow binding-dissociation by strong binding sites is accompanied with fast binding-dissociation via weak sites, especially when strong sites are saturated [172].

In light of the divalent SpA-IgG binding model, we hypothesize that strong binding with slow kinetics might occur due to capture of both IgG binding sites by two different sub-units of the same SpA (which is favored under non-saturating conditions [167, 168]) or two neighbor surface-bound SpA molecules, while monovalent SpA-IgG binding results in weak and fast interaction (under saturating conditions). Indeed, in the relatively low concentration range, the dissociation curve for 100nM rabbit antibodies shows an initial fast drop in signal, accounting for about 5% loss of bound antibodies, followed by a very slow dissociation (**Figure 5.9A**). The same measurements performed with 10nM antibodies, which is consistent with the final IgG concentration used in the staining experiments, show nearly no SpA-IgG dissociation

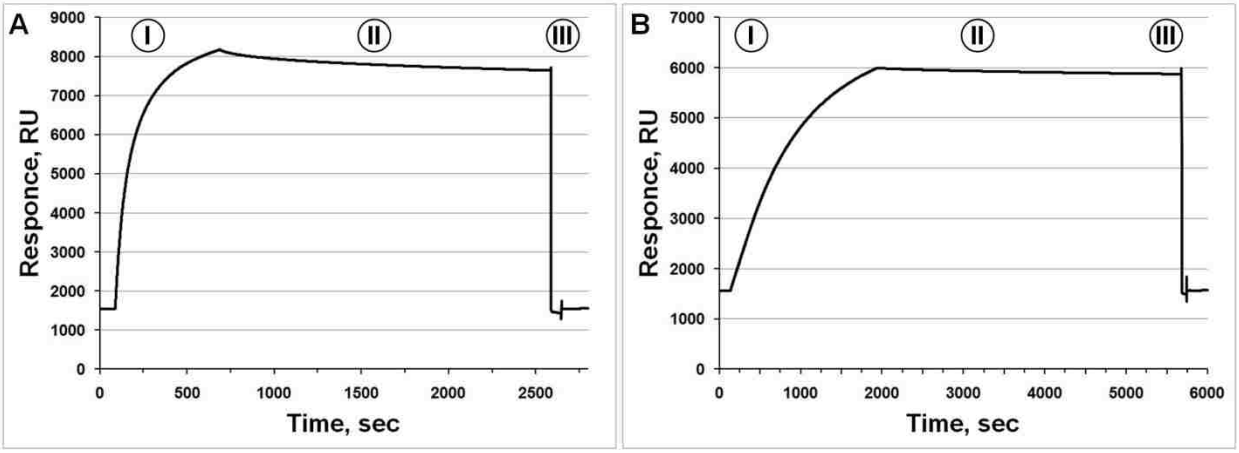

Figure 5.9 SPR analysis of SpA-Antibody bond stability. *Binding (phase I) and dissociation (phase II) of free rabbit anti-mouse IgG to SpA immobilized on the surface of C5 chip is monitored. (A) At 100nM antibody concentration fast saturation of surface binding sites during binding phase and quick initial dissociation of antibodies followed by very slow dissociation kinetics during dissociation phase can be observed. (B) At 10nM antibody concentration only slow dissociation can be observed, yielding an overall retention of >97% bound IgG after 1 hour of washing. Phase III represents chip surface regeneration with low-pH buffer.*

for 60 minutes (**Figure 5.9B**). These results suggest that the SpA-IgG dissociation kinetics is sufficiently slow at the concentration range and time-frame of the cell staining procedure to prevent QDot-SpA-Antibody probe disassembly and release of free antibodies in solution. We should note once again, however, that it is essential to use excess of QDot-SpA over antibodies in the initial probe assembly step to favor formation of stable SpA-IgG bonds and avoid QDot-SpA surface saturation.

To further test the QDot-SpA-Antibody stability and directly answer the question whether crosstalk exists in multicolor cell staining, we have performed dual-color labeling of Lamin A (nuclear envelope protein) in HeLa cells. Specifically, we prepared two QDot-SpA-Antibody probes emitting at 545 and 585 nm using rabbit anti-Lamin A IgG. Immediately before staining, we mixed fully assembled QDot-SpA-Antibody probes with counterpart non-complexed QDot-SpA (*e.g.* QDot545-SpA-IgG mixed with QDot585-SpA, or QDot585-SpA-IgG with QDot545-SpA) and incubated cells with this solution for 1.5 hours. If crosstalk exists, with this setup, the large excess of vacant counterpart QDot-SpA probes would bind any free antibodies released from the QDot-SpA-IgG probes and compete for target binding. In particular, QDot545-SpA and QDot585-SpA platforms mixed together with anti-Lamin A antibodies and incubated with cells efficiently captured free IgG from solution and produced mixed-color Lamin A staining with nearly 50% contribution each, confirming successful capture of free IgG from solution by both probes (**Figure 5.10A**).

Remarkably, we did not observe any crosstalk or interference with either QDot545 or QDot585 pre-assembled probes (**Figure 5.10B,C,D**). Furthermore, presence of a competitor QDot-SpA probe did not interfere with target staining by the pre-assembled QDot-SpA-Antibody probe, as observed signal intensity in a two-probe mixture was comparable to that of 1-color staining experiments in the absence of a competitor probe (**Figure 5.10E**).

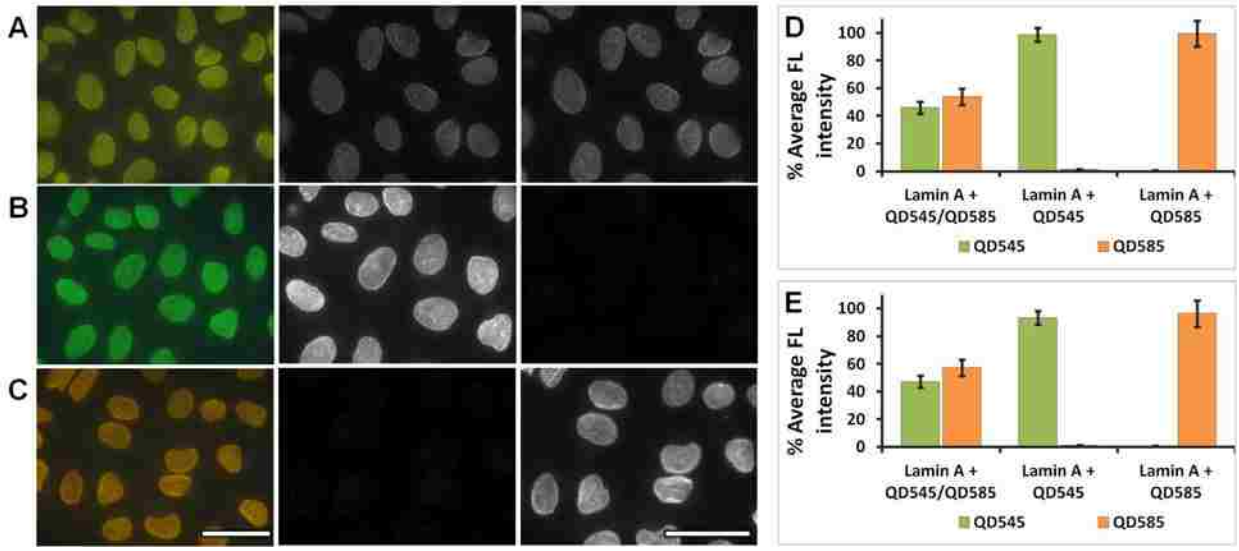

Figure 5.10 Assessment of the QDot-SpA-Antibody probe stability and cross-talk. QDot545-SpA and QDot585-SpA mixed with primary antibodies and immediately applied to cells produce Lamin A staining with approximately 50% contribution from each (A, D). At the same time, regardless of whether QDot545 (B) or QDot585 (C) is pre-assembled with anti-Lamin A antibody, only the pre-assembled probe shows specific nuclear envelope staining, solely contributing to all fluorescence signal registered (D). HSI is used to unmix true-color images (left column) into individual QDot545 (middle column) and QDot585 (right column) channels, remove background, and perform quantitative analysis. Staining intensity from a 2-probe mixture is reported in reference to an overall signal detected (D) and in reference to single-probe staining performed separately (E). Brightness of individual QDot channels is normalized to aid in direct comparison of staining intensity. Intensity of the QDot545 channel is scaled up by a factor of 2 relative to QDot585 channel to compensate for differential QDot brightness. Error bars represent standard deviation of the average staining intensity between 3 different fields of view imaged on the same specimen. Scale bar, 50μm.

From these two independent measurements (SPR analysis and cell staining), we conclude that pre-formed QDot-SpA-Antibody complexes, featuring very slow dissociation kinetics and sterically blocked access to bound antibodies, do not exchange antibodies with other vacant QDot-SpA platforms within the concentration range and time-frame of the cell staining experiment. Additionally, slow diffusion of the relatively large QDot-SpA bioconjugates might further reduce capacity for re-capture of rare free IgG that might be spontaneously released by the QDot-SpA-Antibody probes. This cornerstone property of the QDot-SpA platform forms the foundation for reliable and specific parallel multiplexed staining.

5.2.5 Quantitative analysis of staining with multicolor QDot probes

Finally, we have validated the accuracy of correction factors for adjusting differential QDot brightness and assessed utility of QDot-SpA-Antibody probes for quantitative analysis of staining intensity. Specifically, we performed staining of three model targets localized to different intracellular compartments (Lamin A for nuclear membrane, HSP90 for cytoplasm, and Cox-4 for mitochondria) in HeLa cells with all 5 QDot colors, used HSI for image acquisition and signal analysis, and independently compared differential QDot brightness obtained from individual cell staining experiments and bulk fluorescent measurements (**Figure 5.11**). Consistency of observed differential QDot brightness indicates unhampered access of all QDot-SpA-Antibody probes to intracellular targets and corroborates robustness of HSI-based quantitative analysis of staining intensity. It should be emphasized once again, that variations in imaging instrumentation (*e.g.* different excitation source, wavelength-dependent camera sensitivity) might also affect measured relative QDot brightness. Therefore, assessment of differential QDot brightness should be done for each QDot-SpA batch and for each imaging setup used for quantitative analysis.

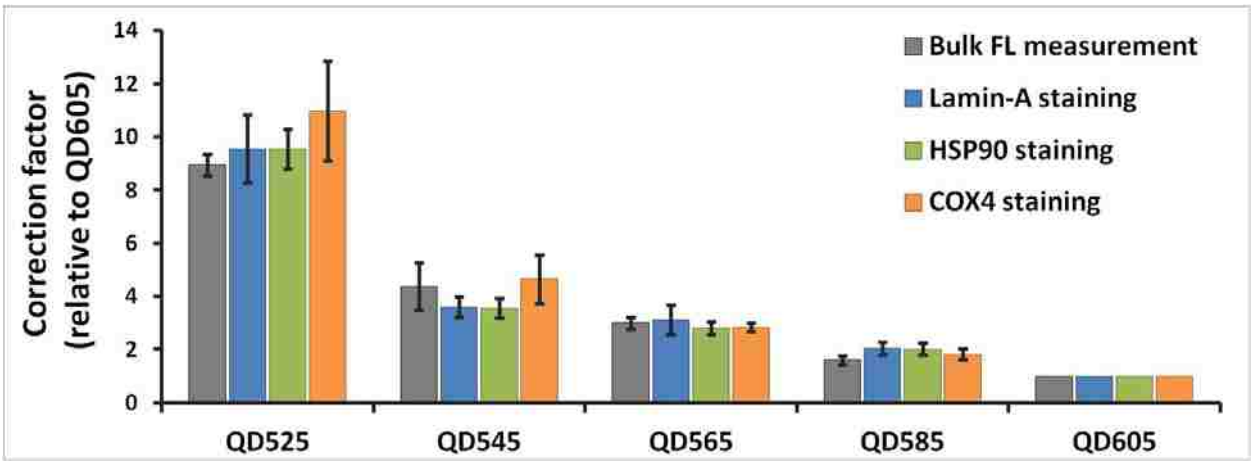

Figure 5.11 Validation of correction factors for quantitative analysis with multicolor QDot probes. Accuracy of correction factors obtained from bulk fluorescence measurements is confirmed by separately staining 3 different molecular targets (Lamin A, HSP90, and Cox4) with all 5 QDot colors in a singleplexed format in HeLa cells and independently comparing differential QDot brightness obtained from cell staining. Error bars represent standard deviation of average signal intensity between 3 different fields of view imaged for cell staining and between 3 different experiments for bulk fluorescence measurements.

5.3 Multiplexed 1-step staining of cultured cells and FFPE tissues

Fixed cultured cells represent a versatile model system for a number of biomedical studies, including examination of signaling pathways, elucidation of cell response to therapeutic intervention, and assessment of pathology-specific molecular signatures. Therefore, we have evaluated the performance of 1-step labeling of multiple targets with self-assembled QDot-Spa-Antibody probes on cultured cells, ensuring that reliable qualitative and quantitative analysis of at least 5 targets can be achieved with our technology. Probe characterization studies have established proper efficiency of probe assembly, sufficient stability of pre-assembled probes, and preserved biological activity of QDot-bound primary antibodies. As a result, it should be straightforward to accomplish simultaneous 5-color

staining through simple mixing of five different pre-assembled QDot-SpA-Antibody probes in a single cocktail for target labeling. The only remaining concern not addressed to this point is the potential interference and non-specific interaction between multiple probes applied in a staining cocktail.

In evaluating the behavior of individual probes in a multiplexed staining cocktail, we have compared the intracellular target distribution and relative abundance (measured by HSI) obtained with (i) multiplexed, (ii) singleplexed multicolor, and (iii) singleplexed single-color staining. Singleplexed multicolor staining eliminates possibility of interaction between dissimilar QDot probes (as only one target is labeled), while labeling each target with the same probe as used in a multiplexed cocktail, thus facilitating assessment of the cocktail composition on the performance of individual probes. Singleplexed single-color staining, in turn, labels all targets separately with the same QDot color, thus highlighting any discrepancies in a behavior of different probes. Specifically, we performed 1-step staining of five model molecular targets (Ki-67, HSP90, Lamin A, Cox-4, and ß-tubulin) in HeLa cells. Individual QDot-SpA bioconjugates (emitting at 525, 545, 565, 585, and 605 nm respectively) and corresponding antibodies were first assembled separately, and then pooled together for staining. In particular, 6µL 1µM QDot-SpA was mixed with 1.5µL 0.2mg/mL primary target-specific rabbit IgG and 0.5µL 6% BSA for 1 hour at room temperature. Then probes were combined in a single microcentrifuge tube for multiplexed staining (or kept separate for singleplexed staining), diluted to 300µL with staining buffer, and incubated with cells for 1.5 hours. HSI reveals that the QDot-SpA-Antibody probes can reliably detect intracellular distribution and relative expression levels of different targets regardless of their cellular location (**Figure 5.12**). Importantly, identical relative target expression profiles are obtained with multiplexed, singleplexed multicolor, and singleplexed single-color staining, confirming

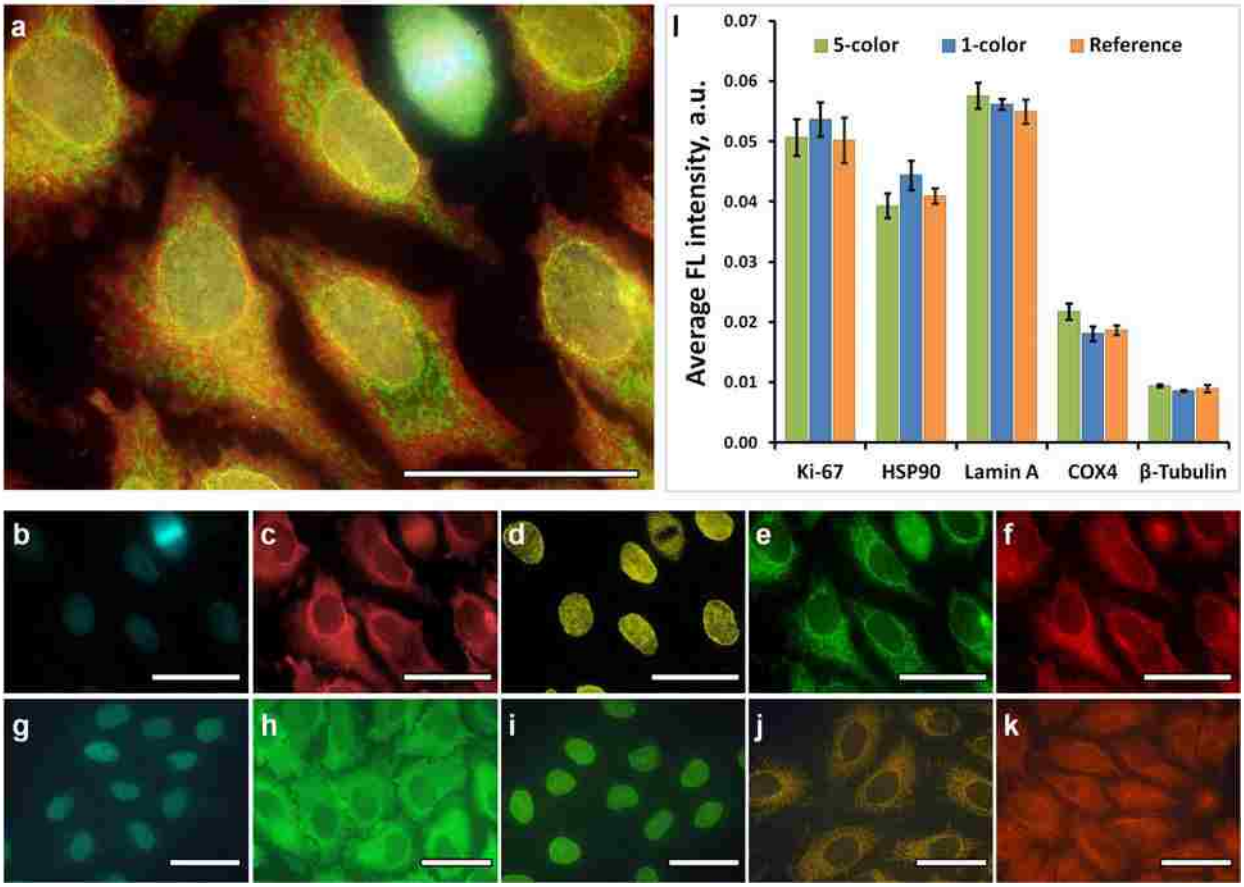

Figure 5.12 Multiplexed cell staining with 5 pre-assembled QDot-SpA-Antibody probes. Ki-67, HSP90, Lamin A, Cox-4, and ß-tubulin are simultaneously stained with a panel of 5 QDot-SpA-Antibody probes (a). HSI is used to extract individual QDot channels (b-f), perform quantitative analysis of staining intensity (l), and reconstruct a false-color composite image (a). Staining patterns obtained in this manner (b-f) are consistent with single-color staining performed with color-matched QDot probes (g-k). Average staining intensities measured with multiplexed staining (5-color bars in l) are consistent with quantitative analysis performed with singleplexed staining using either color-matched QDot-SpA-Antibody probes (1-color bars in l) or reference singleplexed staining performed with same QDot585-SpA-Antibody probe for all targets (Reference bars in l). Error bars represent standard deviation of the average staining intensity between 3 different fields of view imaged on the same specimen. Scale bar, 50µm.

lack of adverse interference between probes in a cocktail and robustness of quantitative signal analysis in a multiplexed format. It is also worth emphasizing once again, that in this multicolor unmixing process the remarkable brightness and photostability of QDots enables reliable image acquisition by scanning through a broad spectral range with narrow bandwidth, while less stable organic fluorophores would rapidly quench during imaging. Taken together, our studies unambiguously demonstrate the utility of self-assembled QDot-SpA-Antibody probes for performing multiplexed labeling and quantitative analysis on cultured cells.

Similarly, we have performed a 3-color staining of Histone H3, ß-Tubulin, and Ki-67 in FFPE prostate tissue microarrays using QDot-SpA-Antibody probes emitting at 565, 585, and 605 nm respectively. First, we re-hydrated specimens according to conventional IHC protocol. Then we performed high-temperature antigen retrieval by incubating slides in pH6 Sodium Citrate buffer with 0.1% Tween-20 in a pressure cooker for 5 minutes and slowly cooling to room temperature for 20 minutes. Finally, slides were washed with TBS, blocked with 2%BSA/0.1%Casein/TBS and incubated with all pre-assembled QDot-SpA-Antibody probes in 6%BSA/TBS for 1.5-2 hours. Following staining, slides were washed, thoroughly dehydrated, and coverslipped using QDot mounting medium (Life Technologies Corporation). Imaging of stained TMAs revealed characteristic staining patterns for all 3 targets (**Figure 5.13A,D**). Notably, multiplexed 1-step staining with self-assembled probes (**Figure 5.13A**) is completely consistent with separately performed singleplexed 2-step staining with commercial QDot-2'Antibody bioconjugates (**Figure 5.13C**). At the same time, control QDot-SpA probes lacking primary antibodies produced only minimal non-specific binding (**Figure 5.13B**). HSI proved especially helpful in removal of the strong tissue autofluorescence signal and accurate unmixing of individual QDot channels. Preliminary affirmative results reported here encourage further evaluation of this technology on variety of FFPE tissue specimens to establish its utility for molecular profiling of clinical specimens. We note, in particular, that off-target

binding by SpA to human IgG, which might be present in tissue specimens, could require additional specimen blocking with free SpA. Poor penetration of large QDot-SpA-Antibody complexes within cross-linked tissue specimens might result in unreliable target labeling, thus calling for modifications in specimen processing protocol and preparation of smaller QDot probes. Finally, development of a universal antigen retrieval methodology might be necessary to ensure robust simultaneous staining of multiple molecular targets within the same tissue specimen.

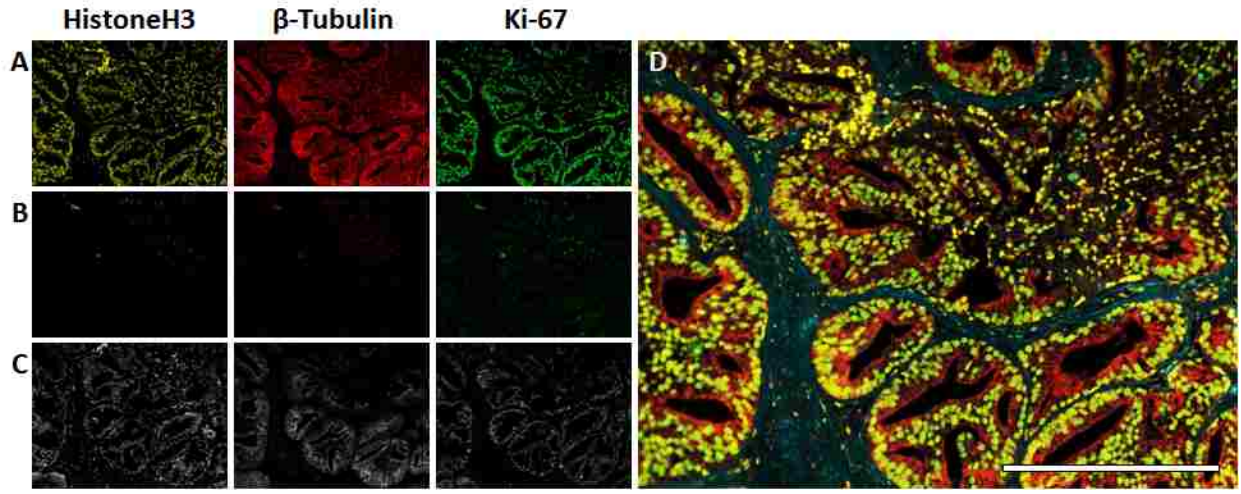

Figure 5.13 Multiplexed 1-step staining of FFPE tissue with self-assembled QDot-SpA-Antibody probes. Incubation of prostate TMAs with a cocktail of 3 QDot probes against Histone H3, ß-Tubulin, and Ki-67 produced characteristic staining patterns in individual QDot channels (A) and yielded a 3-color image (D, with autofluorescence false-colored in cyan). In a control experiment, same probes lacking primary antibodies produced nearly no non-specific staining (B). Notably, staining patterns observed with a 1-step multiplexed staining methodology are completely consistent with those obtained via a conventional 2-step procedure with commercial QDot-2'Antibody bioconjugates (C, shown in grayscale). Scale bar, 250μm. This work was performed in collaboration with Prof. Lawrence True, MD, PhD from the UW Pathology.

5.4 Summary

Direct labeling of molecular targets with multicolor QDots represents the most straightforward approach to utilizing the unique analytical capabilities of these probes. However, requirement for custom preparation of QDot-Antibody bioconjugates, currently performed with technically complex and expensive covalent conjugation procedures, hampers ready adoption of direct labeling approach for addressing biomedical research needs. In contrast, universal QDot-SpA platform described in this chapter offers a simple route for small-scale on-demand purification-free preparation of fully functional QDot-SpA-Antibody probes via non-covalent self-assembly, thus significantly lowering cost, streamlining assay development, and making this method accessible to a wide range of biomedical researchers. With such a versatile platform, preparation of extensive QDot-Antibody libraries becomes easily achievable. Notably, complementary multiplexed staining methodology optimized for use with QDot-SpA-Antibody probes has demonstrated capacity for stoichiometric target labeling and accurate qualitative and quantitative analysis of at least 5 molecular targets in a quick 1-step staining procedure, thus offering a platform for initial single-cell molecular profiling studies.

CHAPTER 6: ANTIGEN ENCODING FOR MULTIPLEXED 2-STEP STAINING

Single-step staining with universal QDot probes described in Chapter 5 offers a simple and direct route for multiplexed quantitative analysis of molecular targets in fixed cultured cells and tissue specimens. Multi-step labeling methodologies, in turn, offer greater flexibility in fine-tuning staining parameters and relax strict criteria for QDot probe design. Specifically, since antibodies and QDots can be applied to specimens in separate steps, the size of individual probes can be substantially reduced, yielding improved staining kinetics and reduced steric hindrance to target recognition. At the same time, staining conditions can be separately tailored to antibodies and QDots, improving specificity and lessening non-specific binding to the specimen. Finally, signal amplification can be employed through multi-step procedure to achieve higher sensitivity of detection. These features are particularly beneficial for applications where highly crosslinked specimens with limited intracellular access are used or when analysis of low-abundance or diffusely expressed targets is desired. Therefore, in addition to a single-step labeling approach, we have further expanded the QDot molecular profiling platform by developing an alternative 2-step multiplexed staining methodology with QDot probes.

Conventional 2-step staining procedures utilize links with no (*e.g.* streptavidin/biotin) or limited (*e.g.* primary/secondary antibodies) selectivity, thus prohibiting highly multiplexed target detection (**Figure 6.1A**). In contrast, we have employed highly selective DNA links to achieve unique assignment of QDot probes to corresponding molecular targets (**Figure 6.1B**). Specifically, each target is first encoded with a unique ssDNA (single-stranded

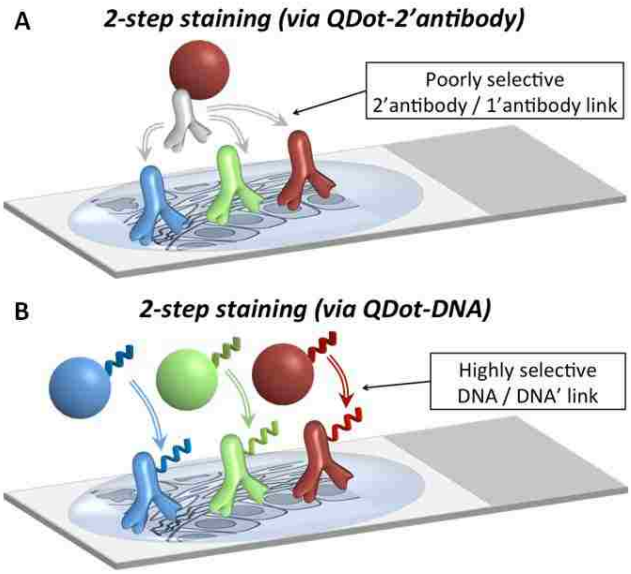

Figure 6.1 Methodologies for 2-step staining with QDots. (A) Conventional procedure utilizing poorly selective intermediate links hampers multiplexed staining. (B) Antigen encoding followed by QDot labeling via DNA linker, in contrast, offers suitable route for labeling of targets with unique QDot probes.

oligonucleotide) tag through recognition by ssDNA-labeled primary antibody. Conversion of target antigenicity information into a DNA sequence code enables performance of a highly multiplexed FISH-like staining procedure with complementary QDot-ssDNA' probes, followed by signal read-out with fluorescence microscopy and HSI (**Figure 6.2**). With this method design, simultaneous DNA encoding of a large number of molecular targets becomes possible, while permitting parallel QDot labeling and analysis of up to 10 targets (currently limited by the availability of suitable QDot scaffolds and unmixing capabilities of HSI).

In implementation of our strategy we have focused on developing the three main components: (i) ssDNA-labeled primary antibodies (Ab-ssDNA); (ii) ssDNA-functionalized QDot

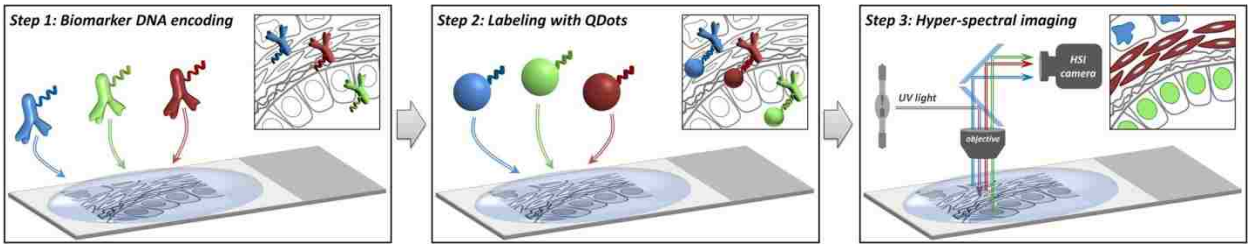

Figure 6.2 Key steps of a multiplexed 2-step staining methodology. Target encoding with unique DNA tags converts antigen information into a DNA sequence. De-coding is then done by hybridization with complementary multicolor QDot-DNA' probes and analysis with HSI.

probes (QDot-ssDNA); and (iii) multiplexed 2-step staining methodology that utilizes DNA-encoding approach for simultaneous labeling of at least 5 molecular targets. Notably, this strategy implies substantial flexibility in probe design depending on particular application needs. We anticipate that two major areas of application will evolve: 1) routine screening of specimens for a pre-defined panel of molecular targets and 2) explorative studies of a wide range of targets. First application comprises of robust specimen staining using stock reagents and well-defined conditions, thus requiring development of methodology for preparation of stable antibody-ssDNA and QDot-ssDNA probe stocks. In contrast, second application involves continuous probe and condition optimization, thus calling for flexibility and simplicity of on-demand small-scale custom probe preparation. We address these needs by employing two strategies in probe engineering: covalent conjugation and non-covalent self-assembly respectively. In particular, labeling of primary antibodies with ssDNA has been achieved with 3 distinct routes (**Figure 6.3**): (i) covalent conjugation with reduced IgG via reaction with sulfhydryl group in Fc region; (ii) covalent conjugation with whole IgG via cross-linking with primary amines; and (iii) non-covalent self-assembly of intact whole IgG with ssDNA-labeled Fc-specific secondary antibodies or Fab fragments. Likewise,

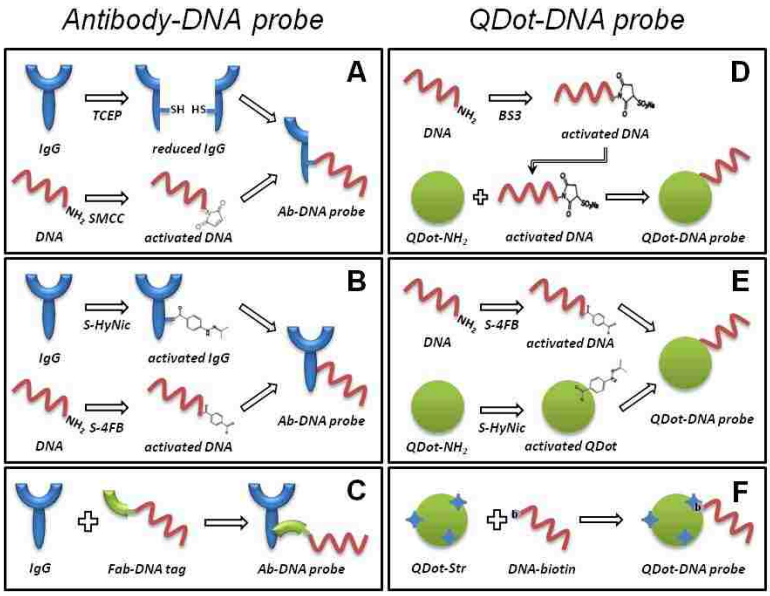

Figure 6.3 Strategies for Antibody-DNA and QDot-DNA probe preparation. Covalent bioconjugation (A,B,D,E) can be employed for preparation of stable stocks, whereas non-covalent self-assembly (C,F) is suitable for small-scale exploratory studies.

preparation of QDot-ssDNA probes has been done based on QDot-PEG scaffold through (i) covalent ssDNA conjugation to the amine-functionalized QDot surface via amine-amine crosslinking and (ii) non-covalent binding of biotinylated ssDNA by streptavidin-functionalized QDots via streptavidin/biotin interaction. In addition, we have explored an alternative route for preparation of compact QDot-ssDNA probes by employing zwitterionic QDot scaffolds and direct covalent conjugation. Each approach has benefits and drawbacks in terms of complexity and yield of conjugation reaction, control over the final structure of bioconjugates, and stability of probes. Therefore, a combination of different methods presented here should provide a versatile staining platform capable of addressing specific needs of a wide range of applications.

6.1 DNA link design

DNA-encoded antibodies prepared with a variety of covalent and non-covalent procedures have been used for a number of bio-analytical methods [173, 174]. At the same time, QDot-oligonucleotide probes have been developed for DNA detection and FISH applications [92, 93, 157, 175-177]. Among these studies, the length and structure of DNA link varies significantly, as different criteria have to be satisfied. However, 12-16 base-pair (bp) overlap appears to be optimal for providing sufficient bond strength, while minimizing formation of unfavorable secondary structures or significant cross-hybridization between non-matching probes. Therefore, to provide a foundation for further application-specific optimization we have designed a panel of 5 unique 16bp oligonucleotide pairs (Table 6.1). Each ssDNA carries a 5' primary amine group on a short PEG spacer to enable covalent conjugation to antibodies and QDots. In addition, a set of biotinilated ssDNA has been used for preparation of probes on QDot-Streptavidin scaffold. Each probe features balanced base content, melting temperature above 45^0C, lack of secondary structures at room temperature, and no more than 4bp homo-

dimers or hetero-dimers with non-matching probes. This set of parameters ensures the unique match between DNA-encoded target and complementary QDot without probe cross-talk even at non-stringent hybridization conditions. HPLC-purified oligonucleotide sequences were purchased from IDT DNA. All DNA analysis was performed with IDT DNA Oligo Analyzer.

Table 6.1 DNA links for antigen encoding

ssDNA	Sequence
1	*5' - (NH_2) - (iSp18) - ATTTCTTGGTGCGACG - 3'*
1'	*5' - (NH_2 or biotin) - (iSp18) - CGTCGCACCAAGAAAT - 3'*
2	*5' - (NH_2) - (iSp18) - ACGTATGGCAAGTCTA - 3'*
2'	*5' - (NH_2 or biotin) - (iSp18) - TAGACTTGCCATACGT - 3'*
3	*5' - (NH_2) - (iSp18) - CCTGGTCTCAAGAATT - 3'*
3'	*5' - (NH_2 or biotin) - (iSp18) - AATTCTTGAGACCAGG - 3'*
4	*5' - (NH_2) - (iSp18) - TGGAGTTTGGGCAGAT - 3'*
4'	*5' - (NH_2 or biotin) - (iSp18) - ATCTGCCCAAACTCCA - 3'*
5	*5' - (NH_2) - (iSp18) - AGATGACGCTTGGGAA - 3'*
5'	*5' - (NH_2 or biotin) - (iSp18) - TTCCCAAGCGTCATCT - 3'*

6.2 Labeling of primary antibodies with ssDNA tags

Encoding of molecular targets with unique DNA tags represents an essential step of the multiplexed QDot staining technology presented here, as encoding directly converts target antigenicity into a DNA sequence code without loss of information. In a sense, histological specimen gets converted into a DNA array, where position and density of oligonucleotides are governed by target distribution and expression levels. DNA sequences, in turn, can be de-coded (*i.e.* labeled and analyzed) in a highly multiplexed manner by employing selectivity of complementary DNA hybridization, unique optical properties of QDots, and analytical

capabilities of HSI. Therefore, great attention has been devoted to development of simple and robust procedures for labeling of primary antibodies with ssDNA tags.

Preparation of a library of antibody-ssDNA bioconjugates has been achieved either via covalent conjugation between primary antibodies and amine-functionalized oligonucleotides or non-covalent self-assembly with between primary antibodies and species-matched Fc-specific ssDNA-labeled secondary half-antibodies or Fab fragments. It should be noted that antibody-DNA probes are successfully used in a number of assays (such as immuno-PCR), exhibiting minimal to no impact of DNA tags onto antibody functionality [173, 174]. At the same time, to this point the use of DNA-labeled antibodies for multiplexed molecular target detection within fixed cells and tissue specimens has not been carefully explored. The potential for major off-target binding originating from ssDNA tags (either through electrostatic interaction, hybridization with intracellular DNA, or interaction with DNA-binding proteins) presents a main challenge for this application. In our experience large number of oligonucleotides deposited on biomolecule (*e.g.* IgG or SpA) lead to enhanced nuclear binding in fixed cells, which cannot be eliminated by conventional DNA blocking or use of stringent hybridization conditions. In developing an antigen encoding procedure, therefore, we have focused on minimizing the number of tags placed onto each antibody molecule and explored alternative methods for blocking undesirable binding of ssDNA tags to the specimen.

6.2.1 Preparation of antibody-ssDNA probes via amine-sulfhydryl cross-linking

One covalent conjugation approach satisfying this criterion employs partial reduction of IgG at the hinge region followed by maleimide-mediated binding of pre-activated ssDNA (**Figure 6.4**). Specifically, 100μL 0.5mg/mL antibody was incubated with 50mM DTT (dithiothreitol) or 10mM TCEP (tris(2-carboxyethyl)phosphine) in PBS for 1 hour, buffer-

exchanged to PBS with 2.5mM EDTA using Zeba spin desalting columns (7K MWCO, Thermo Scientific), and concentrated to 20µL with 50KDa MWCO centrifugal filters (Millipore). This procedure yields primarily half-IgG with free thiol groups on Fc region, facilitating site-controlled conjugation of 1-2 ssDNA tags.

Activation of amine-functionalized 16bp oligonucleotides was done concurrently via incubation of 100µL 60µM ssDNA with 150 molar excess of sulfo-SMCC (sulfosuccinimidyl-4-(N-maleimidomethyl)cyclohexane-1-carboxylate) in PBS for 1 hour. At least 2 consecutive rounds of buffer exchange to PBS/EDTA with Zeba spin desalting columns was performed to completely eliminate excess cross-linker. Activated ssDNA was then added to concentrated reduced IgG solution (achieving ~10:1 ssDNA-to-1/2IgG ratio) and incubated for 4 hours. Reaction was quenched with hydrolyzed sulfo-SMCC, and antibody-ssDNA bioconjugates were purified using 30KDa MWCO centrifugal filters. The final purification step, however, is not essential, as excess unbound ssDNA tags show lack of interaction with the specimen and can be easily washed away after the first staining step (*i.e.* antigen encoding with antibody-ssDNA probes). At the same time, considering the use of common sulfhydryl and amine groups for this conjugation approach, it is important to start with purified IgG (without stabilizing proteins) and ssDNA stocks in amine-free buffers to prevent undesirable side-reactions and quenching of reactive intermediates.

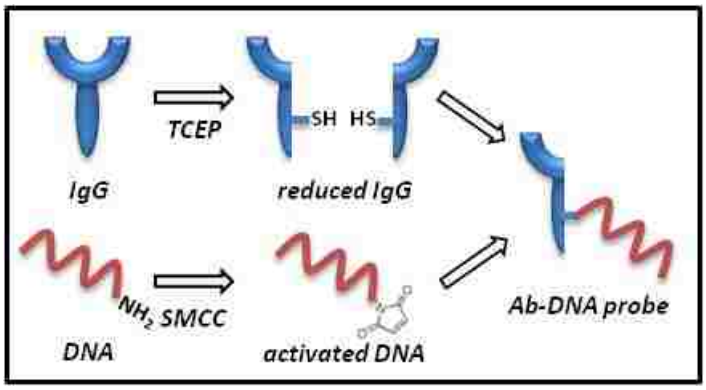

Figure 6.4 Preparation of antibody-ssDNA probes via amine-sulfhydryl cross-linking. IgG is partially reduced, exposing free thiol groups at the hinge region. ssDNA activated with sulfo-SMCC then reacts with available thiols, thus producing 1/2IgG carrying single DNA tag at its Fc region.

An important benefit of this approach comes from the controlled stoichiometry and structure of the antibody-ssDNA bioconjugate. As reaction is limited to 1-2 sites on the Fc region, preparation of antibodies with intact Fab antigen recognition domain and single oligonucleotide attached is readily achievable, which is particularly important for minimizing potential off-target nuclear binding. To probe such off-target binding, we have labeled the same secondary rabbit anti-mouse IgG with 5 different ssDNA tags, incubated with fixed and permeabilized HeLa cells after blocking with shredded salmon sperm DNA, and detected location of those antibody-ssDNA probes using green QDot565 functionalized with goat anti-rabbit $F(ab)_2$ antibodies (**Figure 6.5A**).

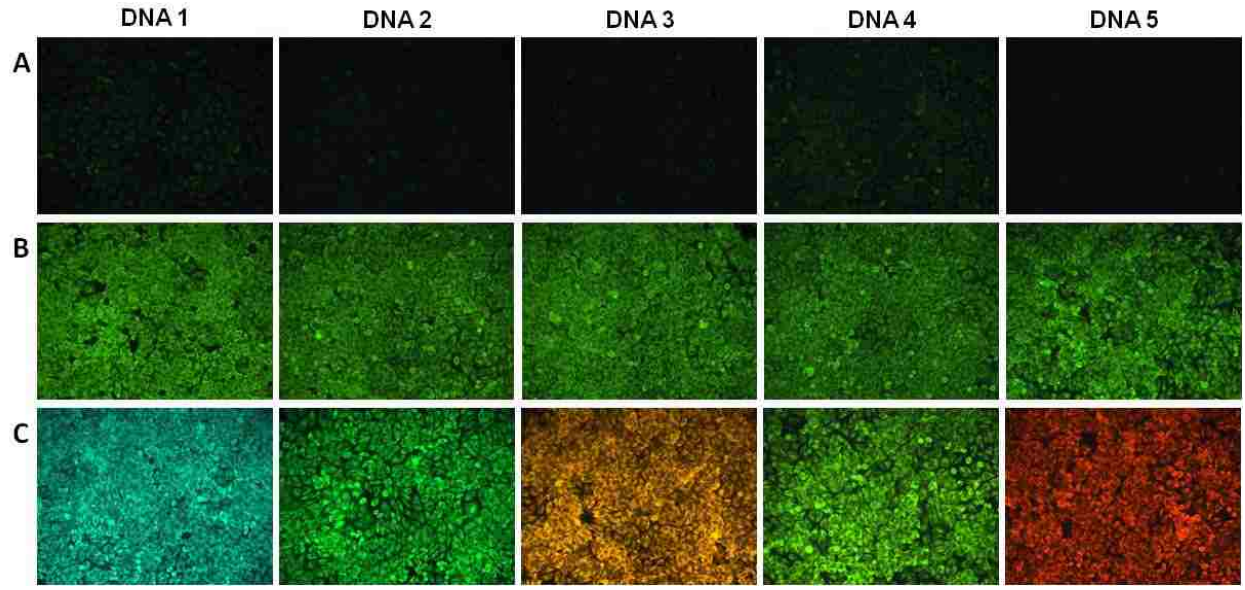

Figure 6.5 Evaluation of the antibody-ssDNA bioconjugate functionality. Rabbit anti-mouse IgG was separately labeled with 5 ssDNA tags via amine-sulfhydryl cross-linking. When incubated with blocked HeLa cells and detected by anti-rabbit QDots, such probes produced minimal non-specific staining (A). At the same time, 3-step labeling with primary mouse anti-HSP90 antibodies, secondary IgG-ssDNA probes, and either anti-rabbit QDots (B) or complementary QDot-ssDNA' probes (C) yielded bright HSP90 staining, confirming successful preparation of fully functional antibody-ssDNA probes.

To evaluate the antigen-binding capacity, in turn, we have first incubated cells with primary mouse anti-HSP90 antibodies, followed by incubation with rabbit anti-mouse IgG-ssDNA and detection with anti-rabbit QDot565 probes (**Figure 6.5B**). Remarkably, only minimal non-specific staining was observed from secondary antibody-ssDNA probes alone, while bright HSP90 staining was achieved with a 3-step procedure when primary antibodies were added, indicating preserved functionality of reduced DNA-labeled antibodies.

Finally, we have assessed the degree of DNA labeling by performing antibody-ssDNA recognition via hybridization with complementary multicolor QDot-ssDNA' probes (see section 6.3 for probe preparation methods) in a 3-step staining procedure (**Figure 6.5C**). Specific HSP90 staining was obtained with all probes, producing staining intensities consistent with those obtained through immunorecognition by anti-rabbit QDot565 probes, thus confirming successful preparation of fully functional antibody-ssDNA bioconjugates.

It should be noted that staining with antibody-ssDNA and QDot-ssDNA' probes has been performed in line with conditions outlined in QDot-optimized IF protocol (see Chapter 3), requiring only addition of scramble DNA to all buffers to block off-target DNA hybridization and, thus, being readily applicable for QDot-based staining applications. At the same time, amine-sulfhydryl conjugation strategy has shown varied efficiency with different antibodies, exhibiting differences in reaction and purification yield. Furthermore, antibody reduction is known to cause adverse effects on antibody functionality and potentially reducing antibody affinity. Therefore, alternative methods for antibody-ssDNA preparation might be explored to circumvent some of these limitations.

6.2.2 Preparation of antibody-ssDNA probes via amine-amine cross-linking

Amine-amine cross-linking presents a convenient approach for conjugation of ssDNA tags to whole IgG with high efficiency. While lacking capacity for precise control of conjugation stoichiometry and final bioconjugate structure, this route better preserves antibody affinity and specificity by avoiding IgG reduction. Out of various amine-amine cross-linking procedures, direct reaction via homo-bifunctional cross-linker BS3 (bis[sulfosuccinimidyl] suberate), which involves initial activation of amine-functionalized oligonucleotides followed by conjugation with antibodies, offers the most straightforward route. However, this reaction proceeded with low efficiency, likely due to hydrolysis of active NHS groups during activation and purification steps.

Therefore, we have employed an alternative conjugation system utilizing an intermediate reaction between hydrazide residues and aldehydes to successfully produce antibody-ssDNA conjugates with varying degree of modification (**Figure 6.6**). In this procedure IgG is activated by S-HyNic cross-linker (succinimidyl-6-hydrazino-nicotinamide, Solulink), which converts primary amines into hydrazide residues reactive towards aldehydes. Amine-modified ssDNA, in turn, is reacted with S-4FB (4-formlbenzamide, Solulink), which converts primary amines into aldehydes. Activated antibodies are

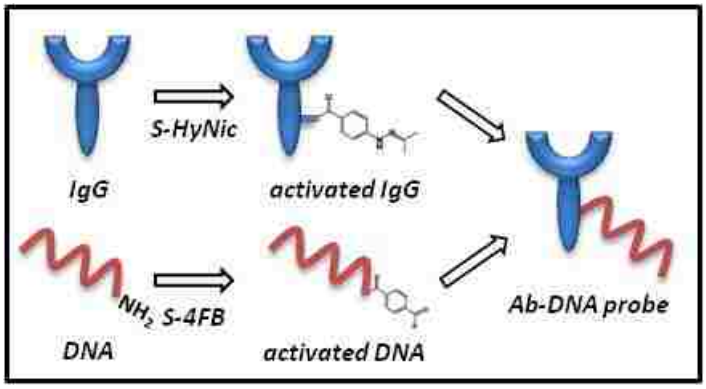

Figure 6.6 Preparation of antibody-ssDNA probes via amine-amine cross-linking. IgG is activated with hydrazide residues, while ssDNA is modified with aldehyde group, both being highly stable intermediates. Reaction between the two yields efficient antibody-ssDNA conjugation.

then conjugated with modified ssDNA via a highly selective and efficient reaction. Specifically, 100μL 0.5mg/mL IgG in PBS was incubated with 50 molar excess of S-HyNic for 4 hours at room temperature. Concurrently, 100μL 50μM amine-modified oligonucleotides in PBS were incubated with 50 molar excess of S-4FB. Following activation, IgG and ssDNA were separately buffer-exchanged to pH5 MES using Zeba spin desalting columns and mixed together (yielding ~7:1 ssDNA-to-IgG excess) for a 5-hour conjugation reaction. With this approach, high stability of reactive intermediates and prolonged reaction time ensure efficient conjugation even with small oligonucleotides excess. At the same time, the degree of ssDNA modification can be controlled by the amount of S-HyNic moieties introduced to antibody and traced with development of characteristic absorbance peak at 354nm, providing flexibility in probe preparation. Yet, similarly to amine-sulfhydryl bioconjugation, purified IgG and DNA stocks in amine-free buffers must be used to ensure proper IgG-DNA coupling.

It should be noted, that amine-amine cross-linking enables significant over-modification of proteins with ssDNA. In certain circumstances such a high degree of DNA tagging might be beneficial (*e.g.* to yield higher staining intensity via binding of multiple reporters per antibody), but it also leads to enhanced off-target nuclear binding in cells. To overcome this limitation we have explored several strategies for blocking DNA binding in cell nucleus. Surprisingly, neither incubation with high excess of free ssDNA nor application of stringent hybridization conditions helped. Instead, partial hybridization of 16bp ssDNA tag with a shorter 11bp ssDNA' nearly completely eliminated all off-target binding, while still allowing hybridization of a QDot-bound full-length 16bp ssDNA' via displacement of a blocking strand for efficient target staining.

6.2.3 Preparation of antibody-ssDNA probes via non-covalent self-assembly

Covalent conjugation procedures produce stable stocks of functional antibody-ssDNA probes suitable for routine examination of a pre-defined library of molecular targets. However, the complexity, relatively high cost, and low yield hamper use of covalent bioconjugation in small-scale synthesis of custom probes for pilot exploratory studies. To address the need for on-demand probe preparation, we have developed a flexible self-assembly methodology capable of labeling miniscule amounts of virtually any antibody with ssDNA tags. Specifically, we employ ssDNA-labeled adaptor molecule (*e.g.* Protein G, SpA, or Fc-specific secondary antibody Fab fragment) to non-covalently link DNA tags onto the Fc region of an intact primary antibody (**Figure 6.7**). While covalent modification of adaptor proteins is required with this strategy, substantially smaller cost and higher stability of such proteins in comparison to primary antibodies allows for preparation and long-term storage of adaptor-ssDNA stocks. At the same time, this approach does not involve purification and chemical modification of primary antibodies, uses very small reagent amounts, and in most cases requires no antibody-ssDNA probe purification (and, thus, no reagent loss). However, non-covalent nature of antibody/adaptor-ssDNA bond brings up concerns regarding probe stability and cross-reactivity, as disassembly and exchange of ssDNA tags become possible. Therefore, we have carefully evaluated the

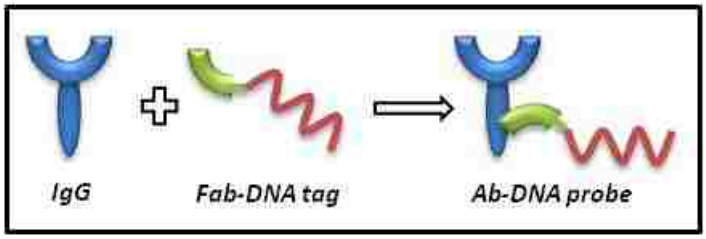

Figure 6.7 Preparation of antibody-ssDNA probes via non-covalent self-assembly. Adaptor molecules (such as Fc-specific Fab secondary antibody) are pre-modified with ssDNA tags and then used for on-demand preparation of antibody-ssDNA probes via non-covalent binding to Fc region of an antibody.

degree of cross-talk and established the utility of self-assembled antibody/adaptor-ssDNA probes for multiplexed encoding of molecular targets.

Among various adaptor molecules for this approach we have closely studied two types, Fc-binding adaptor proteins, such as Protein G and Protein A, and Fc-specific secondary antibodies. Covalent modification of PrG and SpA with oligonucleotides was done in line with reaction conditions described in section 6.2.2 using S-HyNic/S-4FB procedure, whereas DNA-labeling of secondary antibodies or Fab fragments was achieved following sulfhydryl-amine cross-linking described in section 6.2.1. It should be noted that use of whole IgG and $F(ab)_2$ fragments must be avoided, as divalent adaptors might cause aggregation of primary IgG molecules via cross-linking. In particular, we used goat anti-mouse and goat anti-rabbit whole IgG and $F(ab)_2$ fragments as starting materials for probe preparation and achieved complete reduction of disulfide bond at the hinge region via incubation with TCEP. Occasionally this procedure resulted in over-reduction and yielded separated light and heavy antibody chains. In our experience such side-products could also be conjugated with ssDNA and used for labeling of primary antibodies (**Figure 6.8**).

Essential to the success of multiplexed target encoding with self-assembled probes is the lack of antibody/adaptor-ssDNA cross-talk. In this regard, we have tested all the adaptors used and established sufficient probe stability throughout the duration of staining experiment. For example, we used competition test when one adaptor-ssDNA1 is pre-assembled with the primary antibody and another adaptor-ssDNA2 is left vacant to capture any released IgG and serve as an indicator of cross-talk. Specifically, anti-AR primary antibody was first pre-labeled by PrG-ssDNA1, then mixed with PrG-ssDNA2 and incubated with LNCaP cells (**Figure 6.9**). Consistent with high probe stability and lack of DNA tag exchange, only detection of ssDNA1 with complementary QDot-ssDNA1' probe produced characteristic nuclear

staining, whereas detection of ssDNA2 with QDot-ssDNA2' failed to generate signal significantly above the non-specific background.

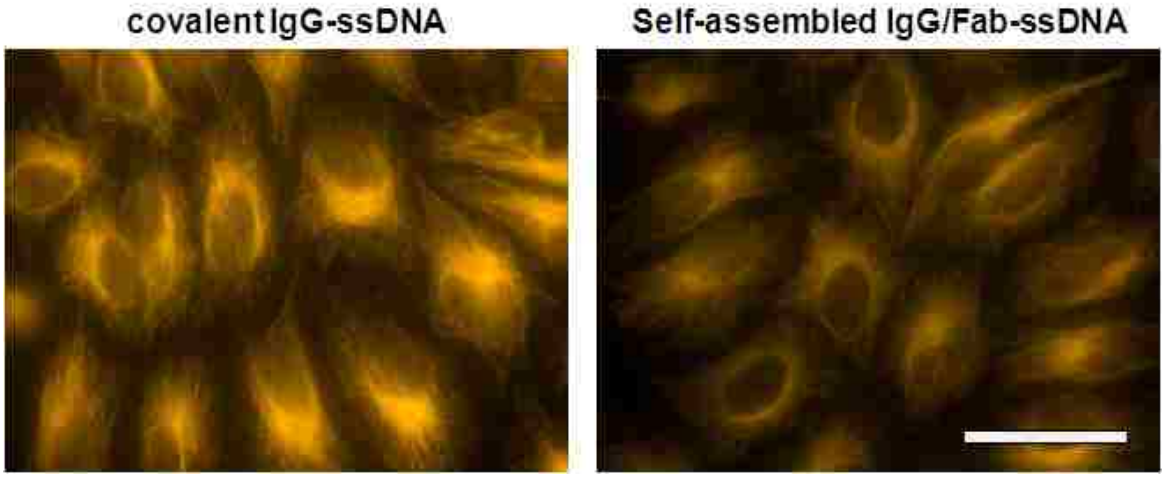

Figure 6.8 Staining specificity with covalent and self-assembled antibody-ssDNA probes. HeLa cells were labeled for ß-Tubulin with either covalent primary IgG-ssDNA probe or self-assembled IgG/Fab-ssDNA probe and stained by complementary QDot585-ssDNA'. Consistent bright staining of microtubules was observed in both cases, affirming utility of covalent and non-covalent probe preparation approaches. Scale bar, 50µm.

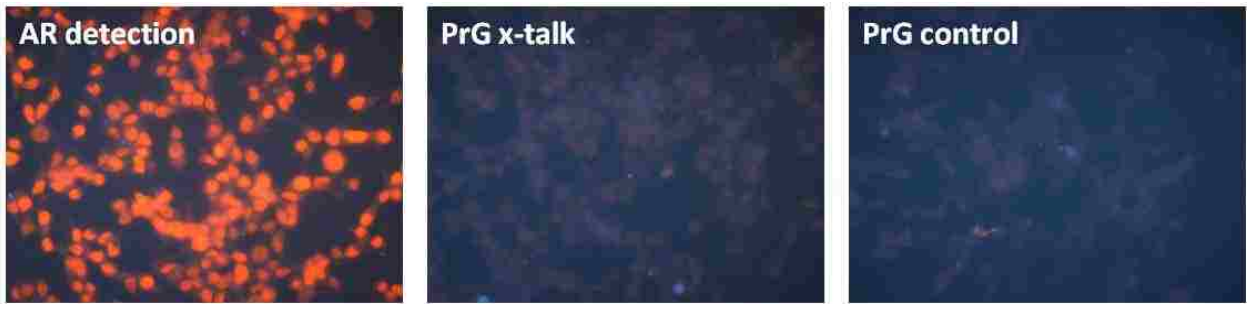

Figure 6.9 Evaluation of the antibody/PrG-ssDNA probe stability. Rabbit anti-AR IgG is pre-assembled with PrG-ssDNA1, mixed with a competitor PrG-ssDNA2 probe, and applied to LNCaP cells for AR labeling. Detection of ssDNA1 via red QDot-ssDNA1' produced characteristic nuclear staining, whereas similar detection of ssDNA2 failed to produce staining significantly above non-specific background, confirming sufficient probe stability and lack of cross-talk.

Similarly, we produced simultaneous dual-target encoding of AR (nuclear) and MAOA (mitochondrial) in LNCaP cells using rabbit primary antibodies pre-assembled with SpA-ssDNA1 and SpA-ssDNA2 respectively, and accurately de-coded it with QDot600-ssDNA1' and QDot565-ssDNA2', observing no cross-talk (**Figure 6.10**).

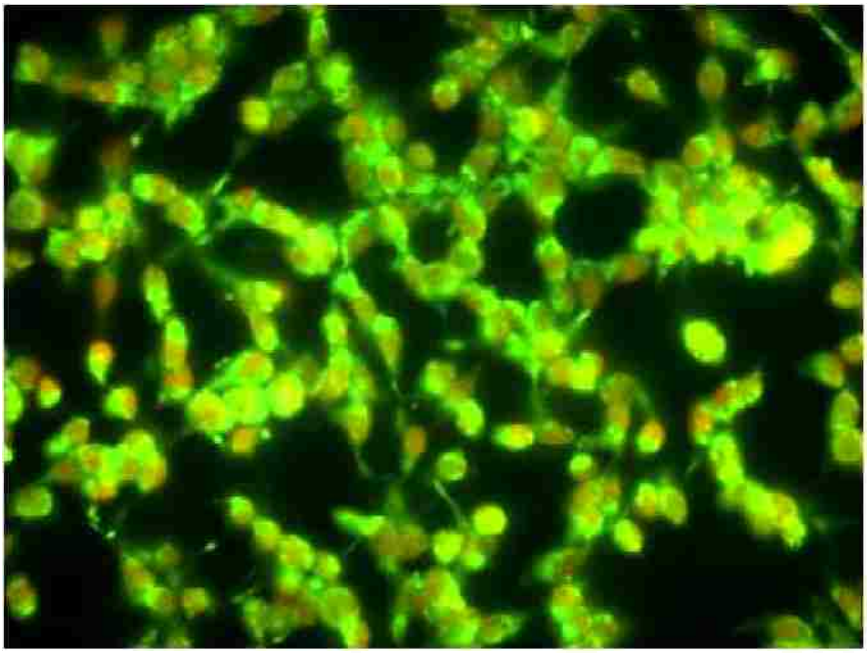

Figure 6.10 Dual-color staining with self-assembled IgG/SpA-ssDNA probes. AR (red) and MAOA (green) were simultaneously labeled in LNCaP cells using rabbit primary antibodies pre-assembled with distinct SpA-ssDNA tags.

In a study on HeLa cells, we used separately pre-assembled probes (goat anti-mouse Fab-ssDNA1 with mouse anti-ß-Tubulin antibody and goat anti-mouse Fab-ssDNA2 with mouse anti-AIF (apoptosis-inducing factor) antibody) to tag microtubules and mitochondria respectively. Non-targeting mouse IgG was added to the staining cocktail to deplete unbound Fab-ssDNA adaptors and block cross-talk. Subsequent simultaneous detection with QDot545-ssDNA1' and QDot585-ssDNA2' produced characteristic staining patterns in respective QDot channels (as detected by HSI, **Figure 6.11**), demonstrating outstanding functionality and lack of cross-talk with self-assembled antibody/Fab-ssDNA probes.

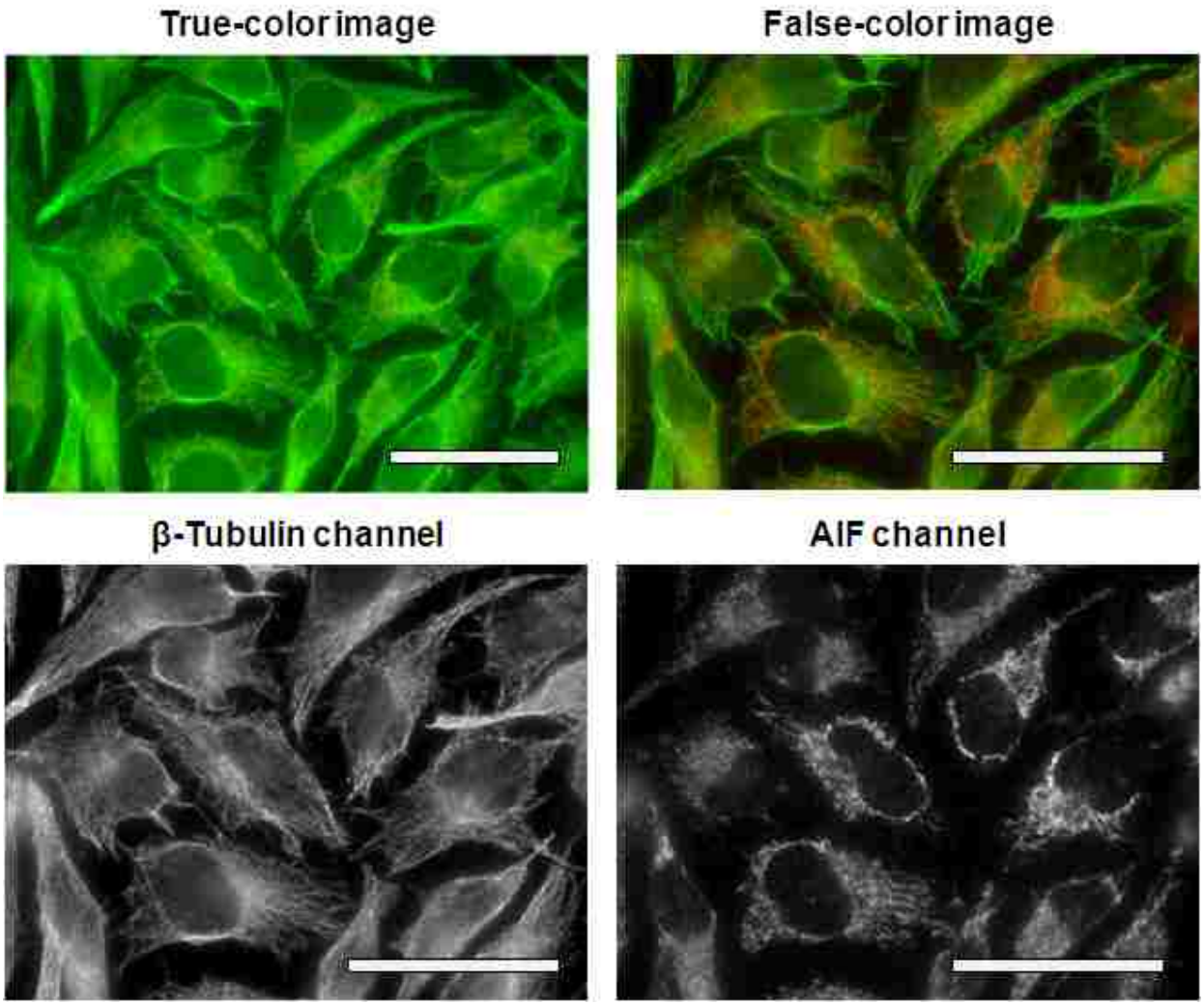

Figure 6.11 Dual-color staining with self-assembled IgG/Fab-ssDNA probes. Beta-tubulin (green) and AIF (orange) were simultaneously labeled in HeLa cells using mouse primary antibodies pre-assembled with anti-mouse Fab-ssDNA tags. True-color image was recorded with QColor5 CCD. HSI of the same subset of cells was used to unmix individual QDot colors into separate channels (bottom panels) and reconstruct a false-color composite image. Scale bar, 50μm.

Notably, benefiting from the great flexibility and simplicity of probe assembly, all studies can be designed and performed within few hours, while using miniscule amounts of reagents (*e.g.* 1-2μL of 0.2mg/mL primary antibodies per specimen can be tagged by 5-10 molar excess of adaptor-ssDNA immediately prior to staining). Requirements imposed on IgG purity and buffer composition are also substantially relaxed in comparison to covalent bioconjugation. For example, presence of stabilizing carrier proteins has no effect on the self-assembly process due to selectivity of antibody binding by adaptors; yet stocks with large amounts of non-specific antibodies (*e.g.* ascites fluid) should be avoided. Finally, purification of assembled antibody/adaptor-ssDNA probes is usually not required, as unbound (and IgG-blocked, in case of Fab-ssDNA) adaptors do not participate in target labeling or significant off-target binding. However, in cases when purification is necessary, efficient elimination of unbound adaptors can be achieved simply by brief incubation with magnetic beads (*e.g.* Dynabeads from Life Technologies Corporation) coated with adaptor-compatible antibodies (*e.g.* rabbit IgG for depletion of SpA and anti-rabbit Fab, or mouse IgG for depletion of PrG and anti-mouse Fab). Magnetic beads are efficiently segregated from the antibody/adaptor-ssDNA sample in a single step by applying a magnet for 1-2 minutes, yielding quick purification with lack of probe loss. Taking together all the features, we conclude that self-assembly between intact primary antibodies and ssDNA-labeled adaptors presents a versatile route for on-demand antibody-ssDNA probe preparation suitable for multiplexed encoding of molecular targets.

6.3 QDot-ssDNA probe preparation

Variety of bioconjugation approaches have been developed for preparation of QDot probes relying on both covalent bond formation and non-covalent self-assembly mechanisms [62, 92, 93, 157, 175-177]. Similarly to development of antibody-ssDNA probes, specific application

requirements govern the choice of QDot-ssDNA probe preparation. Routine use of pre-defined QDot-ssDNA libraries, in particular, might benefit from large-scale synthesis of stable probes via covalent conjugation, whereas exploratory studies make use of flexible small-scale preparation of custom probes via self-assembly. Therefore, we have incorporated both approaches into QDot molecular profiling platform design presented in this chapter.

6.3.1 Preparation of QDot-ssDNA probes via covalent conjugation

Taking into account commercial availability of PEG-coated amine-functionalized QDots and amine-terminated ssDNA, we have focus on exploration of amine-amine cross-linking strategies for QDot-ssDNA probe preparation. In one procedure, we have utilized homo-bifunctional cross-linker BS3 to produce stocks of 5 QDot-ssDNA probes (with emission peaks centered at 525, 545, 565, 585, and 605 nm). This conjugation route relies on efficient activation of 5' primary amines on ssDNA with large excess of BS3, converting each amine group into NHS reactive intermediate, followed by removal of excess cross-linker and reaction with primary amines on the QDot surface (**Figure 6.12**). Specifically, 100µL 40µM amine-terminated ssDNA in 50mM Borate buffer was activated with 100 molar excess of BS3 for 30 minutes, purified with Zeba spin desalting columns, and incubated with 100µL 2µM amine-functionalized QDot-PEG (Qdot ITK amino (PEG) quantum dots from Life Technologies Corporation) overnight at room

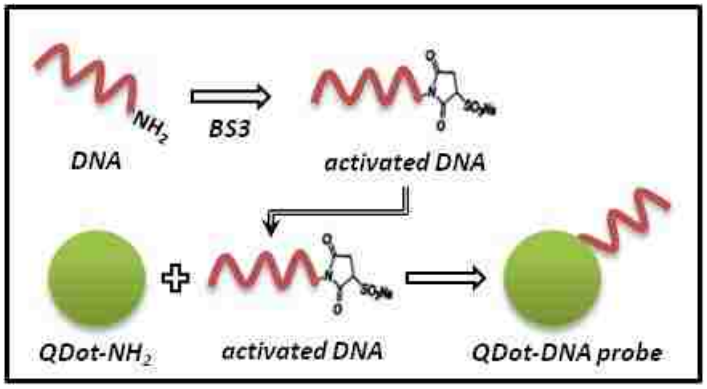

Figure 6.12 Preparation of QDot-ssDNA probes via covalent conjugation. Amine-terminated oligonucleotides are first activated with BS3, which converts amines into reactive NHS moieties, and then reacted with amine-functionalized PEG-coated QDots.

temperature. Probes were then purified by ultrafiltration for 5-6 times with 100KDa MWCO centrifugal filter and dispersed in Borate buffer to a final concentration of 1μM for storage. Probes remained stable and functional for several months when stored at 4^0C. DLS registered lack of significant change in an overall QDot hydrodynamic size upon conjugation, reporting particle distributions centered at 13-14nm in diameter. At the same time, indicative of successful conjugation, agarose gel electrophoresis showed slightly increased motility of QDot-ssDNA bioconjugates in comparison to PEG-coated QDots due to additional negative charge brought to the QDot surface by ssDNA (**Figure 6.13, top panel**). We have further confirmed functionality of QDot-ssDNA probes by separately tagging HSP90 in LNCaP cells with 5 different ssDNA followed by labeling with complementary multicolor QDot-ssDNA' probes, obtaining characteristic cytoplasmic staining (**Figure 6.13, bottom panels**).

Benefiting from its simplicity and relatively low cost, amine cross-linking strategy utilizing BS3 might prove most suitable for preparation of QDot-ssDNA stocks. However, rapid hydrolysis of reactive NHS groups often yields poor conjugation efficiency, especially when QDot scaffolds with non-fouling surface coating, such as PEG, are used. We have successfully circumvented this issue by repeated addition of EDC into the reaction, facilitating re-activation of hydrolyzed NHS (*i.e.* carboxylic acid groups) and promoting conjugation reaction. Surprisingly, besides re-activating ssDNA, EDC also interacted with carboxylic acid groups buried underneath PEG shell, causing irreversible reduction of QDot negative charge and producing nearly neutral particles. Such a side reaction was found to be quite favorable, as increase in QDot negative charge associated with ssDNA conjugation could induce undesirable electrostatic interactions with fixed cells.

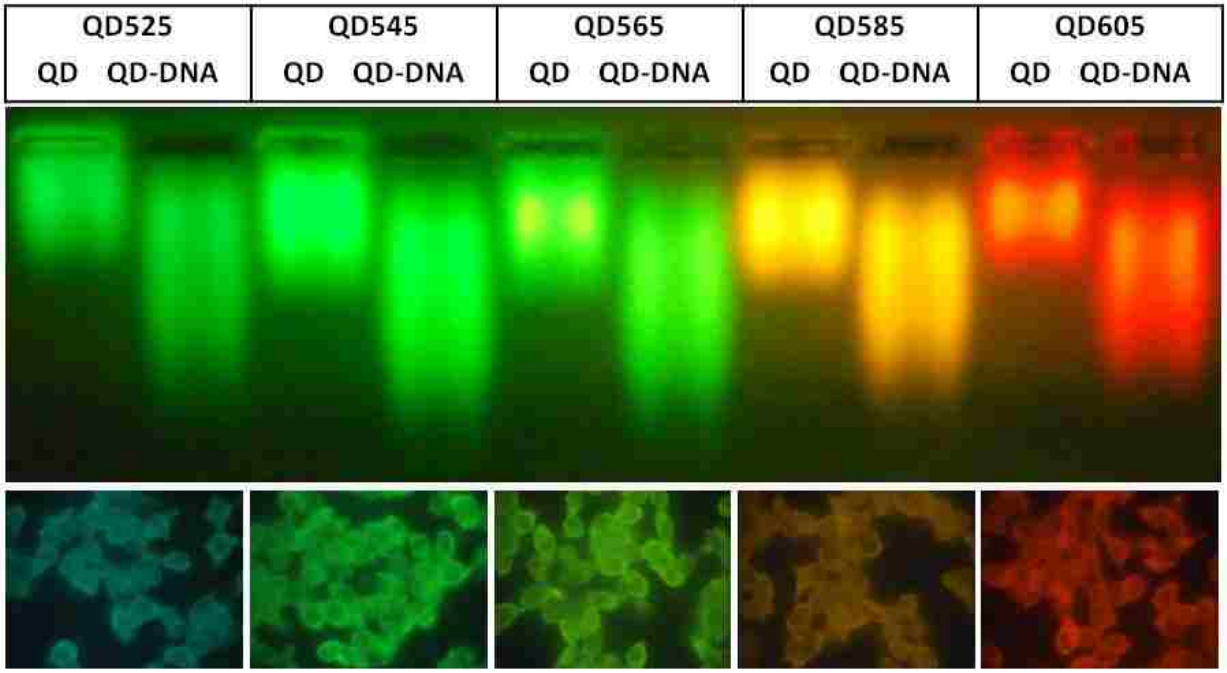

Figure 6.13 Characterization of covalent QDot-ssDNA bioconjugates. Agarose gel electrophoresis shows enhanced particle motility, likely originating from increased QDot surface negative charge, thus indirectly confirming successful conjugation to ssDNA tags. Bright and specific HSP90 staining achieved via hybridization with antibody-ssDNA probes (bottom panels) further corroborates desirable probe functionality.

Alternatively, in line with discussion on antibody-ssDNA conjugation, substantially improved QDot-DNA coupling efficiency can be achieved with S-HyNic/S-4FB bioconjugation system. QDot surface is activated with hydrazide residues, while DNA 5' terminal is converted to an aldehyde group to achieve highly specific and efficient coupling reaction (**Figure 6.14**). High stability of reactive intermediates in this system facilitates efficient reaction between DNA and PEG shells of QDots over prolonged incubation.

In our evaluation of the utility of other QDot scaffolds for preparation of stable QDot-ssDNA probes we have covalently conjugated amine-terminated oligonucleotides to PMAT-coated and PMAL-coated QDots (see Chapter 4) via EDC-mediated coupling. In one implementation of this strategy, negatively-charged QDot-PMAT scaffolds featuring readily-

accessible carboxylic acid groups on the surface were incubated with a large excess of EDC and 10-20 molar excess of oligonucleotides overnight. Following conjugation reaction, the QDot surface was back-filled with 3' or 4' amines to yield zwitterionic coating (see section 4.3 for detailed procedure).

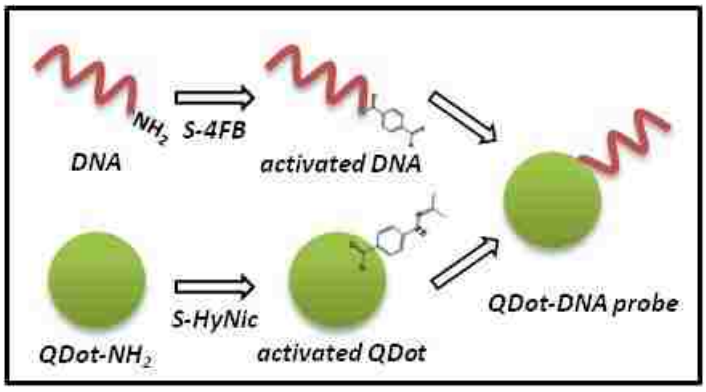

Figure 6.14 Efficient QDot-ssDNA conjugation via stable reactive intermediates. S-HyNic/S-4FB system offers an alternative route for covalent conjugation. Unlike NHS, hydrizide and aldehyde intermediates used here are highly stable, thus maintaining reactivity for extended incubation periods.

In another implementation, QDots pre-coated with zwitterionic polymer PMAL were used. However, unlike PMAT-coated QDots, access to carboxylic acid groups on PMAL is sterically hindered by abundance of bulky tertiary amines spaced away from the QDot surface by C3 linkers. Therefore, while providing very good barrier from non-specific interactions with biomolecules, chemical modification of such surface has proven to be challenging. Furthermore, oligonucleotide amine group placed at the end of PEG spacer on a hydrophobic C6 linker exhibited poor accessibility in aqueous buffers. Therefore, to resolve accessibility issues, EDC-mediated conjugation between PMAL-coated QDots and amine-modified oligonucleotides should be performed in a 100% DMSO or DMF solution. Unlike PMAT-coated QDots that show severe aggregation in DMSO/DMF, QDot-PMAL particles remain single even after addition of a small amount of EDC (small aggregates might form upon addition of larger amounts of EDC, but fall apart upon resuspension in Borate buffer). QDot-ssDNA probes were extensively purified using ultrafiltration. Successful conjugation of 3-4 oligonucleotides per QDot was confirmed by detection of absorption peak

at 260 nm in QDot-ssDNA solution and slight increase in hydrodynamic size from 10 to 11-13 nm (depending on the number of ssDNA conjugated).

6.3.2 Preparation of QDot-ssDNA probes via non-covalent self-assembly

Covalent conjugation strategies enable efficient large-scale synthesis of stable QDot-ssDNA stock libraries based on QDot-PEG, QDot-PMAT, and QDot-PMAL scaffolds, thus satisfying requirements of a wide range of molecular profiling applications. At the same time, flexibility in preparing on-demand probes necessary for quick testing of new DNA sequences and staining modalities cannot be gained from covalent bioconjugation. Instead, non-covalent self-assembly mechanisms might be employed for this purpose. In particular, we have developed a versatile procedure for small-scale QDot-ssDNA probe preparation that comprises functionalization of streptavidin-coated QDots (Qdot Streptavidin Conjugates from Life Technologies Corporation) with biotin-terminated ssDNA (from IDT DNA) followed by quick probe purification with streptavidin-coated magnetic beads (**Figure 6.15**). Specifically, to prepare a probe for 1 staining experiment, 1μL 1μM QDot-Streptavidin was mixed with 1μL 10μM ssDNA-biotin and 3μL PBS for 30 minutes. Then 5μL 10mg/mL pre-washed magnetic beads (Dynabeads MyOne Streptavidin C1 from Life Technologies Corporation) in 1%BSA/PBS was added, and mixture was incubated for 15 minutes on rotator, depleting all unbound ssDNA-biotin from solution. Finally, magnet was applied to the side of the tube to

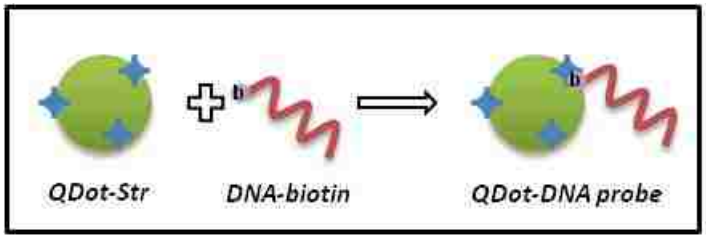

Figure 6.15 Preparation of QDot-ssDNA probes via non-covalent self-assembly. Streptavidin-functionalized QDots are used for efficient binding of biotinylated oligonucleotides, while quick purification with streptavidin-coated magnetic beads yields pure probes. As a result, small-scale on-demand probe preparation is easily achievable.

segregate magnetic beads, purified QDot-ssDNA solution was transferred to a new tube, and remaining binding sites on streptavidin were blocked with free biotin solution for 10 minutes. Unlike the common case with antibody-ssDNA probes, complete removal of unbound ssDNA-biotin is essential here in order to prevent blocking of complementary ssDNA' tags on the specimen during staining procedure. Due to much smaller size and faster diffusion, free ssDNA efficiently inhibits hybridization of QDot-ssDNA probes. At the same time, streptavidin blocking with free biotin is necessary to avoid off-target binding to endogenous biotin that might be present in the specimen.

In a remarkable contrast to covalent conjugation approaches, probe preparation via self-assembly between QDot-Streptavidin and ssDNA-biotin proceeds rapidly and with high efficiency. We have found that even small excess of ssDNA (*e.g.* 2DNA : 1QDot) results in efficient formation of monovalent and divalent QDot-ssDNA probes (**Figure 6.16**), whereas deposition of 4-5 ssDNA is possible with larger oligonucleotides excess, should multivalent probes be desirable for a particular application. For example, we have explored one potential mechanism for signal amplification, which is based on hybridization of a second "layer" of QDot-ssDNA probes, thus requiring the first "layer" to be comprised of multivalent QDot-

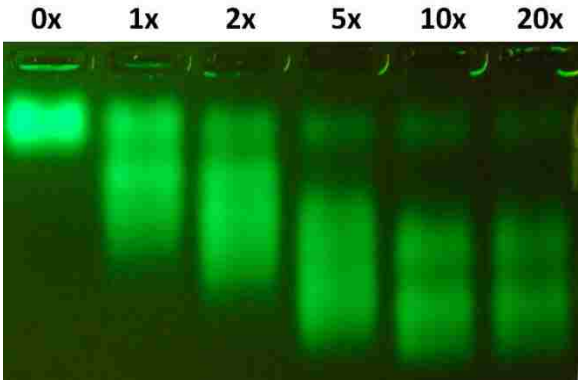

Figure 6.16 Characterization of the QDot-ssDNA probe self-assembly. QDot-Streptavidin efficiently captures biotinylated ssDNA even at slight DNA excess, as indicated by formation of QDot-DNA bands on agarose gel. QDot-Streptavidin conjugates show minimal gel motility (0x line), whereas upon ssDNA binding particles become more negatively charged and move faster.

ssDNA' probes and feature unoccupied ssDNA' for hybridization. While carrying multiple oligonucleotides on the surface, each QDot-ssDNA' probe likely hybridizes via only one ssDNA', thus exposing the rest of unoccupied oligonucleotides and converting original layer of ssDNA tags (from antibody-ssDNA probes) into a yet larger number of ssDNA' tags. Detection of those tags with a same-color QDot-ssDNA, therefore, yields signal amplification. Moreover, second layer of staining is also driven by specific DNA hybridization, thus being completely compatible with the multiplexed staining modality. Regardless of the modification degree, all QDot-Streptavidin-ssDNA' probes demonstrate highly accurate target labeling via sequence-specific hybridization with a complementary ssDNA tag on the specimen. Among disadvantages of this method, however, might be higher cost of reagents and larger overall QDot-ssDNA probe size.

6.4 Multiplexed 2-step staining of cultured cells and FFPE tissues

Multiplexed 2-step staining methodology involves recognition and DNA encoding of molecular targets on the first step by appropriate antibody-ssDNA probes and labeling of ssDNA tags with complementary QDot-ssDNA' probes on the second step. Since the link between the first and second steps is established by DNA hybridization, sequence-specific recognition of multiple targets without cross-talk between probes is possible, thus limiting the maximum number of targets detected in parallel only by the current availability of suitable QDot scaffolds and the capabilities of HSI and unmixing algorithms. In particular, we have employed 5 commercially available QDot-PEG or QDot-Streptavidin scaffolds (with emission peaks centered at 525, 545, 565, 585, and 605 nm) in preparation of QDot-ssDNA probes for simultaneous imaging of up to 5 molecular targets.

In most generic staining of fixed cells antibody-ssDNA and QDot-ssDNA' probes prepared via any suitable route (covalent conjugation or non-covalent self-assembly) can be successfully used, as described in previous sections. For example, we have assessed the performance of covalent antibody-ssDNA and self-assembled antibody-ssDNA probes in labeling of intracellular targets in reference to 2-step staining with unmodified primary antibodies and QDot-2'Antibody bioconjugates. Specifically, we prepared formalin-fixed and permeabilized prostate cancer LNCaP cells, blocked cells with 6%BSA/TBS buffer with 0.1mg/mL of sheared salmon sperm DNA, and incubated with either antibody-ssDNA probes or unmodified primary antibodies for 1 hour at room temperature. Following washing, QDot-ssDNA' probes or QDot-2'Antibody probes, respectively, were applied to cells for another hour. Completely consistent staining patterns obtained in a single-color staining of AR (nuclear) and MAOA (mitochondrial) targets with all probes corroborate our conclusions (**Figure 6.17**).

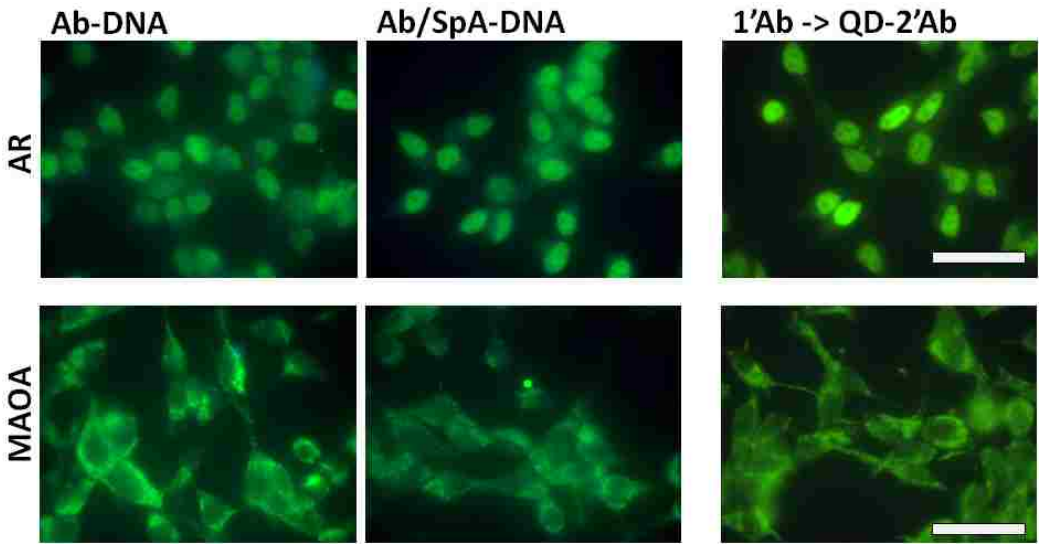

Figure 6.17 Singleplexed staining with covalent and self-assembled antibody-ssDNA probes. AR (nuclear) and MAOA (mitochondrial) staining patterns obtained on LNCaP cells with both types of probes are consistent with conventional 2-step staining with QDot-2'Antibody conjugates. Scale bar, 50μm.

Comprehensive evaluation of the multiplexed 2-step staining methodology has been performed on fixed and permeabilized HeLa cells using a panel of 5 molecular targets featuring distinct intracellular localization patterns and variable expression levels. In particular, we have labeled Lamin A (nuclear envelope), HSP90 (cytoplasm), Histone H3 (nucleus), ß-Tubulin (microtubules), and AIF (mitochondria) with covalent antibody-ssDNA and complementary covalent QDot-ssDNA' probes. First, we assessed the functionality of antibody-ssDNA probes for all targets. Specifically, we incubated cells with either unmodified or ssDNA-modified antibodies during the first staining step and detected localization of antibodies either via immunorecognition with QDot-2'Antibody bioconjugates or DNA hybridization with QDot-ssDNA' probes during the second staining step (**Figure 6.18**). Staining via immunorecognition by a secondary antibody is used here to detect all primary antibodies bound to the specimen, regardless of the degree of ssDNA labeling. At the same time, staining via hybridization is used to confirm successful antibody-ssDNA probe preparation and lack of cross-talk between various ssDNA tags. Consistent patterns achieved with both staining routes along with lack of staining by QDot-ssDNA' probes in a control study (where non-complementary DNA links were used) demonstrate good accuracy and efficiency of antigen encoding and subsequent staining.

Building upon robust performance of our 2-step staining methodology in a singleplexed format, we have combined a panel of 5 antibody-ssDNA probes matched with 5 QDot-ssDNA' probes for evaluation of the multiplexing capacity. In line with singleplexed studies, cells were pre-blocked and incubated with a cocktail containing all 5 antibody-ssDNA probes, followed by washing and incubation with a cocktail containing all 5 QDot-ssDNA' probes. HSI was used to unmix the image cube into individual QDot channels (see section 3.4). Low-magnification image demonstrates consistent staining patterns of all targets through a large

number of cells, while highlighting variability of target expression levels depending on the cell cycle stage (**Figure 6.19**).

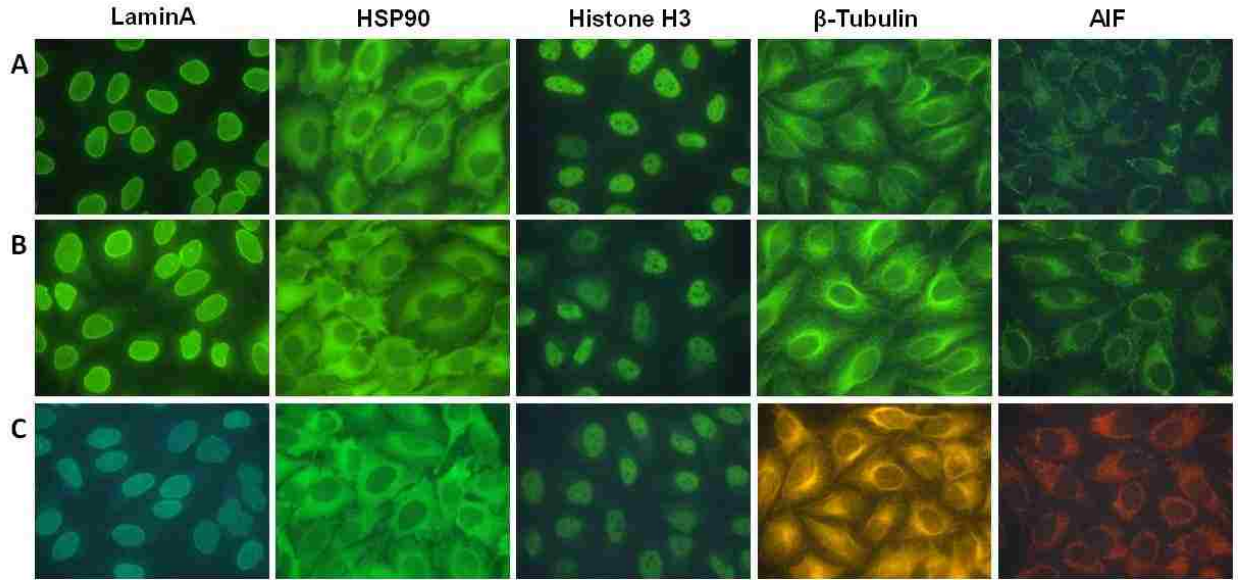

Figure 6.18 Verification of an antibody-ssDNA probe panel for 5-target encoding. HeLa cells were labeled separately with five covalent primary antibody-ssDNA bioconjugates, each carrying a unique DNA tag. Upon IgG detection via immunorecognition with QDot565-2'Antibody, DNA-tagged antibodies (B) demonstrated staining specificity consistent with unmodified antibodies (A). At the same time, IgG-ssDNA probes could be detected by complementary QDot-ssDNA' reporters (C), confirming successful preparation of a functional antibody-ssDNA probe stock panel.

To further evaluate the capacity for single-cell molecular profiling at sub-cellular resolution, we have performed staining of Lamin A, ß-Tubulin, and Ki-67 in HeLa cells and examined a small number of cells with 100x oil-immersion objective (**Figure 6.20**). Remarkably, here we were able to clearly observe chromosome condensation (via Ki-67 staining), mitotic spindle formation (via ß-Tubulin staining), and dissolution of the nuclear membrane (via Lamin A staining) in a sole dividing cell. Finally, we have employed self-assembled antibody/Fab-ssDNA and QDot-Streptavidin-ssDNA probes for dual-color labeling of

Histone H3 and ß-Tubulin in fixed LNCaP cells, achieving characteristic nuclear and microtubule staining respectively. Lack of cross-talk between QDot channels further supports the utility of self-assembled probes for multiplexed target labeling. Summarizing results of all validation studies, we have established the utility of the 2-step QDot staining platform for detailed multiplexed examination of adherent cell cultures, providing a highly versatile platform for further design of single-cell molecular profiling applications.

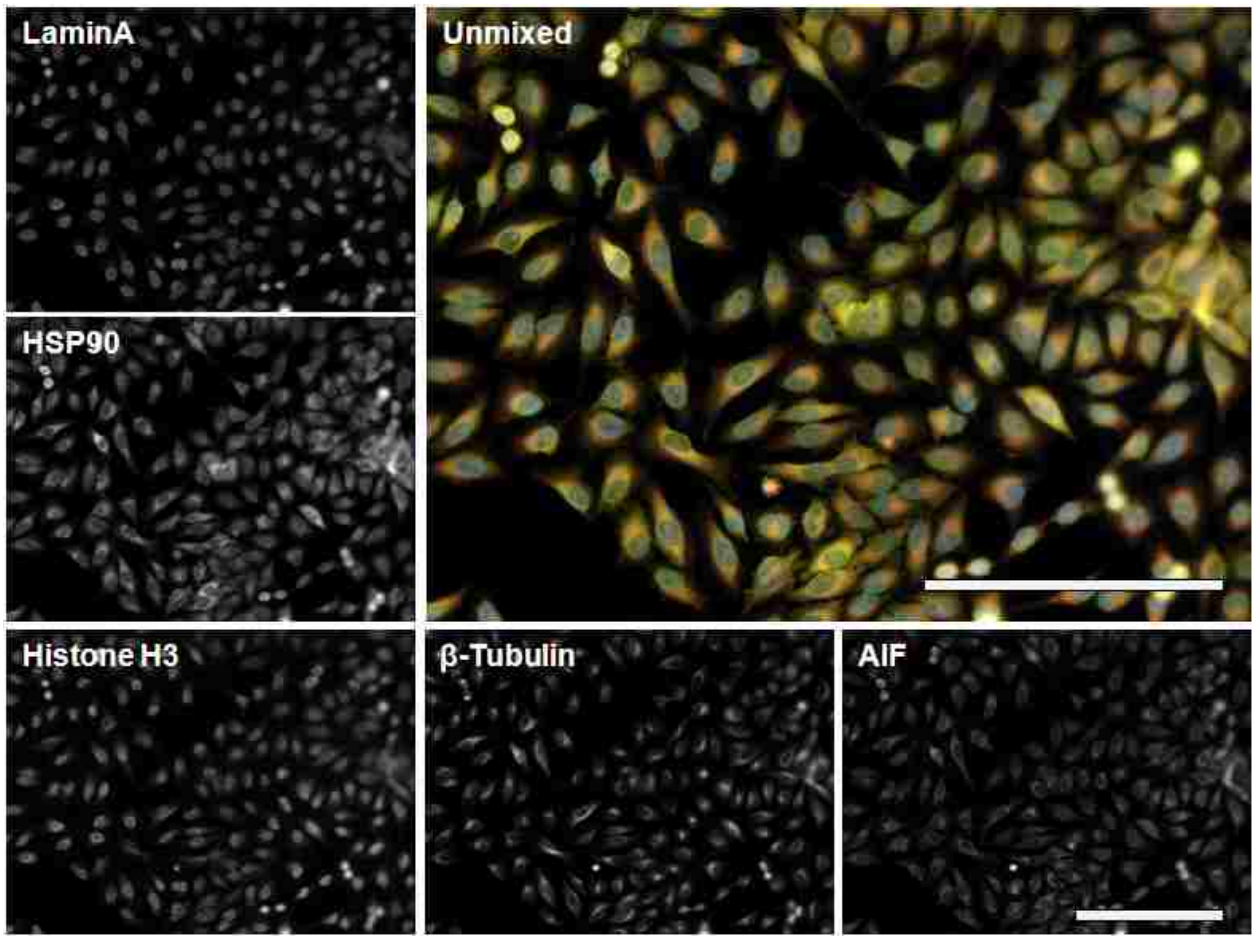

Figure 6.19 Simultaneous labeling of a 5-target panel via 2-step staining methodology. HeLa cells were first incubated with a set of covalent antibody-ssDNA probes targeting Lamin A, HSP90, Histone H3, ß-Tubulin, and AIF, followed by sequence-specific hybridization with complementary QDot-ssDNA' probes. Characteristic staining patterns obtained for each target corroborate capacity of antigen encoding strategy for highly multiplexed staining with QDot probes in a multi-step format. Scale bar, 250µm.

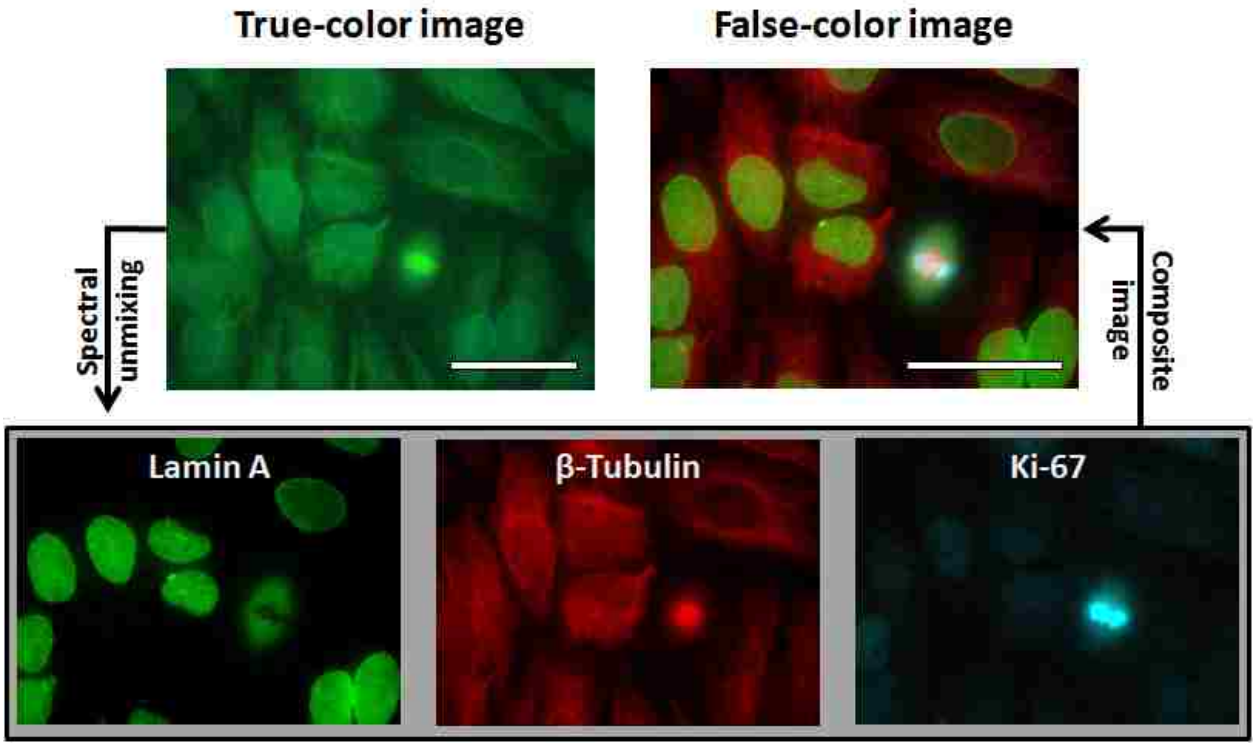

Figure 6.20 Detailed examination of a 3-target panel at sub-cellular resolution. HeLa cells were labeled with covalent antibody-ssDNA bioconjugates targeting Lamin A, ß-Tubulin, and Ki-67 and stained by complementary QDot probes emitting at 525, 545, and 565 nm respectively. While closely spaced QDot colors are hard to distinguish with true-color imaging, HSI reliably unmixes them into individual channels, providing an insight into molecular events within a sole dividing cell. Scale bar, 50μm.

Building upon robust performance of 2-step staining methodology in cultured cells we have applied self-assembled antibody-ssDNA probes for multiplexed labeling of FFPE brain sections. Specifically, we tested a section of brain deteriorated by Alzheimer's disease for a set of three characteristic biomarkers, Tau5, PHF-Tau, and Tau2. We simultaneously labeled all targets with primary antibody/Fab-ssDNA probes and subsequently stained with covalent QDot-ssDNA' probes emitting at 545, 565, and 585 nm respectively. As a result, we were able to observe co-localization of all three biomarkers within the bodies of most neurons (**Figure 6.21**), which also matched reference singleplexed labeling.

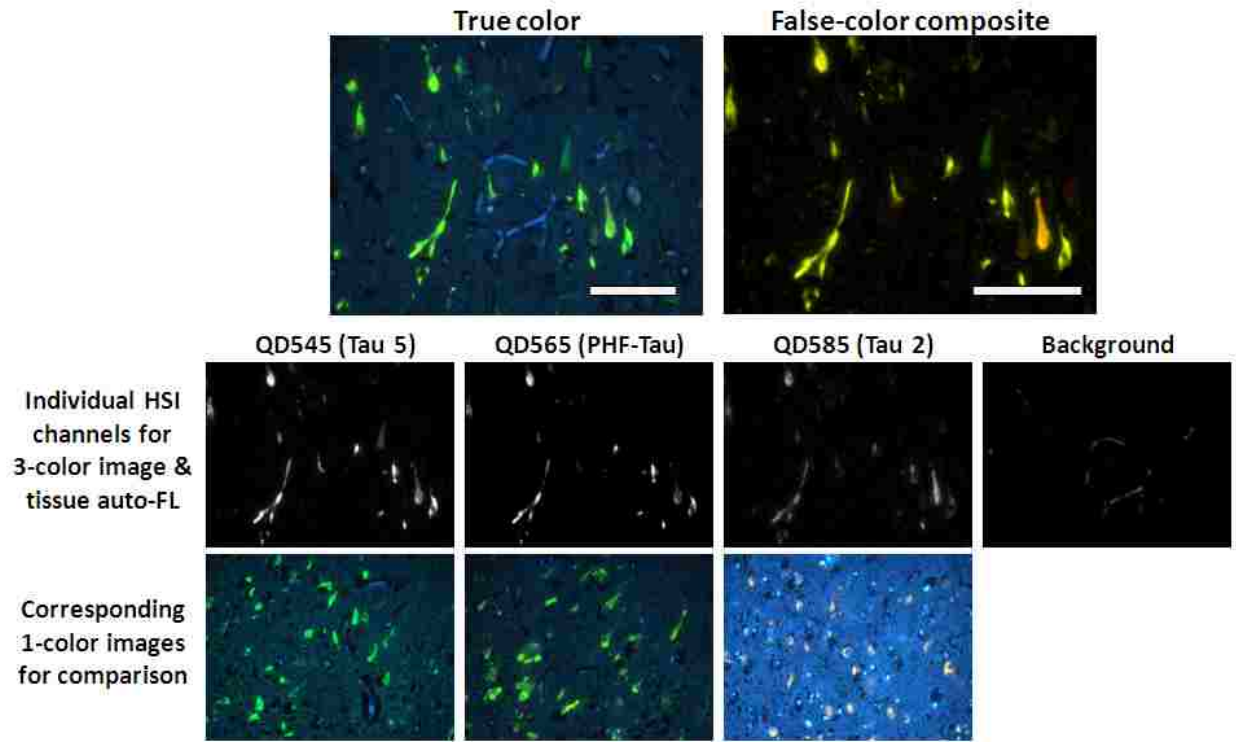

Figure 6.21 Multiplexed 2-step staining of FFPE tissue sections. Human brain sections (from Alzheimer's patients) were stained for Tau5, PHF-Tau, and Tau2 with self-assembled antibody-ssDNA probes and covalent QDot-ssDNA' probes. HSI and spectral unmixing yielded consistent staining patterns for all targets, indicating co-localization in the bodies of most neurons. Scale bar, 100μm. This work was performed in collaboration with Prof. Jing Zhang, MD, PhD and Dr. Bertrand Huber, MD from the UW Pathology.

6.5 Summary

Multiplexed 2-step staining methodology described in this chapter presents a simple and highly versatile approach to staining of various molecular targets capable of addressing unique design criteria of a wide range of molecular profiling applications. Combination of high-content information carriers, such as biomolecule antigenicity, DNA sequence code, and QDot emission profile, enable direct translation of target-specific molecular information into a detectable signal that can be measured and analyzed, while individual steps are separated

to allow for optimization of target recognition and DNA hybridization conditions. In some sense, histological specimen is converted into a DNA array, where position and density of DNA sequences are governed by expression profiles of corresponding molecular targets. As a result, first step of staining procedure is performed similarly to conventional IHC and IF, whereas second step resembles a less demanding FISH procedure [92, 93, 157]. Such a combination is highly beneficial for further translation of QDot technology into practice, as common pre-staining specimen processing along with antibody incubation step can be performed with minimal modifications to conventional methodology. Furthermore, FISH-like labeling with DNA-decorated QDots reduces potential for non-specific probe interaction with the specimen, prevents probe cross-reactivity, and facilitates deeper penetration into specimen due to smaller probe size, all of which improve robustness and flexibility of the QDot molecular profiling technology. At the same time, a comprehensive set of covalent and non-covalent procedures described here offers great flexibility in preparation of custom-designed probes (Table 6.2). Being substantially more versatile than 1-step staining platform presented in Chapter 5, 2-step QDot-based staining methodology might prove most suitable for performing exploratory molecular profiling studies on a single-cell level within the context of intact specimen morphology.

Table 6.2 Comparison of methods for IgG-ssDNA and QDot-ssDNA probe preparation

	Antibody-ssDNA probe		**QDot-ssDNA probes**	
	Covalent	**Self-assembled**	**Covalent**	**Self-assembled**
Application	Stock library	Custom tests	Stock library	Custom tests
Benefits	Long-term stability	On-demand preparation	Long-term stability	On-demand preparation
Drawbacks	IgG chemical modification	Poor stability	Complex conjugation	Large size Higher cost

CHAPTER 7: CYCLIC STAINING METHODOLOGY FOR ANALYSIS OF EXPANDED MOLECULAR PROFILES

A truly comprehensive single-cell molecular profiling requires imaging and quantitative analysis of tens of molecular targets on the same specimens. QDot imaging platforms based either on a single-step target labeling with QDot-SpA-Antibody probes (see Chapter 5) or multi-step labeling via DNA encoding and de-coding with QDot-ssDNA probes (see Chapter 6) present a versatile foundation for initial exploratory studies with relatively small multiplexing capacity for simultaneous examination of up to 7-10 targets. While our staining methodology allows for much greater multiplexing, spectral overlap between multicolor QDots imposes a limit on the number of probes that can be reliably distinguished in a mix. In fact, 10 colors of spectrally distinguishable QDots are commercially available at this time, which is coincident with the current color deconvolution capability of HSI. Preparation of QDots with narrower emission peaks and improvements in HSI could further increase the multiplexing capability of parallel staining beyond 10. Indeed, recent work on QDot bandgap engineering has produced particles with emission profile as narrow as 14nm FWHM (full width at half maximum) [178], in contrast to commonly used commercial QDots with typical 25-30nm FWHM. Yet, such improvements are likely to be incremental.

To break the fundamental limitations of parallel multiplexing and increase the multiplexing power of the QDot imaging platform by another magnitude, we have developed a cyclic staining methodology [162]. Generally, cyclic staining involves separate labeling and imaging of a sub-set of molecular targets alternated by de-staining steps, during which

fluorescent labels are either quenched or completely removed from the specimen to prevent interference with subsequent cycles. In other words, identical 5-10 color staining procedure is performed multiple times on the same specimen, each time using a different selection of antibody probes, thus enabling molecular profiling of expanded target libraries.

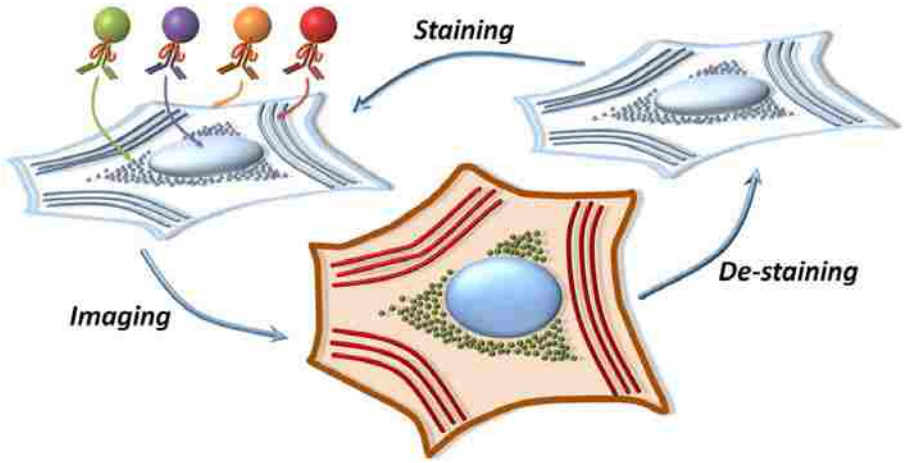

Figure 7.1 Schematic of a cyclic staining methodology. In general terms, this procedure involves multiplexed labeling of a sub-set of targets, hyper-spectral imaging and unmixing of multicolor QDots, and de-staining (or specimen regeneration), which enables staining and imaging of another sub-set of targets during the next cycle.

Cyclic staining method consists of 3 main steps (**Figure 7.1**). First, specimen is labeled with multicolor QDot probes (either in 1-step or 2-step procedure) for parallel multiplexed staining. In the second step, fluorescence microscopy with HSI capability is utilized to acquire and unmix signals from each QDot color to generate quantitative antigen expression profiles in separate channels, depicting the relative antigen distribution in a merged image. In the third step, complete de-staining of the specimen is done by brief washing with a regeneration buffer, enabling the next full cycle of IF staining for a different subset of targets. With each staining cycle, N targets can be analyzed, where N depends on the number of spectrally

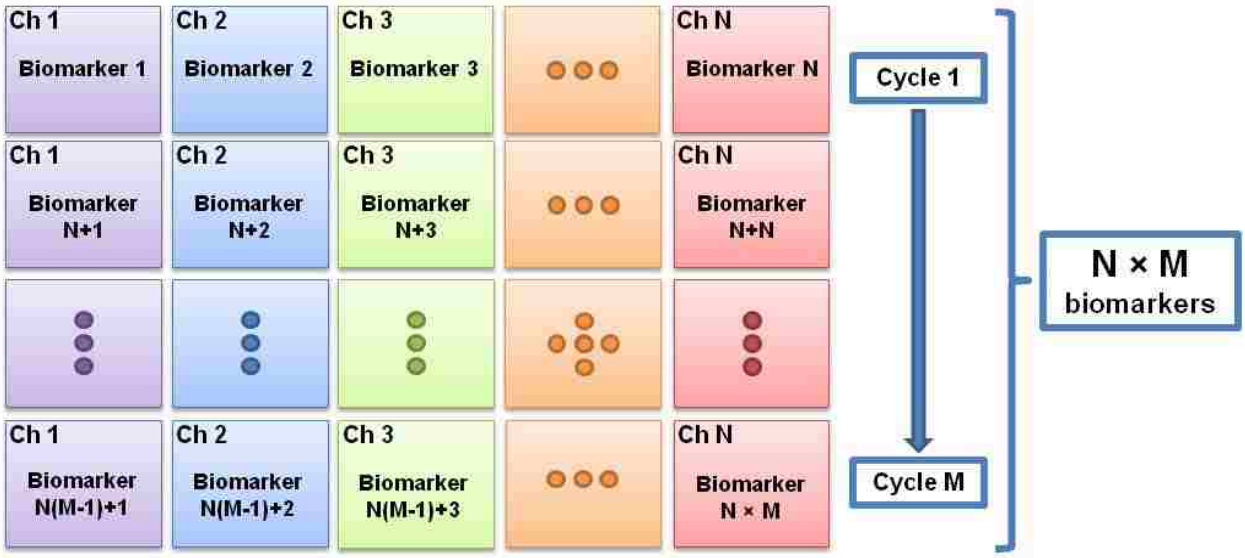

Figure 7.2 Expanded multiplexing capacity enabled by cyclic staining. Sequential repetition of N-plexed parallel staining for M cycles enables labeling of NxM molecular targets. With utilization of QDot probes featuring narrow emission profiles, molecular profiling for over 100 targets becomes achievable.

distinct fluorescent probes that can be detected simultaneously. Performing IF staining for M sequential cycles generates M subsets of data for the same specimen, thus yielding an overall molecular profile consisting of N x M targets (**Figure 7.2**). For example, when the staining/imaging procedure is carried out for 10 cycles using 10 spectrally distinguishable QDot probes, 10x10 (100) molecular targets can be studied within a single sample. Therefore, cyclic staining modality dramatically expands the capability of the QDot imaging platform for comprehensive evaluation of single-cell molecular profiles.

7.1 Design criteria for cyclic staining methodology

Cyclic immunofluorescence critically depends on complete specimen regeneration after each cycle, including removal or blocking of all the probe components and elimination of fluorescence signal. In particular, successful regeneration should achieve (i) complete de-

staining after each IF cycle to avoid false-positive detection due to signals carried over from previous cycles, (ii) complete removal or blocking of target-bound primary and/or secondary antibodies to preclude binding of probes during further cycles, and (iii) preservation of specimen morphology and target antigenicity to gain consistent staining intensity on every cycle. Microwave treatment [45], strong acidic conditions [46-48], and specimen dehydration [47] have been used with some success for cyclic staining procedures based on conventional IF and IHC. However, elimination of large staining complexes (often consisting of crosslinked primary and secondary antibodies conjugated with enzymes or streptavidin and surrounded by precipitated chromogens) proves to be challenging and requires extensive chemical or thermal treatment, which often lead to specimen degradation.

Self-assembled QDot-SpA-Antibody probes described in Chapter 5 are uniquely suited for quick and efficient specimen regeneration via chemical stripping. Directly benefiting from the non-covalent semi-stable nature of the QDot-SpA-Antibody probe assembly and direct biomarker-QDot binding (lacking multilayer probe build-up and cross-linking) featured by the 1-step labeling methodology, complete removal of QDot-Antibody probes can be achieved via brief exposure to low-pH/detergent-based regeneration buffer. Dissociation of labile antibody-antigen and antibody-SpA bonds offers quick probe disassembly and enables efficient elution of individual probe components, thus achieving complete specimen restoration to pre-staining conditions, while exerting minimal adverse effect on biomarker antigenicity. Furthermore, trace amounts of residual QDots, which might remain bound to the specimen due to non-specific interactions, can be completely and irreversibly quenched, thus prohibiting fluorescence signal build-up and carry-over between different cycles.

Similarly, cyclic staining can be employed with a DNA-encoding platform described in Chapter 6, as labile DNA links can be easily disrupted to facilitate efficient elution of

individual probe components for specimen regeneration, while highly selective binding of QDot probes via DNA links prevents cross-reactivity between cycles even if trace amounts of probes are left behind. Yet, an extra encoding step lengthens the procedure. Therefore, we have primarily focused on implementation and characterization of cyclic staining methodology using self-assembled QDot-SpA-Antibody probes and single-step direct target labeling.

7.2 Specimen de-staining and regeneration of biomarker antigenicity

In identifying a suitable regeneration buffer for cyclic staining with self-assembled QDot-SpA-Antibody probes we have focused on satisfying following criteria: (i) all probe components should be completely (or nearly completely) removed from the specimen, (ii) trace amounts of QDots remaining in the specimen should be completely quenched, (iii) trace amounts of primary antibodies should remain inaccessible to unoccupied QDot-SpA probes, (iv) probe components remaining on the specimen should not interfere with subsequent staining cycles, and (v) specimen antigenicity should be preserved through multiple regeneration cycles.

Through preliminary studies we have tested a number of regeneration buffers, primarily aiming at achieving complete removal of probe components. In particular, we labeled Lamin A in HeLa cells with green QDot525-SpA-Antibody probes and measured probe components before and after 15-minute de-staining: (i) QDot-SpA-Antibody probe fluorescence was recorded directly from target labeling, (ii) amount of primary antibodies was determined via secondary staining with red QDot655-2'Antibody probes, and (iii) amount of QDot-SpA-Antibody probes was determined indirectly via staining of SpA with primary anti-SpA antibody followed by yellow QDot565-2'Antibody probes (**Figure 7.3**). All low-pH buffers (such as pH1.5 Glycine-HCl, Elution Buffer, and Regeneration Buffer from Thermo Scientific) removed about

70% of probe components. Elution and Regeneration buffers, despite being specifically formulated for antibody and antigen elution from affinity resins, could not achieve complete removal of probes from fixed cells. Interestingly, Gentle Elution Buffer (Thermo Scientific), formulated for IgG elution from SpA resins at near-neutral pH, indeed yielded good dissociation of SpA-Antibody bond (leading to removal of ~70% of QDot-SpA), while failing in breaking antibody-antigen bond (leading to even higher immunorecognition of primary antibodies with QDot-2'Antibody probes). To facilitate dissociation of all non-covalent bonds, we added anionic detergent, SDS (sodium dodecyl sulfate), at a final concentration of 0.5%w/v to regeneration buffers, achieving improved elution of ~90% of probe components. Since SDS-supplemented Elution Buffer achieved the same efficiency of de-staining as pH1.5 Glycine-HCl-SDS under less acidic conditions (pH 2.8), we established IgG Elution Buffer with 0.5% SDS as a suitable candidate condition for specimen regeneration purposes.

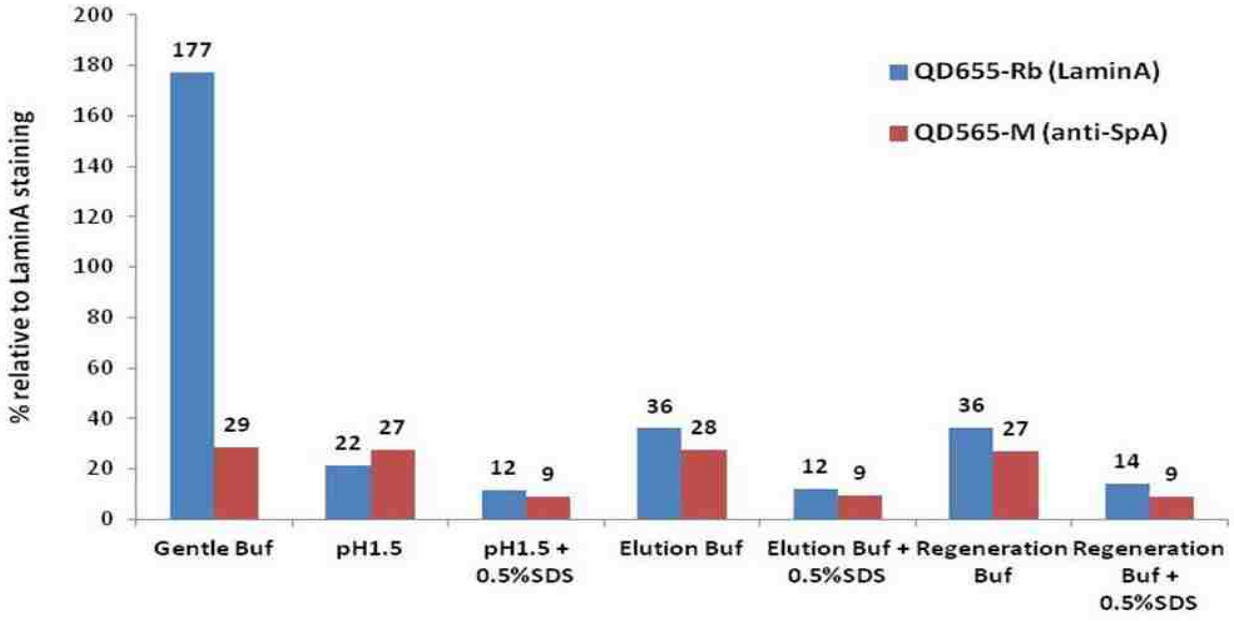

Figure 7.3 Evaluation of specimen regeneration conditions. Lamin A is stained with QDot-SpA-Antibody probes. Post-elution detection is done via 1' antibody labeling with QDot655-2'Antibody and QDot-SpA labeling via 2-step SpA staining with QDot565. Low pH (1.5-3.0) generally achieves removal of ~70% probes, whereas further addition of anionic surfactant SDS yields nearly complete regeneration.

Thorough characterization studies have been performed to evaluate compliance of the candidate regeneration buffer with the five criteria outlined above. First, we have confirmed the nearly complete elution and complete quenching of QDot-SpA probes upon treatment with regeneration buffer (**Figure 7.4**). Specifically, Lamin A in HeLa cells was stained with red QDot605-SpA-Antibody probes followed by incubation with either TBS (Reference) or regeneration buffer (De-staining) for 15 minutes and analysis with HSI. QDot605 labeling was observed directly and indirectly via SpA staining with green QDot565 probes. Remarkably, no leftover QDot605 signal could be detected after de-staining (**Figure 7.4B**). Secondary detection of QDot605-SpA probes through SpA staining revealed that nearly all QDot-SpA probes were eluted from the specimen during de-staining (less than 10% of probes remained bound to cells, **Figure 7.4D,E**). At the same time, when QDot605-SpA-Antibody probes were covalently cross-linked to cells, all probes remained bound to their targets, but produced no fluorescence signal due to irreversible quenching of QDot fluorescence (**Figure 7.4C,F**). In line with preliminary evaluation of regeneration buffers, these results confirm that de-staining is achieved primarily by dissociation of QDot-SpA-Antibody probes, either as separate components or as a whole complex, from the specimen and completed by quenching of leftover QDots, thus restoring the specimen to pre-staining condition.

Notably, specimen regeneration through QDot-SpA-Ab probe elution releases targets of their labels, thus preventing probe interference and enabling complete re-staining of the same targets during subsequent cycles. For example, Lamin A stained with QDot545 can be re-stained again after de-staining with pre-assembled QDot545-SpA-Antibody probes. At the same time, "blank" QDot545-SpA fails to produce any staining, confirming the lack of accessible primary antibodies left on the specimen, which is critical for preventing cross-talk between staining cycles (**Figure 7.5A-D**). Similarly, in a dual-color staining of Lamin A and HSP90 with QDot545 and QDot585 probes respectively (**Figure 7.5E-H**) we achieve complete

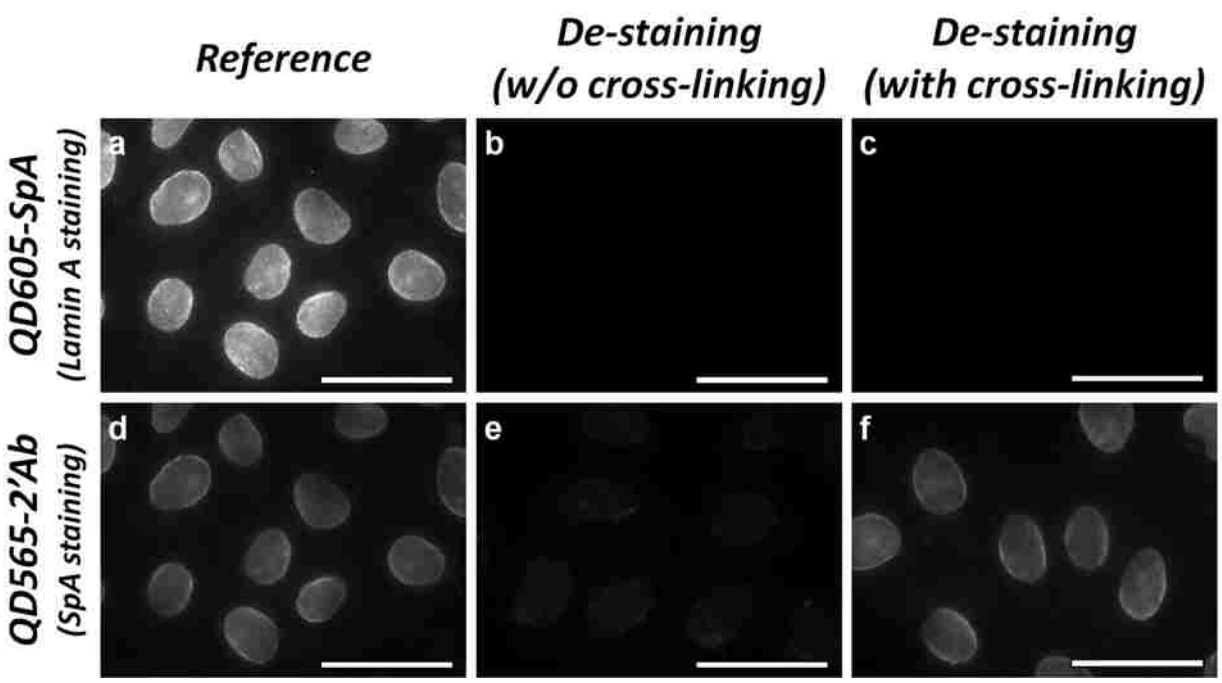

Figure 7.4 Confirmation of complete specimen regeneration during low-pH/detergent-mediated de-staining. Lamin A staining with QDot605-SpA-Antibody probe shows characteristic nuclear envelope staining pattern in QDot605 spectral channel (A). At the same time, presence of QDot-SpA probes can be detected by further staining of SpA using anti-SpA antibody (mouse anti-SpA IgG) and anti-mouse QDot565-2'Antibody (D). After de-staining QDot605 signal is completely eliminated (B), while barely detectable QDot565 staining of SpA highlights trace amounts (< 10%) of leftover QDot605-SpA probes (E), indicating that majority of QDot-SpA probes are efficiently eluted from the specimen, whereas remaining probes are completely quenched. In contrast, post-staining crosslinking of QDot-SpA-Antibody probes to specimen hinders elution, as indirectly evidenced by preserved SpA staining in QDot565 channel (F), keeping all QDot-SpA-Antibody probes attached to the specimen. Yet, even in this case QDot605 signal is completely eliminated following de-staining (C), proving low-pH-mediated QDot quenching as a sufficient method for elimination of non-specific fluorescence background build-up through staining cycles. Brightness of all images is normalized to (A) to facilitate in direct comparison of staining intensity. Scale bar, 50μm.

exchange of fluorescent reporters during the second cycle (**Figure 7.5I-L**) and measure identical relative average staining intensities for these targets during both cycles (data not shown). While re-staining of targets might be un-necessary for majority of cell profiling applications, complete removal of QDot-SpA-Antibody probes is still desirable to avoid any steric hindrance or interference that may be encountered by nanoprobes during cyclic staining of closely spaced targets. Therefore, given re-staining results, it is reasonable to conclude that such an issue should not arise with cyclic staining methodology utilizing chemical stripping of self-assembled QDot-SpA-Antibody probes.

Expansion of QDot imaging platform to profiling of over 100 molecular targets, nonetheless, requires that at least 10 cycles of staining are performed (assuming parallel use of 10 QDot colors complemented by 10-channel HSI), thus placing restrictions on regeneration conditions. Acknowledging this requirement, we have verified that the candidate regeneration buffer allows performance of up to (but not limited to) 10 regeneration cycles with no detrimental effect on specimen morphology and target antigenicity. This study was performed via quantitative evaluation of Lamin A and HSP90 staining in HeLa cells and AR staining in LNCaP cells. Specifically, we designed experiments using cells located in separate wells of the same 24-well plate, thus ensuring that all cells were prepared under identical conditions. Cells were exposed to M regeneration cycles (where M ranged from 0 to 10). Each cycle consisted of de-staining with SDS-supplemented pH2.8 IgG Elution Buffer, blocking, incubation with staining buffer, and washing, imitating a full IF staining cycle. Following the multicycle treatment, targets were stained, and HSI was used for quantitative analysis of average staining intensities. Notably, consistent staining was observed for all targets regardless of the number of regeneration cycles performed, corroborating further expansion of the QDot imaging platform with the multicycle staining methodology.

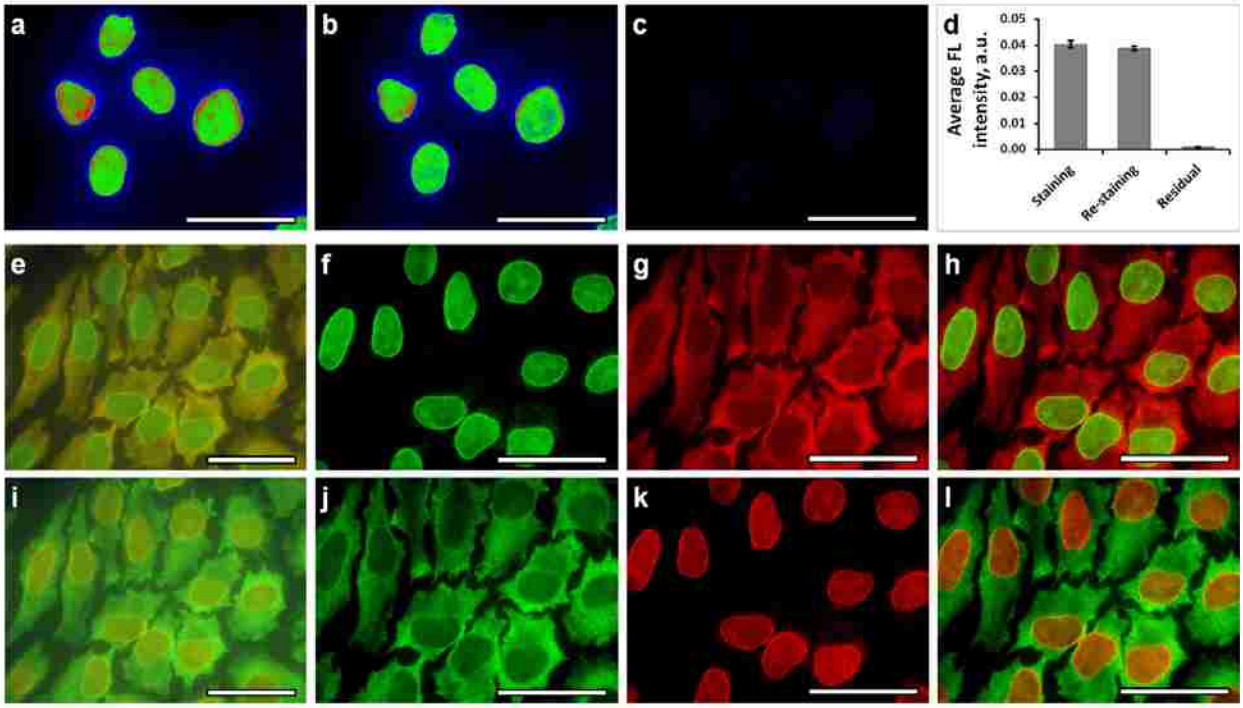

Figure 7.5 Specimen regeneration and target re-staining with multicycle staining procedure. (**a**) Characteristic nuclear envelope staining is obtained with QDot545-SpA probes pre-assembled with anti-Lamin A antibody. Brief incubation with regeneration buffer removes QDot-SpA-Antibody probes, achieving specimen restoration to pre-staining condition and enabling nearly complete target re-staining (**b, d**).Incubation of regenerated specimen with "blank" QDot545-SpA probes (lacking target-specific antibodies) fails to produce any residual staining (**c, d**), confirming complete removal of 1' antibodies during de-staining. Same subset of cells is imaged, normalized by intensity, and false-colored with a heat-map. Error bars represent standard deviation of the average staining intensity between 3 different fields of view imaged on the same specimen. (**e-l**) Application of the cyclic staining procedure to dual-color cell labeling enables complete exchange of QDot reporters between 2 different molecular targets. In particular, parallel staining of Lamin A with QDot545 and HSP90 with QDot585 is achieved (**e-h**). HSI reveals distinct Lamin A staining pattern in QDot545 channel (**f**) and HSP90 pattern in QDot585 channel (**g**). Following de-staining, during the second cycle the same targets are stained with the counterpart QDot probes (**i-l**), yielding clear HSP90 pattern in QDot545 channel (**j**) and Lamin A pattern in QDot585 channel (**k**). (**e**) and (**i**) are true-color images and (**h**) and (**l**) are false-color composite images. Fluorescence intensity of individual channels is adjusted to achieve clear target representation in composite false-color images. Same sub-population of cells is imaged after each step to aid in direct comparison of staining patterns. Scale bar, 50μm.

It is advisable to perform evaluation of specimen degradation for all targets of interest as well as for alternative pre-staining specimen processing conditions, as some antigens might demonstrate greater susceptibility to degradation. For example, we have found that incomplete cell fixation achieved by incubation with formaldehyde in TBS for 10 minutes (in contrast to 20-30 minutes with optimized procedure, see section 3.1) resulted in over 40% AR signal drop in LNCaP cells after 10 degradation cycles (**Figure 7.6**), while fixation with formaldehyde in PBS followed by Triton X-100 permeabilization failed to preserve biomarker antigenicity even after one de-staining.

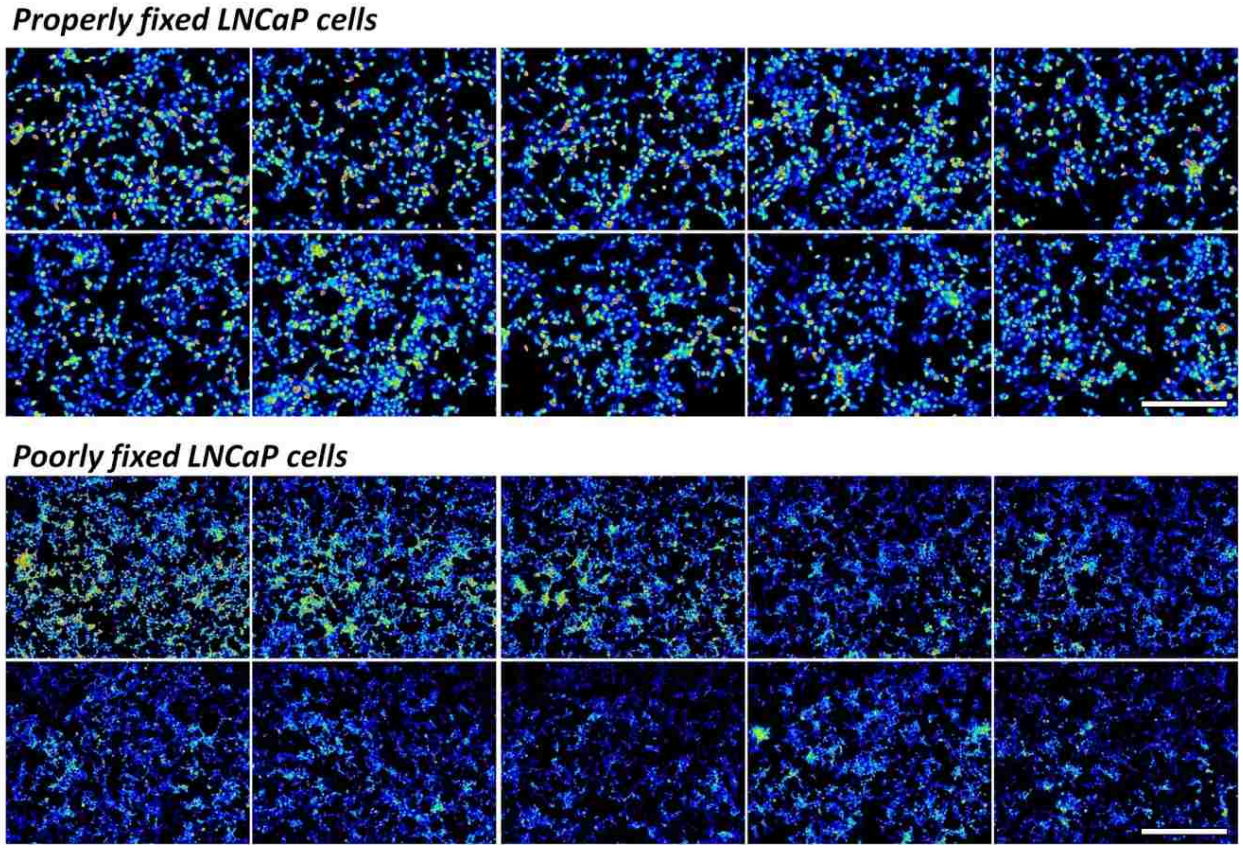

Figure 7.6 **Antigen preservation via proper pre-staining specimen processing.** LNCaP cells were treated for 1-10 (left-to-right) regeneration cycles, after which AR was stained. Significant target degradation is observed in poorly fixed cells (bottom panels), but not in properly processed ones (top panels). Images are normalized by intensity and false-colored with a heat-map for this study. Scale bar, 500μm.

7.3 Cyclic staining with self-assembled QDot-Antibody probes

Complete specimen regeneration paired with lack of specimen degradation enables robust singleplex cyclic staining and quantitative analysis of multiple molecular targets in fixed cells regardless of the target expression levels and staining sequence. For example, we have sequentially stained HSP90, MAOA, AR, pAkt, and ß-Tubulin in LNCaP cells from low- to high-expression level as well as the opposite in a multi-cycle procedure and observed consistent target distribution and staining intensity independent of the staining sequence, with no carry-over or cross-talk signal being detectable throughout the 5 cycles (**Figure 7.7**).

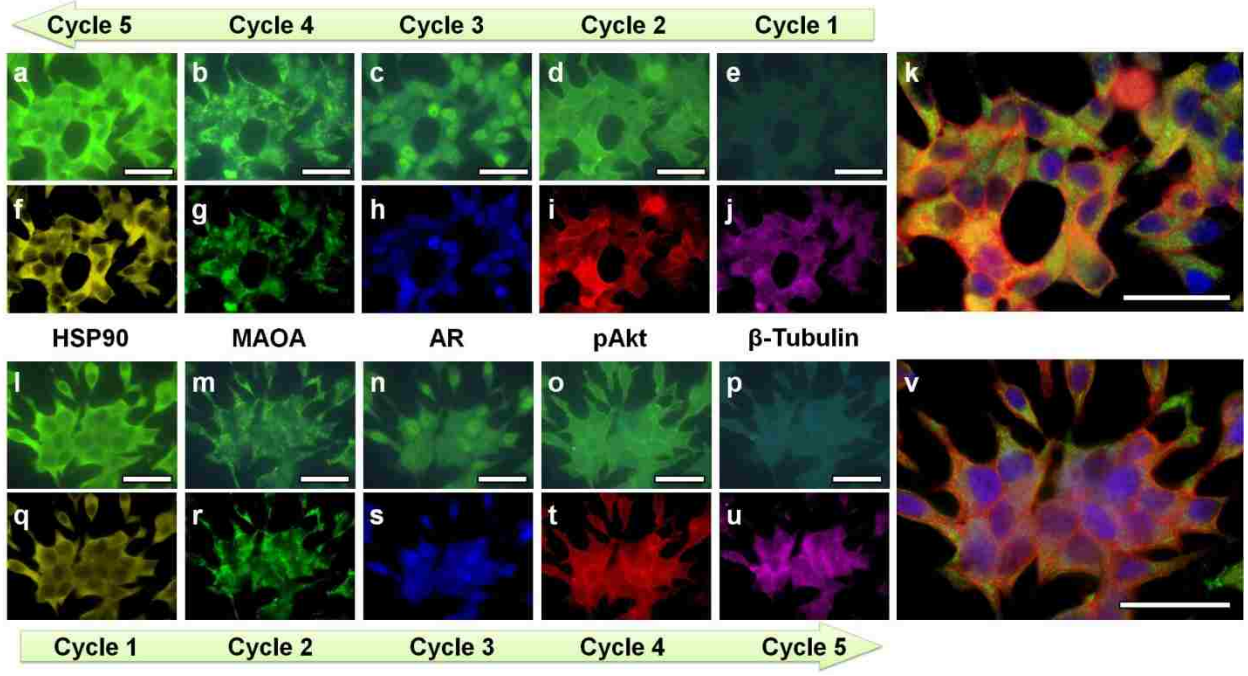

Figure 7.7 Evaluation of the robustness of sequential staining procedure in LNCaP cells. Single-color staining of 5 targets on the same cell sub-population is performed in sequential manner in the order from low-abundance to high-abundance target (**a-k**) and from high-abundance to low-abundance target (**l-v**). Independent of the order, all targets are reliably stained, showing correct staining pattern and relative staining intensity. True-color images (**a-e,l-p**) are converted to false-color images (**f-j,g-u**) with background removed and intensity adjusted for clear representation of each biomarker in composite false-color images (**k,v**). Scale bar, 50µm.

A more rigorous quantitative analysis has been performed on HeLa cells with a 5-target panel consisting of Lamin A, HSP90, Ki-67, Cox4, and ß-Tubulin (**Figure 7.8**). Here, again, we observe correct staining pattern and target expression profiles for staining sequence from highly condensed down to diffusely distributed targets (**Figure 7.8A-K**) and in reverse (**Figure 7.8L-V**). Remarkably, relative molecular profiles obtained with both staining sequences are completely consistent between each other as well as the reference singleplex single-cycle staining performed with QDot-SpA-Antibody probes (**Figure 7.8W**).

It is worth noting, that single-color multicycle experiment serves as a suitable platform for validation of cyclic staining methodology and evaluation of potential cross-talk or interference between cycles on variety of specimens. In particular, labeling of all targets with the same QDot color facilitates direct quantitative comparison of target expression, since it completely rules out such potential complications as inaccurate hyperspectral unmixing, CCD sensitivity to different wavelengths of light, or QDot fluorescence intensity fluctuation among different colors. At the same time, imaging of the same sub-set of cells through all cycles eliminates staining pattern and intensity fluctuations that originate from cell heterogeneity, thus enabling accurate evaluation of changes in cell morphology and target distribution at sub-cellular resolution. One technical note should be made here, though. Since cyclic staining involves repeated imaging of the same area of the specimen, a strategy for finding the same sub-set of cells after each staining cycle is required. We have achieved this objective by placing a reference mark (using fine-tip permanent marker) on the bottom of each well and stepping a set distance from the mark for imaging. Accuracy of imaging frame alignment can be further improved by overlaying the unique cell culture morphology between different cycles. Minor mismatch is then manually corrected with image-processing software.

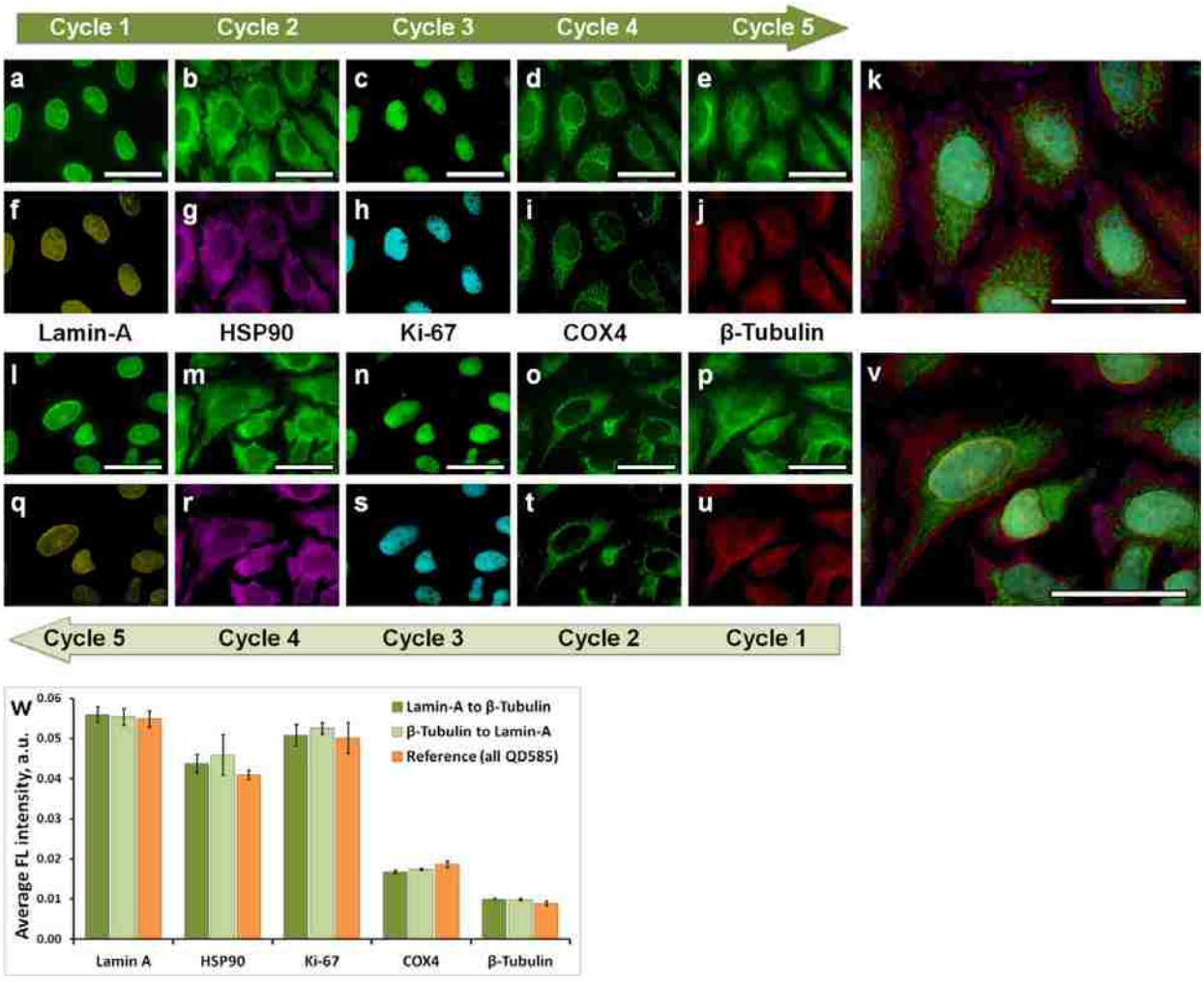

Figure 7.8 Evaluation of the robustness of sequential staining procedure in HeLa cells. Similarly to study with LNCaP cells, single-color staining of 5 molecular targets on the same cell sub-population is performed using QDot545-SpA-Antibody probes in sequential manner. Quantitative analysis of target staining intensity for both sequences in comparison to reference single-cycle single-color staining performed with QDot585-SpA probes is shown in (**w**). Independent of the order, all targets are reliably stained, showing correct staining pattern and relative staining intensity. No carry-over fluorescence, build-up of background fluorescence, or cross-staining between cycles can be observed. Original images obtained with HSI (**a-e,l-p**) are false-colored, aligned, and cropped (**f-j,q-u**) for clear representation of each target in composite false-color images (**k,v**). Error bars represent standard deviation of the average staining intensity between 3 different fields of view imaged on the same specimen. Scale bar, 50μm.

With augmenting multiplexed 1-step staining procedure (see Chapter 5) by a cyclic staining modality described here, a comprehensive single-cell molecular profiling becomes possible. Parallel multicolor staining features capacity for simultaneous analysis of up to 10 targets, whereas cyclic single-color staining also enables robust interrogation of at least 10 (or more) targets through several cycles without causing specimen degradation. Therefore, when combined together, these modalities potentially offer access to quantitative molecular profiles consisting of 100+ molecular targets.

We have demonstrated the feasibility or such an extensive molecular profiling capacity by performing a 25-target analysis in a 5-color x 5-cycle format. Specifically, we re-stained the same model 5-target panel (Ki-67, HSP90, Lamin A, Cox-4, and ß-tubulin) with multicolor QDot-SpA-Antibody probes for 5 cycles and performed quantitative analysis of staining intensity after each cycle with HSI. Such setup facilitates not only the demonstration of the concept, but also further evaluation of the technology robustness, including assessment of the target staining pattern consistency, preservation of sub-cellular and cell culture morphology, and uniformity of relative target expression profiles measured through different staining cycles. Notably, all 5 targets were consistently stained through five cycles yielding accurate staining patterns and identical average staining intensity profiles (**Figure 7.9**), while producing no carry-over of fluorescence signal between cycles (**Figure 7.10**). Furthermore, low-magnification imaging of the same field of view demonstrates complete preservation of cell culture morphology through 5 cycles (**Figure 7.11**). Therefore, it is reasonable to expect the multiplexed cyclic staining achieved by combination of 1-step target labeling with self-assembled QDot-SpA-Antibody probes and specimen de-staining via chemical stripping to become a technically straightforward, yet analytically powerful imaging platform for comprehensive *in situ* single-cell molecular profiling.

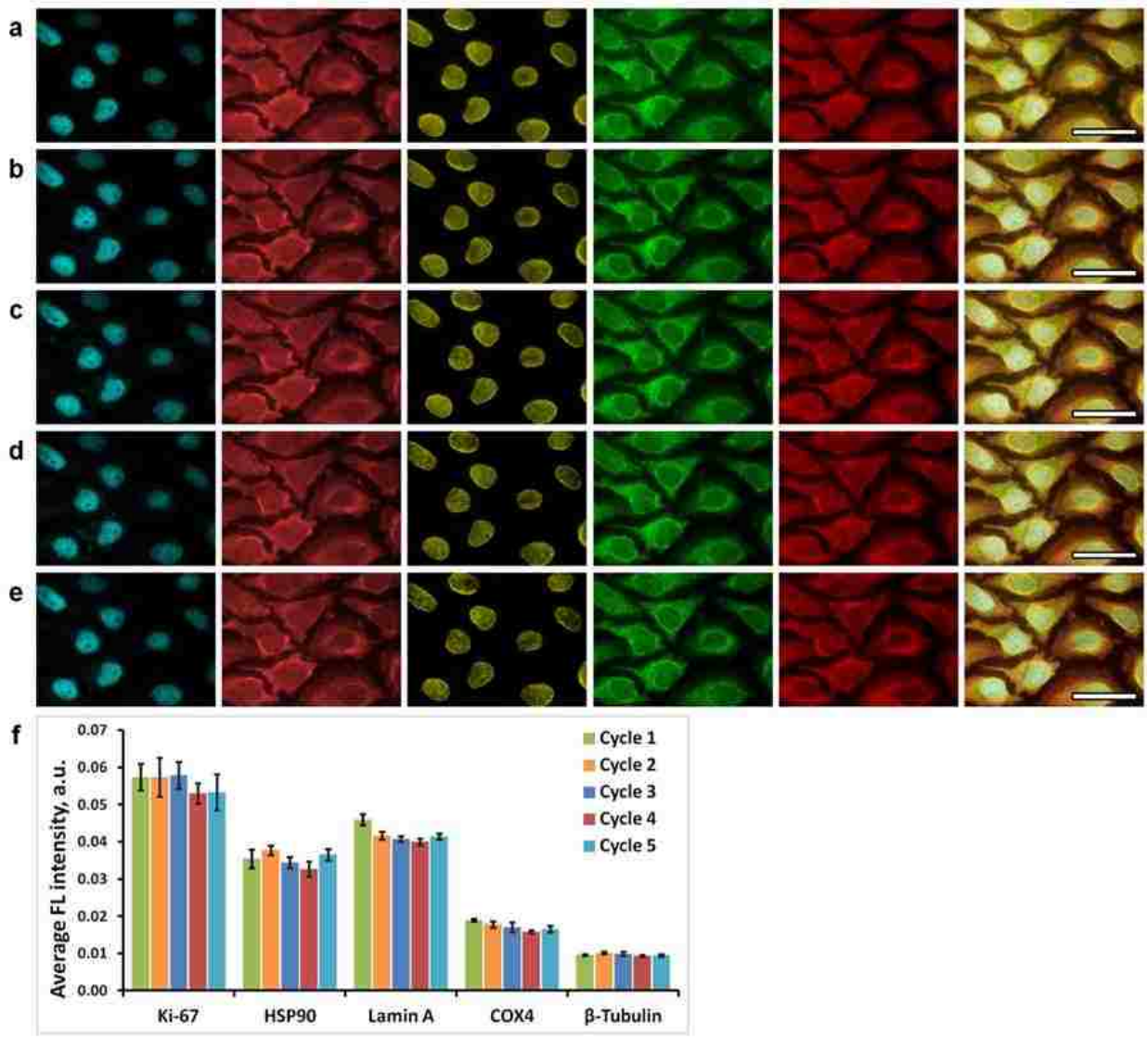

Figure 7.9 Validation of multiplexed multicycle staining for comprehensive single-cell molecular profiling. Utility of QDot imaging technology for molecular profiling is demonstrated by re-staining the same set of 5 model molecular targets (Ki-67, HSP90, Lamin A, Cox-4, and ß-tubulin labeled with QDot-SpA-Antibody probes emitting at 525, 545, 565, 585, and 605 nm respectively) through 5 cycles (**a-e**) and performing quantitative analysis of average staining intensity for each target at every cycle (**f**). Qualitative evaluation of individual QDot channels (columns 1-5 in **a-e**) as well as composite images (column 6 in **a-e**) of the same cell sub-population imaged after every cycle shows robust re-staining of each target with precisely preserved sub-cellular morphology, whereas quantitative analysis (**f**) demonstrates consistency of target staining profiles throughout all cycles. Error bars represent standard deviation of the average staining intensity between 3 different fields of view imaged on the same specimen. Scale bar, 50µm.

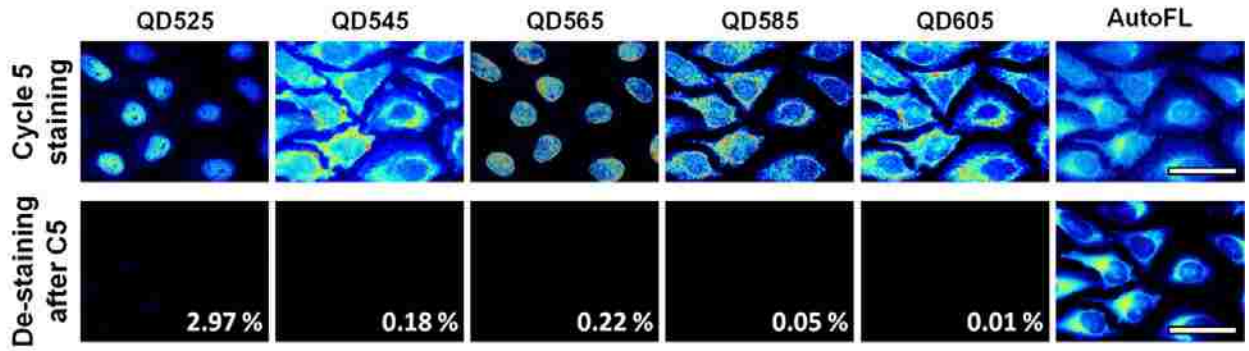

Figure 7.10 Verification of the lack of QDot fluorescence signal carry-over through 5 cycles of 5-color staining. To confirm complete specimen regeneration and removal of all QDot signal by a de-staining step through multiple cycles, a set of 5 model molecular targets is re-labeled with a matching QDot-SpA-Antibody probes, as described for 25-target labeling. After the 5th cycle, cells are once again de-stained, and the same sub-set of cells is analyzed with HSI. To facilitate direct comparison of fluorescence signal intensities, unmixed cell images obtained after cycle 5 staining (**top row**) and consequent de-staining (**bottom row**) are presented. Signal intensity within each individual QDot channel (columns QD525 through QD605) as well as cell autofluorescence channel (column AutoFL) are normalized and false-colored with a heat map. Residual signal intensity after de-staining is indicated as a % fraction of the Cycle 5 staining intensity within each QDot channel. Qualitative and quantitative analysis of cell imaging data unambiguously demonstrate complete removal of the QDot signal during de-staining step. At the same time specimen autofluorescence remains nearly unaffected, outlining preserved cell morphology. Slightly higher levels of residual fluorescence detected in QDot525 channel might also be attributed to "spectral leakage" contributed by cell autofluorescence, which is most pronounced in a blue-green spectral range. Scale bar, 50μm.

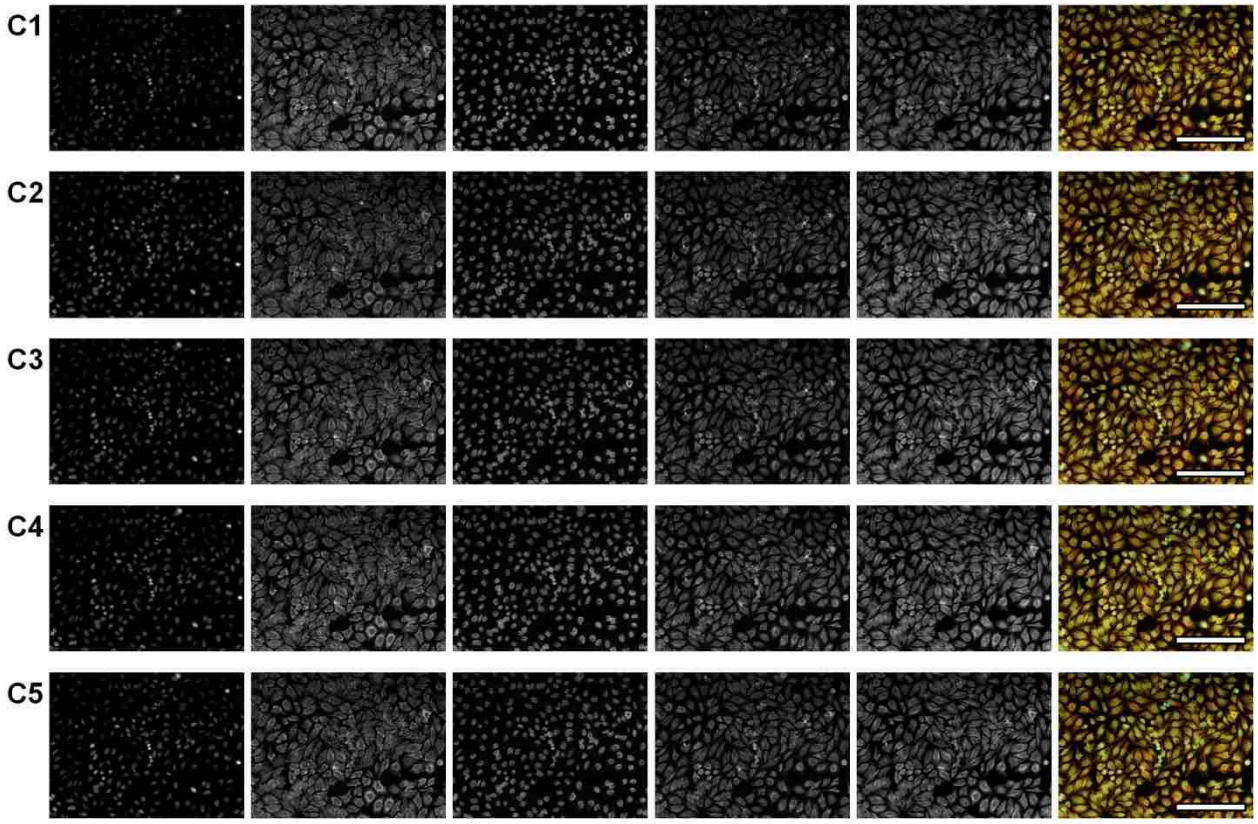

Figure 7.11 Preservation of the specimen morphology throughout 5 cycles of 5-color target re-staining. The same set of 5 model molecular targets (from left to right, Ki-67, HSP90, Lamin A, Cox-4, and ß-tubulin labeled with QDot-SpA-Antibody probes emitting at 525, 545, 565, 585, and 605 nm respectively) is re-stained through 5 cycles (C1-C5). Qualitative evaluation of individual QDot channels (columns 1-5) as well as composite images (column 6) of the same cell sub-population imaged at low magnification after every cycle shows robust re-staining of each target with preserved specimen morphology. Note that complete specimen regeneration is achieved after each cycle, leaving no detectable fluorescence signal (see **Figure 7.10**), thus ensuring that observed staining is generated by incubation of cells with a new QDot-SpA-Antibody cocktail during each cycle. Scale bar, 250µm.

7.4 Summary

Sole translation of the versatile 1-step and 2-step QDot imaging platforms presented in this dissertation into biomedical research already provides a solid foundation for initial exploratory molecular profiling studies examining panels of 5-10 molecular targets. Addition of a multicycle staining modality, in turn, dramatically expands the analytical capabilities of this platform far beyond the parallel multiplexing limitations imposed by QDot probes and HSI. In general, N color staining performed for M cycles allows N x M molecular targets being probed. We have demonstrated the utility of this technology using self-assembled QDot-SpA-Antibody probes for examination of 5 molecular targets as a model system. Unique features of the novel QDot-SpA nanoprobes offer a straightforward approach to preparation of an extensive customized QDot-Antibody library. At the same time, dual use of intermediate SpA-Antibody bond stability (i) prevents probe crosstalk during parallel multiplexed staining, while (ii) enabling quick probe dissociation and elution during specimen regeneration. As a result, several cycles of multicolor staining can be performed with a range of spectrally distinguishable QDot probes on same specimens. Importantly, in developing the cyclic staining methodology we have ensured that the specimen antigenicity and morphology remain unperturbed, while complete elimination of fluorescent signal and elution of probe components are achieved during de-staining. In this regard we'd like to highlight the importance of proper pre-staining specimen processing for target preservation.

CHAPTER 8: SUMMARY AND FUTURE DIRECTIONS

Personalized molecular diagnostics and targeted therapy are essential for making progress towards combating such complex diseases as cancer, immune system disorders, and neurological disorders. Realization of these objectives might become possible through comprehensive examination of the phenotypic heterogeneity within large cell populations, study of low-abundance events often masked or completely erased by batch processing, and elucidation of biomarker signatures of diseases, all of which are attainable with single-cell molecular profiling. However, implementation of this strategy remains elusive. "Methods to watch" column of the Nature Methods magazine has recently highlighted the importance of single-cell analysis for addressing cell heterogeneity and exploring complexity of biological systems, praising potentially groundbreaking impact these tools can bring to the study of cell biology and disease pathogenesis [11]. At the same time, limitations faced by single-cell technologies and the need for innovative technological advances have been emphasized. Unique properties of nanomaterials inspire enthusiasm for overcoming the fundamental limitations of existing technologies and hold promise of advancing the field of personalized medicine.

Incorporation of novel QDot-based tools will undoubtedly play a major role in bringing single-cell molecular profiling into biomedical practice. Unique photo-physical properties and versatile bio-functionalization capabilities make QDots well suited for multiplexed sensitive quantitative analysis of target expression profiles in cells and tissue specimens. Furthermore, an increasing number of proof-of-concept studies along with more applied and clinically

relevant QDot-based tools appearing in a variety of fields ranging from *ex vivo* molecular fingerprinting of individual cells to *in vivo* diagnostics and image-guided therapy highlight the exciting opportunities that become available through implementation of nanomedicine. However, there are still a number of challenges on the way to integration of QDot technology into biomedical practice.

Fairly uncommon behavior of nanomaterials and lack of clinical experience of utilizing QDot-based assays often raise concerns of result reproducibility, reliability, and comparability between each other and conventional techniques. Therefore, a number of proof-of-concept studies is actively exploring and validating a wide range of possible areas for QDot applications. A forthcoming leap towards technologies working in clinical settings along with wide-scale "test-drives" of QDot tools and training of technical personnel should encourage interest in QDot-based tools, increase familiarity and hands-on experience working with QDot probes, and establish confidence in this technology within scientific and medical communities. Among first steps towards this goal, standardization of QDot-based assays will be beneficial for making data from different research centers comparable and enabling large-scale clinical studies. Strategies for QDot signal calibration and accurate quantitative analysis, optimized protocols for specimen processing and staining, and straightforward probe preparation procedures described in this dissertation might prove instrumental in development of standardized robust QDot assays.

Technical limitations imposed by multi-step staining modalities and complex QDot-Antibody bioconjugation procedures also hamper wide adoption of QDot technology for fundamental research and clinical diagnostics. In this regard, the highly potent QDot imaging platform described in this dissertation overcomes the fundamental limitations of conventional methods by employing the full parallel multiplexing potential of QDot probes for direct

labeling of molecular targets and dramatically expanding this capacity via implementation of multi-cycle staining methodology. Importantly, this technology features simple and versatile probe preparation strategies capable of addressing specific need of a variety of molecular profiling applications.

In addition to the remarkable multiplexing and analytical capability, QDot platform offers all the benefits of fluorescence imaging of intact cell and tissue specimens, providing valuable 3D morphological information and addressing phenotypic heterogeneity within large cell populations. In particular, biomarker co-localization and intracellular translocation studies, cell morphometric analysis, and assessment of specimen morphology becomes available with QDot imaging platform, further enriching single-cell molecular information. For example, accurate quantitative analysis of biomarker expression might reveal strength of individual signaling nodes, whereas tracking of biomarker translocation and/or co-localization represents a straightforward way for detecting biomarker activation (particularly useful when antibodies to activated target form are not available) and assessing inter-molecular interactions. Examination of cell heterogeneity, in turn, is important for study of complex cell or tissue cultures, elucidation of drug-resistant cells, analysis of rare cell types, and accurate mapping of intra- and inter-cellular signaling mechanisms [179, 180]. As a result, our platform holds a potential of providing access to unique multi-parametric information for in-depth study of molecular mechanisms underlying normal cell physiology, disease pathogenesis, and response to therapeutic intervention on a single-cell level. To the best of our knowledge, this type of comprehensive cell characterization is not accessible through existing state-of-the-art techniques.

Certainly, current implementation of QDot imaging platform is far from being ideal, leaving plenty of room for improvement, primarily through modification of existing and

development of novel QDot and antibody probe designs. For example, smaller probes employing zwitterionic QDot platform (prepared via either polymer encapsulation or ligand exchange) that lacks spacious PEG shell might be employed for labeling of highly crosslinked specimens or tightly packed molecular targets. Alternatively, protein surface density can be decreased down to immobilization of a single ssDNA tag or a single adaptor protein per nanoparticle (*e.g.* following gel electrophoresis-based technology for preparation of monovalent QDot-Antibody probes developed in our laboratory [181]) to gain better control over probe architecture and stoichiometry. Further development of the cyclic staining methodology should benefit from integrating QDot-based labeling with automated staining-imaging instruments. For example, an automated system consisting of a fluorescence microscope and a pump-driven flow chamber can be engineered to achieve easy alignment of images obtained from different staining cycles and substantially reduce the labor requirement.

In conclusion, we envision that practical implementation of QDot-based single-cell molecular profiling technology will offer exciting opportunities in systems biology, signaling pathway analysis, gene expression studies, molecular diagnostics, and drug discovery, finding use in a wide range of research endeavors and providing a powerful tool for advancing biomedical research and clinical practice.

Literature Cited

1. Chen, H., et al., *Trends in nanotechnology patents.* Nat Nanotechnol, 2008. **3**(3): p. 123-5.
2. Massoud, T.F. and S.S. Gambhir, *Molecular imaging in living subjects: seeing fundamental biological processes in a new light.* Genes & development, 2003. **17**(5): p. 545-80.
3. Mankoff, D.A., *A definition of molecular imaging.* J Nucl Med, 2007. **48**(6): p. 18N, 21N.
4. Zrazhevskiy, P. and X. Gao, *Multifunctional Quantum Dots for Personalized Medicine.* Nano Today, 2009. **4**(5): p. 414-428.
5. True, L.D. and X. Gao, *Quantum dots for molecular pathology: their time has arrived.* J Mol Diagn, 2007. **9**(1): p. 7-11.
6. Paik, S., et al., *A multigene assay to predict recurrence of tamoxifen-treated, node-negative breast cancer.* N Engl J Med, 2004. **351**(27): p. 2817-26.
7. Sotiriou, C. and L. Pusztai, *Gene-Expression Signatures in Breast Cancer.* N. Engl. J. Med., 2009. **360**(8): p. 790-800.
8. Jain, K.K., *Personalised medicine for cancer: from drug development into clinical practice.* Expert Opin. Pharmacother., 2005. **6**(9): p. 1463-1476.
9. Chamary, J.V., J.L. Parmley, and L.D. Hurst, *Hearing silence: non-neutral evolution at synonymous sites in mammals.* Nat Rev Genet, 2006. **7**(2): p. 98-108.
10. Sauna, Z.E., et al., *Silent polymorphisms speak: how they affect pharmacogenomics and the treatment of cancer.* Cancer Res, 2007. **67**(20): p. 9609-12.
11. de Souza, N., *Single-cell methods.* Nat. Meth., 2012. **9**(1): p. 35-35.
12. Smith, A.M., et al., *Multicolor quantum dots for molecular diagnostics of cancer.* Expert Review of Molecular Diagnostics, 2006. **6**(2): p. 231-244.
13. Alivisatos, A.P., W. Gu, and C. Larabell, *Quantum dots as cellular probes.* Annual review of biomedical engineering, 2005. **7**: p. 55-76.
14. Geho, D.H., et al., *Nanotechnology in clinical proteomics.* Nanomedicine (London, England), 2007. **2**(1): p. 1-5.

15. Jemal, A., et al., *Cancer statistics, 2005.* Ca-a Cancer Journal for Clinicians, 2005. **55**(1): p. 10-30.

16. Liu, A.Y., M.P. Roudier, and L.D. True, *Heterogeneity in primary and metastatic prostate cancer as defined by cell surface CD profile.* American Journal of Pathology, 2004. **165**(5): p. 1543-1556.

17. Elledge, R.M., et al., *Estrogen receptor (ER) and progesterone receptor (PgR), by ligand-binding assay compared with ER, PgR and pS2, by immuno-histochemistry in predicting response to tamoxifen in metastatic breast cancer: A Southwest Oncology Group Study.* International Journal of Cancer, 2000. **89**(2): p. 111-117.

18. Konecny, G., et al., *Quantitative association between, HER-2/neu and steroid hormone receptors in hormone receptor-positive primary breast cancer.* Journal of the National Cancer Institute, 2003. **95**(2): p. 142-153.

19. Vogel, C.L., et al., *Efficacy and safety of trastuzumab as a single agent in first-line treatment of HER2-overexpressing metastatic breast cancer.* Journal of Clinical Oncology, 2002. **20**(3): p. 719-726.

20. Arora, A. and E.M. Scholar, *Role of tyrosine kinase inhibitors in cancer therapy.* J Pharmacol Exp Ther, 2005. **315**(3): p. 971-9.

21. Mayr, L.M. and D. Bojanic, *Novel trends in high-throughput screening.* Curr. Opin. Pharmacol., 2009. **9**(5): p. 580-588.

22. Brouzes, E., et al., *Droplet microfluidic technology for single-cell high-throughput screening.* Proc. Natl. Acad. Sci. U. S. A., 2009. **106**(34): p. 14195-14200.

23. Inglese, J., et al., *High-throughput screening assays for the identification of chemical probes.* Nat. Chem. Biol., 2007. **3**(8): p. 466-479.

24. Butcher, E.C., *Can cell systems biology rescue drug discovery?* Nat. Rev. Drug Discov., 2005. **4**(6): p. 461-467.

25. Macarron, R., et al., *Impact of high-throughput screening in biomedical research.* Nat. Rev. Drug Discov., 2011. **10**(3): p. 188-195.

26. Tanaka, M., et al., *An Unbiased Cell Morphologyâ€“Based Screen for New, Biologically Active Small Molecules.* PLoS Biol, 2005. **3**(5): p. e128.

27. Lang, P., et al., *Cellular imaging in drug discovery.* Nat Rev Drug Discov, 2006. **5**(4): p. 343-356.

28. Chaurand, P., et al., *Proteomics in diagnostic pathology: profiling and imaging proteins directly in tissue sections.* Am J Pathol, 2004. **165**(4): p. 1057-68.

29. Liotta, L. and E. Petricoin, *Molecular profiling of human cancer.* Nat Rev Genet, 2000. **1**(1): p. 48-56.

30. Gorg, A., W. Weiss, and M.J. Dunn, *Current two-dimensional electrophoresis technology for proteomics.* Proteomics, 2004. **4**(12): p. 3665-85.

31. Aebersold, R. and M. Mann, *Mass spectrometry-based proteomics.* Nature, 2003. **422**(6928): p. 198-207.

32. Gleason, D.F. and G.T. Mellinger, *Prediction of prognosis for prostatic adenocarcinoma by combined histological grading and clinical staging.* J. Urol., 1974. **111**(1): p. 58-64.

33. Liotta, L.A. and E.C. Kohn, *The microenvironment of the tumour-host interface.* Nature, 2001. **411**(6835): p. 375-379.

34. Ma, C., et al., *A clinical microchip for evaluation of single immune cells reveals high functional heterogeneity in phenotypically similar T cells.* Nat. Med., 2011. **17**(6): p. 738-43.

35. Salehi-Reyhani, A., et al., *A first step towards practical single cell proteomics: a microfluidic antibody capture chip with TIRF detection.* Lab. Chip, 2011. **11**(7): p. 1256-61.

36. Chattopadhyay, P.K., et al., *Quantum dot semiconductor nanocrystals for immunophenotyping by polychromatic flow cytometry.* Nat. Med., 2006. **12**(8): p. 972-7.

37. Bendall, S.C., et al., *Single-cell mass cytometry of differential immune and drug responses across a human hematopoietic continuum.* Science, 2011. **332**(6030): p. 687-96.

38. Umemura, S. and R.Y. Osamura, *Utility of immunohistochemistry in breast cancer practice.* Breast Cancer, 2004. **11**(4): p. 334-8.

39. True, L.D., *Quantitative immunohistochemistry: a new tool for surgical pathology?* Am J Clin Pathol, 1988. **90**(3): p. 324-5.

40. Pedersen, L., et al., *Interobserver and Intraobserver Variability in the Histopathological Diagnosis of Medullary Carcinoma of the Breast, and Its Prognostic Implications.* Breast Cancer Research and Treatment, 1989. **14**(1): p. 91-99.

41. Thomson, T.A., et al., *HER-2/neu in breast cancer: interobserver variability and performance of immunohistochemistry with 4 antibodies compared with fluorescent in situ hybridization.* Mod Pathol, 2001. **14**(11): p. 1079-86.

42. Ghazani, A.A., et al., *High throughput quantification of protein expression of cancer antigens in tissue microarray using quantum dot nanocrystals.* Nano Lett, 2006. **6**(12): p. 2881-6.

43. Furuya, T., et al., *A novel technology allowing immunohistochemical staining of a tissue section with 50 different antibodies in a single experiment.* J. Histochem. Cytochem., 2004. **52**(2): p. 205-10.

44. Englert, C.R., G.V. Baibakov, and M.R. Emmert-Buck, *Layered expression scanning: rapid molecular profiling of tumor samples.* Cancer Res., 2000. **60**(6): p. 1526-30.

45. Toth, Z.E. and E. Mezey, *Simultaneous visualization of multiple antigens with tyramide signal amplification using antibodies from the same species.* J. Histochem. Cytochem., 2007. **55**(6): p. 545-54.

46. Pirici, D., et al., *Antibody elution method for multiple immunohistochemistry on primary antibodies raised in the same species and of the same subtype.* J. Histochem. Cytochem., 2009. **57**(6): p. 567-75.

47. Glass, G., J.A. Papin, and J.W. Mandell, *SIMPLE: a sequential immunoperoxidase labeling and erasing method.* J. Histochem. Cytochem., 2009. **57**(10): p. 899-905.

48. Wahlby, C., et al., *Sequential immunofluorescence staining and image analysis for detection of large numbers of antigens in individual cell nuclei.* Cytometry, 2002. **47**(1): p. 32-41.

49. Micheva, K.D., et al., *Single-synapse analysis of a diverse synapse population: proteomic imaging methods and markers.* Neuron, 2010. **68**(4): p. 639-53.

50. Schubert, W., et al., *Analyzing proteome topology and function by automated multidimensional fluorescence microscopy.* Nat. Biotechnol., 2006. **24**(10): p. 1270-8.

51. Schwamborn, K. and R.M. Caprioli, *Molecular imaging by mass spectrometry--looking beyond classical histology.* Nat. Rev. Cancer, 2010. **10**(9): p. 639-46.

52. Wollscheid, B., et al., *Mass-spectrometric identification and relative quantification of N-linked cell surface glycoproteins.* Nat. Biotechnol., 2009. **27**(4): p. 378-86.

53. Caldwell, R.L. and R.M. Caprioli, *Tissue profiling by mass spectrometry - A review of methodology and applications*. Molecular & Cellular Proteomics, 2005. **4**(4): p. 394-401.

54. Zrazhevskiy, P. and X. Gao, *Quantum dots for cancer molecular imaging*. Minerva Biotecnologica, 2009. **21**(1): p. 37-52.

55. Medintz, I.L. and H. Mattoussi, *Quantum dot-based resonance energy transfer and its growing application in biology*. Phys. Chem. Chem. Phys., 2009. **11**(1): p. 17-45.

56. Medintz, I.L., H. Mattoussi, and A.R. Clapp, *Potential clinical applications of quantum dots*. Int. J. Nanomedicine, 2008. **3**(2): p. 151-67.

57. Misra, R.D., *Quantum dots for tumor-targeted drug delivery and cell imaging*. Nanomed, 2008. **3**(3): p. 271-4.

58. Resch-Genger, U., et al., *Quantum dots versus organic dyes as fluorescent labels*. Nat. Methods, 2008. **5**(9): p. 763-75.

59. Smith, A.M., et al., *Bioconjugated quantum dots for in vivo molecular and cellular imaging*. Adv Drug Deliv Rev, 2008. **60**(11): p. 1226-40.

60. Tholouli, E., et al., *Quantum dots light up pathology*. J. Pathol., 2008. **216**(3): p. 275-85.

61. Xing, Y. and J. Rao, *Quantum dot bioconjugates for in vitro diagnostics & in vivo imaging*. Cancer Biomark, 2008. **4**(6): p. 307-19.

62. Zrazhevskiy, P., M. Sena, and X.H. Gao, *Designing multifunctional quantum dots for bioimaging, detection, and drug delivery*. Chem. Soc. Rev., 2010. **39**(11): p. 4326-4354.

63. Alivisatos, A.P., *Perspectives on the physical chemistry of semiconductor nanocrystals*. Journal of Physical Chemistry, 1996. **100**(31): p. 13226-13239.

64. Alivisatos, A.P., *Semiconductor clusters, nanocrystals, and quantum dots*. Science, 1996. **271**(5251): p. 933-937.

65. Bruchez, M., Jr., et al., *Semiconductor nanocrystals as fluorescent biological labels*. Science, 1998. **281**(5385): p. 2013-6.

66. Medintz, I.L., et al., *Quantum dot bioconjugates for imaging, labelling and sensing*. Nat Mater, 2005. **4**(6): p. 435-46.

67. Chan, W.C., et al., *Luminescent quantum dots for multiplexed biological detection and imaging.* Curr Opin Biotechnol, 2002. **13**(1): p. 40-6.

68. Chattopadhyay, P.K., et al., *Quantum dot semiconductor nanocrystals for immunophenotyping by polychromatic flow cytometry.* Nat. Med., 2006. **12**(8): p. 972-7.

69. Yezhelyev, M.V., et al., *In Situ Molecular Profiling of Breast Cancer Biomarkers with Multicolor Quantum Dots.* Adv. Mater., 2007. **19**(20): p. 3146-3151.

70. Fountaine, T.J., et al., *Multispectral imaging of clinically relevant cellular targets in tonsil and lymphoid tissue using semiconductor quantum dots.* Mod. Pathol., 2006. **19**(9): p. 1181-91.

71. Gao, X. and S. Nie, *Molecular profiling of single cells and tissue specimens with quantum dots.* Trends Biotechnol, 2003. **21**(9): p. 371-3.

72. Wu, X.Y., et al., *Immunofluorescent labeling of cancer marker Her2 and other cellular targets with semiconductor quantum dots.* Nat. Biotechnol., 2003. **21**(1): p. 41-46.

73. Yezhelyev, M.V., et al., *In situ molecular profiling of breast cancer biomarkers with multicolor quantum dots.* Adv. Mater., 2007. **19**(20): p. 3146-3151.

74. Tokumasu, F. and J. Dvorak, *Development and application of quantum dots for immunocytochemistry of human erythrocytes.* J Microsc, 2003. **211**(Pt 3): p. 256-61.

75. Cui, B., et al., *One at a time, live tracking of NGF axonal transport using quantum dots.* Proc Natl Acad Sci U S A, 2007. **104**(34): p. 13666-71.

76. Derfus, A.M., W.C.W. Chan, and S.N. Bhatia, *Probing the cytotoxicity of semiconductor quantum dots.* Nano Letters, 2004. **4**(1): p. 11-18.

77. Dubertret, B., et al., *In vivo imaging of quantum dots encapsulated in phospholipid micelles.* Science, 2002. **298**(5599): p. 1759-1762.

78. Gao, X., et al., *In vivo cancer targeting and imaging with semiconductor quantum dots.* Nature biotechnology, 2004. **22**(8): p. 969-76.

79. Klostranec, J.M. and W.C.W. Chan, *Quantum dots in biological and biomedical research: Recent progress and present challenges.* Advanced Materials, 2006. **18**(15): p. 1953-1964.

80. Mews, A., et al., *Structural and spectroscopic investigations of CdS/HgS/CdS quantum-dot quantum wells.* Physical Review B, 1996. **53**(20): p. 13242-13245.

81. Gao, X., et al., *In vivo molecular and cellular imaging with quantum dots.* Curr Opin Biotechnol, 2005. **16**(1): p. 63-72.

82. Pinaud, F., et al., *Advances in fluorescence imaging with quantum dot bio-probes.* Biomaterials, 2006. **27**(9): p. 1679-87.

83. Dahan, M., et al., *Time-gated biological imaging by use of colloidal quantum dots.* Optics Letters, 2001. **26**(11): p. 825-827.

84. Grecco, H.E., et al., *Ensemble and single particle photophysical properties (two-photon excitation, anisotropy, FRET, lifetime, spectral conversion) of commercial quantum dots in solution and in live cells.* Microsc Res Tech, 2004. **65**(4-5): p. 169-79.

85. Lao, U.L., A. Mulchandani, and W. Chen, *Simple conjugation and purification of quantum dot-antibody complexes using a thermally responsive elastin-protein L scaffold as immunofluoresecent agents.* J. Am. Chem. Soc., 2006. **128**(46): p. 14756-7.

86. Medintz, I.L., et al., *Self-assembled nanoscale biosensors based on quantum dot FRET donors.* Nat. Mater., 2003. **2**(9): p. 630-8.

87. Goldman, E.R., et al., *Avidin: a natural bridge for quantum dot-antibody conjugates.* J. Am. Chem. Soc., 2002. **124**(22): p. 6378-82.

88. Mattoussi, H., et al., *Self-assembly of CdSe-ZnS quantum dot bioconjugates using an engineered recombinant protein.* J. Am. Chem. Soc., 2000. **122**(49): p. 12142-12150.

89. Yezhelyev, M.V., et al., *Emerging use of nanoparticles in diagnosis and treatment of breast cancer.* Lancet Oncol, 2006. **7**(8): p. 657-67.

90. Xiao, Y. and P.E. Barker, *Semiconductor nanocrystal probes for human metaphase chromosomes.* Nucleic Acids Res, 2004. **32**(3): p. e28.

91. Tholouli, E., et al., *Imaging of multiple mRNA targets using quantum dot based in situ hybridization and spectral deconvolution in clinical biopsies.* Biochemical and biophysical research communications, 2006. **348**(2): p. 628-36.

92. Chan, P., et al., *Method for multiplex cellular detection of mRNAs using quantum dot fluorescent in situ hybridization.* Nucleic Acids Res, 2005. **33**(18): p. e161.

93. Matsuno, A., et al., *Three-dimensional imaging of the intracellular localization of growth hormone and prolactin and their mRNA using nanocrystal (Quantum dot) and confocal laser scanning microscopy techniques.* J. Histochem. Cytochem., 2005. **53**(7): p. 833-8.

94. Xing, Y., et al., *Bioconjugated quantum dots for multiplexed and quantitative immunohistochemistry.* Nat. Protoc., 2007. **2**(5): p. 1152-65.

95. Shi, C., et al., *Quantum dots-based multiplexed immunohistochemistry of protein expression in human prostate cancer cells.* Eur. J. Histochem., 2008. **52**(2): p. 127-34.

96. Liu, J., et al., *Multiplexed detection and characterization of rare tumor cells in Hodgkin's lymphoma with multicolor quantum dots.* Anal. Chem., 2010. **82**(14): p. 6237-43.

97. Liu, J., et al., *Molecular mapping of tumor heterogeneity on clinical tissue specimens with multiplexed quantum dots.* ACS Nano, 2010. **4**(5): p. 2755-65.

98. Chen, C., et al., *Quantum-dot-based immunofluorescent imaging of HER2 and ER provides new insights into breast cancer heterogeneity.* Nanotechnology, 2010. **21**(9): p. 095101.

99. Sweeney, E., et al., *Quantitative multiplexed quantum dot immunohistochemistry.* Biochem. Biophys. Res. Commun., 2008. **374**(2): p. 181-6.

100. Huang, D.H., et al., *Comparison and Optimization of Multiplexed Quantum Dot-Based Immunohistofluorescence.* Nano Research, 2010. **3**(1): p. 61-68.

101. Wu, X., et al., *Immunofluorescent labeling of cancer marker Her2 and other cellular targets with semiconductor quantum dots.* Nat. Biotechnol., 2003. **21**(1): p. 41-6.

102. Ghazani, A.A., et al., *High throughput quantification of protein expression of cancer antigens in tissue microarray using quantum dot nanocrystals.* Nano Lett., 2006. **6**(12): p. 2881-6.

103. Zeng, R.S., et al., *Aqueous synthesis of type-II CdTe/CdSe core-shell quantum dots for fluorescent probe labeling tumor cells.* Nanotechnology, 2009. **20**(9): p. -.

104. Zheng, Y.G., Z.C. Yang, and J.Y. Ying, *Aqueous synthesis of glutathione-capped ZnSe and Zn1-xCdxSe alloyed quantum dots.* Adv. Mater., 2007. **19**(11): p. 1475-1479.

105. Murray, C.B., D.J. Norris, and M.G. Bawendi, *Synthesis and characterization of nearly monodisperse CdE (E = sulfur, selenium, tellurium) semiconductor nanocrystallites.* J. Am. Chem. Soc., 1993. **115**(19): p. 8706-8715.

106. Peng, Z.A. and X.G. Peng, *Formation of high-quality CdTe, CdSe, and CdS nanocrystals using CdO as precursor*. J. Am. Chem. Soc., 2001. **123**(1): p. 183-184.

107. Peng, Z.A. and X. Peng, *Nearly monodisperse and shape-controlled CdSe nanocrystals via alternative routes: nucleation and growth*. J. Am. Chem. Soc., 2002. **124**(13): p. 3343-53.

108. Li, L.S., et al., *High Quality ZnSe and ZnS Nanocrystals Formed by Activating Zinc Carboxylate Precursors*. Nano Lett., 2004. **4**(11): p. 2261-2264.

109. Peng, X., J. Wickham, and A.P. Alivisatos, *Kinetics of II-VI and III-V Colloidal Semiconductor Nanocrystal Growth: Focusing of Size Distributions*. J. Am. Chem. Soc., 1998. **120**(21): p. 5343-5344.

110. Zhong, X.H., et al., *Alloyed ZnxCd1-xS nanocrystals with highly narrow luminescence spectral width*. J. Am. Chem. Soc., 2003. **125**(44): p. 13559-13563.

111. Kim, S., et al., *Type-II quantum dots: CdTe/CdSe(core/shell) and CdSe/ZinTe(core/shell) heterostructures*. J. Am. Chem. Soc., 2003. **125**(38): p. 11466-11467.

112. Pietryga, J.M., et al., *Pushing the band gap envelope: Mid-infrared emitting colloidal PbSe quantum dots*. J. Am. Chem. Soc., 2004. **126**(38): p. 11752-11753.

113. Qu, L. and X. Peng, *Control of photoluminescence properties of CdSe nanocrystals in growth*. J. Am. Chem. Soc., 2002. **124**(9): p. 2049-55.

114. Smith, A.M., X. Gao, and S. Nie, *Quantum dot nanocrystals for in vivo molecular and cellular imaging*. Photochem. Photobiol., 2004. **80**(3): p. 377-85.

115. Zhong, X.H., et al., *Composition-tunable ZnxCd1-xSe nanocrystals with high luminescence and stability*. J. Am. Chem. Soc., 2003. **125**(28): p. 8589-8594.

116. Bailey, R.E. and S.M. Nie, *Alloyed semiconductor quantum dots: Tuning the optical properties without changing the particle size*. J. Am. Chem. Soc., 2003. **125**(23): p. 7100-7106.

117. Giepmans, B.N., et al., *Correlated light and electron microscopic imaging of multiple endogenous proteins using Quantum dots*. Nat. Methods, 2005. **2**(10): p. 743-9.

118. Nisman, R., et al., *Application of quantum dots as probes for correlative fluorescence, conventional, and energy-filtered transmission electron microscopy*. J Histochem Cytochem, 2004. **52**(1): p. 13-8.

119. Alivisatos, A.P., *Perspectives on the Physical Chemistry of Semiconductor Nanocrystals*. J. Phys. Chem., 1996. **100**(31): p. 13226-13239.

120. Oberdorster, G., E. Oberdorster, and J. Oberdorster, *Nanotoxicology: an emerging discipline evolving from studies of ultrafine particles*. Environ. Health Perspect., 2005. **113**(7): p. 823-39.

121. Bryant, G.W. and W. Jaskolski, *Surface effects on capped and uncapped nanocrystals*. J. Phys. Chem. B, 2005. **109**(42): p. 19650-6.

122. Gomez, D.E., M. Califano, and P. Mulvaney, *Optical properties of single semiconductor nanocrystals*. Phys. Chem. Chem. Phys., 2006. **8**(43): p. 4989-5011.

123. Dabbousi, B.O., et al., *(CdSe)ZnS Core Shell Quantum Dots: Synthesis and Characterization of a Size Series of Highly Luminescent Nanocrystallites*. The Journal of Physical Chemistry B, 1997. **101**(46): p. 9463-9475.

124. Hines, M.A. and P. Guyot-Sionnest, *Synthesis and Characterization of Strongly Luminescing ZnS-Capped CdSe Nanocrystals*. J. Phys. Chem., 1996. **100**(2): p. 468-471.

125. Peng, X., et al., *Epitaxial Growth of Highly Luminescent CdSe/CdS Core/Shell Nanocrystals with Photostability and Electronic Accessibility*. J. Am. Chem. Soc., 1997. **119**(30): p. 7019-7029.

126. Efros, A.L. and M. Rosen, *Random telegraph signal in the photoluminescence intensity of a single quantum dot*. Phys. Rev. Lett., 1997. **78**(6): p. 1110-1113.

127. Michalet, X., et al., *Properties of Fluorescent Semiconductor Nanocrystals and their Application to Biological Labeling*. Single Molecules, 2001. **2**(4): p. 261-276.

128. Nirmal, M., et al., *Fluorescence intermittency in single cadmium selenide nanocrystals*. Nature, 1996. **383**(6603): p. 802-804.

129. Comparelli, R., et al., *Improved optical properties of CdS quantum dots by ligand exchange*. Materials Science and Engineering: C, 2003. **23**(6-8): p. 1083-1086.

130. Li, J.J., et al., *Large-scale synthesis of nearly monodisperse CdSe/CdS core/shell nanocrystals using air-stable reagents via successive ion layer adsorption and reaction*. J. Am. Chem. Soc., 2003. **125**(41): p. 12567-75.

131. Talapin, D.V., et al., *Highly Luminescent Monodisperse CdSe and CdSe/ZnS Nanocrystals Synthesized in a Hexadecylamine-Trioctylphosphine Oxide-Trioctylphospine Mixture*. Nano Lett., 2001. **1**(4): p. 207-211.

132. Chan, W.C. and S. Nie, *Quantum Dot Bioconjugates for Ultrasensitive Nonisotopic Detection*. Science, 1998. **281**(5385): p. 2016-2018.

133. Choi, H.S., et al., *Renal clearance of quantum dots*. Nat. Biotechnol., 2007. **25**(10): p. 1165-70.

134. Law, W.C., et al., *Aqueous-phase synthesis of highly luminescent CdTe/ZnTe core/shell quantum dots optimized for targeted bioimaging*. Small, 2009. **5**(11): p. 1302-10.

135. Aldana, J., Y.A. Wang, and X. Peng, *Photochemical instability of CdSe nanocrystals coated by hydrophilic thiols*. J. Am. Chem. Soc., 2001. **123**(36): p. 8844-50.

136. Algar, W.R. and U.J. Krull, *Luminescence and stability of aqueous thioalkyl acid capped CdSe/ZnS quantum dots correlated to ligand ionization*. ChemPhysChem, 2007. **8**(4): p. 561-8.

137. Liu, W., et al., *Compact biocompatible quantum dots functionalized for cellular imaging*. J Am Chem Soc, 2008. **130**(4): p. 1274-84.

138. Sukhanova, A., et al., *Biocompatible fluorescent nanocrystals for immunolabeling of membrane proteins and cells*. Anal. Biochem., 2004. **324**(1): p. 60-7.

139. Jiang, W., et al., *Design and characterization of lysine cross-linked mereapto-acid biocompatible quantum dots*. Chem. Mater., 2006. **18**(4): p. 872-878.

140. Smith, A.M. and S. Nie, *Minimizing the hydrodynamic size of quantum dots with multifunctional multidentate polymer ligands*. J. Am. Chem. Soc., 2008. **130**(34): p. 11278-9.

141. Gerion, D., et al., *Synthesis and properties of biocompatible water-soluble silica-coated CdSe/ZnS semiconductor quantum dots*. J. Phys. Chem. B, 2001. **105**(37): p. 8861-8871.

142. Pinaud, F., et al., *Bioactivation and cell targeting of semiconductor CdSe/ZnS nanocrystals with phytochelatin-related peptides*. J Am Chem Soc, 2004. **126**(19): p. 6115-23.

143. Whaley, S.R., et al., *Selection of peptides with semiconductor binding specificity for directed nanocrystal assembly*. Nature, 2000. **405**(6787): p. 665-8.

144. Pellegrino, T., et al., *Hydrophobic nanocrystals coated with an amphiphilic polymer shell: A general route to water soluble nanocrystals*. Nano Letters, 2004. **4**(4): p. 703-707.

145. Dubertret, B., et al., *In vivo imaging of quantum dots encapsulated in phospholipid micelles.* Science (New York, N.Y, 2002. **298**(5599): p. 1759-62.

146. Smith, A.M., et al., *A systematic examination of surface coatings on the optical and chemical properties of semiconductor quantum dots.* Phys. Chem. Chem. Phys., 2006. **8**: p. 3895 - 3903.

147. Cui, B., et al., *One at a time, live tracking of NGF axonal transport using quantum dots.* Proc. Natl. Acad. Sci. U. S. A., 2007. **104**(34): p. 13666-71.

148. Dahan, M., et al., *Diffusion dynamics of glycine receptors revealed by single-quantum dot tracking.* Science, 2003. **302**(5644): p. 442-5.

149. Barat, B., et al., *Cys-diabody Quantum Dot Conjugates (ImmunoQdots) for Cancer Marker Detection.* Bioconjug. Chem., 2009. **20**(8): p. 1474-1481.

150. Medintz, I.L., et al., *Proteolytic activity monitored by fluorescence resonance energy transfer through quantum-dot-peptide conjugates.* Nat. Mater., 2006. **5**(7): p. 581-9.

151. Delehanty, J.B., et al., *Self-assembled quantum dot-peptide bioconjugates for selective intracellular delivery.* Bioconjug. Chem., 2006. **17**(4): p. 920-7.

152. Goldman, E.R., et al., *Conjugation of luminescent quantum dots with antibodies using an engineered adaptor protein to provide new reagents for fluoroimmunoassays.* Anal. Chem., 2002. **74**(4): p. 841-847.

153. Mattoussi, H., et al., *Self-Assembly of CdSe/ZnS Quantum Dot Bioconjugates Using an Engineered Recombinant Protein.* J. Am. Chem. Soc., 2000. **122**(49): p. 12142-12150.

154. Fernandez-Arguelles, M.T., et al., *Synthesis and characterization of polymer-coated quantum dots with integrated acceptor dyes as FRET-based nanoprobes.* Nano Lett., 2007. **7**(9): p. 2613-2617.

155. Lin, C.A.J., et al., *Design of an amphiphilic polymer for nanoparticle coating and functionalization.* Small, 2008. **4**(3): p. 334-341.

156. Alivisatos, A.P., *Birth of a nanoscience building block.* ACS nano, 2008. **2**(8): p. 1514-6.

157. Tholouli, E., et al., *Imaging of multiple mRNA targets using quantum dot based in situ hybridization and spectral deconvolution in clinical biopsies.* Biochem. Biophys. Res. Commun., 2006. **348**(2): p. 628-36.

158. Zhong, X.H., et al., *Embryonic nuclei-induced alloying process for the reproducible synthesis of blue-emitting ZnxCd1-xSe nanocrystals with long-time thermal stability in size distribution and emission wavelength.* J. Phys. Chem. B, 2004. **108**(40): p. 15552-15559.

159. Levenson, R.M., *Spectral Imaging and Pathology: Seeing More*. Lab Medicine, 2004. **35**(4): p. 244-251.

160. Byers, R.J., et al., *Semiautomated multiplexed quantum dot-based in situ hybridization and spectral deconvolution.* J. Mol. Diagnostics, 2007. **9**(1): p. 20-9.

161. Ghazani, A.A., et al., *High throughput quantification of protein expression of cancer antigens in tissue microarray using quantum dot nanocrystals.* Nano Lett., 2006. **6**(12): p. 2881-2886.

162. Zrazhevskiy, P. and X. Gao, *Quantum dot imaging platform for single-cell molecular profiling.* Nat Commun, 2013. **4**: p. 1619.

163. Jaiswal, J.K., et al., *Long-term multiple color imaging of live cells using quantum dot bioconjugates*. Nat. Biotechnol., 2003. **21**(1): p. 47-51.

164. Jin, T., et al., *Antibody-protein A conjugated quantum dots for multiplexed imaging of surface receptors in living cells.* Mol. BioSyst., 2010. **6**(11): p. 2325-31.

165. Moks, T., et al., *Staphylococcal protein A consists of five IgG-binding domains.* Eur. J. Biochem., 1986. **156**(3): p. 637-43.

166. Atkins, K.L., et al., *S. aureus IgG-binding proteins SpA and Sbi: host specificity and mechanisms of immune complex formation.* Mol. Immunol., 2008. **45**(6): p. 1600-11.

167. Hanson, D.C., M.L. Phillips, and V.N. Schumaker, *Electron microscopic and hydrodynamic studies of protein A-immunoglobulin G soluble complexes.* J. Immunol., 1984. **132**(3): p. 1386-96.

168. Hanson, D.C. and V.N. Schumaker, *A model for the formation and interconversion of protein A-immunoglobulin G soluble complexes.* J. Immunol., 1984. **132**(3): p. 1397-409.

169. Mota, G., V. Ghetie, and J. Sjoquist, *Characterization of the soluble complex formed by reacting rabbit IgG with protein A of S. aureus.* Immunochemistry, 1978. **15**(9): p. 639-42.

170. Chen, S.F., et al., *Strong resistance of phosphorylcholine self-assembled monolayers to protein adsorption: Insights into nonfouling properties of zwitterionic materials.* J. Am. Chem. Soc., 2005. **127**(41): p. 14473-14478.

171. Michalet, X., et al., *Quantum dots for live cells, in vivo imaging, and diagnostics.* Science, 2005. **307**(5709): p. 538-544.

172. Myhre, E.B. and G. Kronvall, *Immunochemical Aspects of Fc-Mediated Binding of Human-Igg Subclasses to Group-a, Group-C and Group-G Streptococci.* Mol. Immunol., 1980. **17**(12): p. 1563-1573.

173. Bailey, R.C., et al., *DNA-encoded antibody libraries: a unified platform for multiplexed cell sorting and detection of genes and proteins.* J. Am. Chem. Soc., 2007. **129**(7): p. 1959-67.

174. Lind, K. and M. Kubista, *Development and evaluation of three real-time immuno-PCR assemblages for quantification of PSA.* J. Immunol. Methods, 2005. **304**(1-2): p. 107-16.

175. Cady, N.C., A.D. Strickland, and C.A. Batt, *Optimized linkage and quenching strategies for quantum dot molecular beacons.* Mol. Cell. Probes, 2007. **21**(2): p. 116-24.

176. Gueroui, Z. and A. Libchaber, *Single-molecule measurements of gold-quenched quantum dots.* Phys. Rev. Lett., 2004. **93**(16): p. 166108.

177. Lim, S.H., et al., *Specific nucleic acid detection using photophysical properties of quantum dot probes.* Anal. Chem., 2010. **82**(3): p. 886-91.

178. Zhong, X., et al., *Alloyed ZnxCd1-xS Nanocrystals with Highly Narrow Luminescence Spectral Width.* J. Am. Chem. Soc., 2003. **125**(44): p. 13559-13563.

179. Denysenko, T., et al., *Glioblastoma cancer stem cells: heterogeneity, microenvironment and related therapeutic strategies.* Cell Biochem. Funct., 2010. **28**(5): p. 343-51.

180. Sachs, K., et al., *Causal protein-signaling networks derived from multiparameter single-cell data.* Science, 2005. **308**(5721): p. 523-9.

181. Liu, H.Y. and X. Gao, *Engineering monovalent quantum dot-antibody bioconjugates with a hybrid gel system.* Bioconjug. Chem., 2011. **22**(3): p. 510-7.